New Jersey Institute of Technology
Digital Commons @ NJIT

Dissertations | Theses and Dissertations

Spring 2007

In vitro studies of degradation and bioactivity of aliphatic polyesther composites

Georgia Chouzouri
New Jersey Institute of Technology

Follow this and additional works at: https://digitalcommons.njit.edu/dissertations

 Part of the Chemical Engineering Commons

Recommended Citation
Chouzouri, Georgia, "In vitro studies of degradation and bioactivity of aliphatic polyesther composites" (2007). *Dissertations*. 814.
https://digitalcommons.njit.edu/dissertations/814

This Dissertation is brought to you for free and open access by the Theses and Dissertations at Digital Commons @ NJIT. It has been accepted for inclusion in Dissertations by an authorized administrator of Digital Commons @ NJIT. For more information, please contact digitalcommons@njit.edu.

Copyright Warning & Restrictions

The copyright law of the United States (Title 17, United States Code) governs the making of photocopies or other reproductions of copyrighted material.

Under certain conditions specified in the law, libraries and archives are authorized to furnish a photocopy or other reproduction. One of these specified conditions is that the photocopy or reproduction is not to be "used for any purpose other than private study, scholarship, or research." If a, user makes a request for, or later uses, a photocopy or reproduction for purposes in excess of "fair use" that user may be liable for copyright infringement,

This institution reserves the right to refuse to accept a copying order if, in its judgment, fulfillment of the order would involve violation of copyright law.

Please Note: The author retains the copyright while the New Jersey Institute of Technology reserves the right to distribute this thesis or dissertation

Printing note: If you do not wish to print this page, then select "Pages from: first page # to: last page #" on the print dialog screen

The Van Houten library has removed some of the personal information and all signatures from the approval page and biographical sketches of theses and dissertations in order to protect the identity of NJIT graduates and faculty.

ABSTRACT

IN VITRO STUDIES OF DEGRADATION AND BIOACTIVITY OF ALIPHATIC POLYESTER COMPOSITES

by

Georgia Chouzouri

In spite of numerous publications on the potential use of combinations of aliphatic polyester composites containing bioactive fillers for bone regeneration, little information exists on the combined *in vitro* mechanisms involving simultaneously diffusion for polymer degradation and bioactivity through nucleation and growth of apatite in simulated body fluid (SBF) solution. The objective of this study is to contribute to the understanding of the fundamentals in designing non-porous, solid materials for bone regeneration, from experimental data along with their engineering interpretation.

Bioactivity, in terms of apatite growth, was assessed through several experimental methods such as scanning electron microscopy (SEM), energy dispersive X-ray analysis (EDX), X-ray-diffraction (XRD) and changes in ion concentration. In the case of the six neat fillers evaluated, the filler shape, form and chemical structure showed significant differences in bioactivity response. Bioglass and calcium silicate fillers showed faster nucleation and growth rates in the screening experiments.

Composites at 30 % by weight filler were prepared by solution and/or melt mixing. Polycaprolactone (PCL) composites containing five different fillers were evaluated. Solution processed PCL/calcium silicate (CS) samples showed faster bioactivity, as determined by apatite growth, compared to melt mixed samples. The onset time for bioactivity was different for all PCL composites. The limited bioactivity in the

PCL composites over longer periods of time could be attributed to the PCL hydrophobicity leading to a slow polymer degradation rate, and also to the lack of SBF replenishment. For both polylactic acid (PLA) composites containing CS and bioglass, significant growth was observed after one week and in the case of CS was still evident after four weeks immersion. However, at prolonged time periods no further bioactivity was observed, although ion release results indicated a faster release rate that would eventually lead to a faster polymer degradation and possibly continuing bioactivity.

The presence of silicate fillers enhanced the hydrolytic degradation rate of both PCL and PLA as shown from kinetic data calculations based on molecular weight measurements. Unfilled PLA samples showed significant embrittlement after two weeks immersion, whereas for the CS filled system more significant changes could be observed in the compressive strength and modulus after the same time period.

Experimental data were also fitted into an equation proposed to calculate erosion number; in the case of unfilled PLA predictions were found to agree with literature results suggesting bulk erosion. By assuming impermeable, randomly dispersed glass flakes, water transport in a composite system, prior to significant polymer degradation could be modeled. However, modeling of transport in the case of the composite consisting of a degrading polymer and a reactive decaying filler was challenging, particularly in the case of directional bioactive reinforcements, due to the occurrence of simultaneous time dependent diffusion phenomena that altered the integrity of the sample.

IN VITRO STUDIES OF DEGRADATION AND BIOACTIVITY OF ALIPHATIC POLYESTER COMPOSITES

by
Georgia Chouzouri

A Dissertation
Submitted to the Faculty of
New Jersey Institute of Technology
In Partial Fulfillment of the Requirements for the Degree of
Doctor of Philosophy in Chemical Engineering

Otto H. York Department of Chemical Engineering

May 2007

Copyright © 2007 by Georgia Chouzouri

ALL RIGHTS RESERVED

APPROVAL PAGE

IN VITRO STUDIES OF DEGRADATION AND BIOACTIVITY OF ALIPHATIC POLYESTER COMPOSITES

Georgia Chouzouri

Dr. Marino Xanthos, Dissertation Advisor — Date
Professor, Otto H. York Department of Chemical Engineering, NJIT

Dr. Treena Livingston Arinzeh, Committee Member — Date
Associate Professor, Biomedical Engineering, NJIT

Dr. Michael Jaffe, Committee Member — Date
Research Professor, Biomedical Engineering, NJIT

Dr. Laurent Simon, Committee Member — Date
Assistant Professor, Otto H. York Department of Chemical Engineering, NJIT

Dr. Jing Wu, Committee Member — Date
Assistant Professor, Otto H. York Department of Chemical Engineering, NJIT

BIOGRAPHICAL SKETCH

Author: Georgia Chouzouri

Degree: Doctor of Philosophy

Date: May 2007

Undergraduate and Graduate Education:

- Doctor of Philosophy in Chemical Engineering,
  New Jersey Institute of Technology, Newark, NJ, 2007

- Master of Science in Chemical Engineering,
  New Jersey Institute of Technology, Newark, NJ, 2003

- Bachelor of Science in Chemical Engineering.
  National Technical University of Athens, Athens, Greece, 1998

Major: Chemical Engineering

Presentations and Publications:

G. Chouzouri, M. Xanthos, "Bioactive Fillers", Chapter 22, pp. 387-399 in M. Xanthos, Ed., *"Functional Fillers for Plastics"*, Wiley-VCH, Weinheim, Germany (2005).

G. Chouzouri and M. Xanthos, "Degradation of Aliphatic Polyesters in the Presence of Inorganic Fillers", *Journal of Plastic Film and Sheeting,* 23, 19-36 (2007).

G. Chouzouri and M. Xanthos, "In vitro Bioactivity and Degradation of Polycaprolactone Composites containing Silicate Fillers", *Acta Biomaterialia.* Available on line. doi:10.1016/j.actbio.2007.01.005.

G. Chouzouri and M. Xanthos, "Polycaprolactone Composites for Biomedical Applications", *Proc. 23rd Annual Meeting of the Polymer Processing Society, PPS- 23,* Salvador, Brazil, Accepted for presentation May 27-31, 2007.

M. Xanthos, G. Chouzouri and Q. Zhou, "Effects of Fillers-Nanofillers on the Degradation Characteristics of Aliphatic Polyesters", *Intertech-PIRA Conference*, San Antonio, Texas, February 21-23, 2007.

G. Chouzouri and M. Xanthos, "Assessment of Bioactivity of Aliphatic Polyester Composites", *Proc. 64th Annual Technical Conference Society of Plastics Engineers*, SPE, **52**, 1361, (2006).

G. Chouzouri and M. Xanthos, "Degradation of Aliphatic Polyesters in the Presence of Inorganic Fillers", *Proc. 64th Annual Technical Conference Society of Plastics Engineers*, SPE, **52**, 1750, (2006).

G. Chouzouri, D. Abdeljabbar and M. Xanthos, "Biodegradable Polymeric Matrix Composites for Tissue Regeneration Applications", *Proc. 21st Annual Meeting of the Polymer Processing Society, PPS 21, Paper SL10.5,* Leipzig, Germany, June 19-23, 2005.

N. S. Patel, T. G. Gopakumar, G. Chouzouri and M. Xanthos, "Effect of Nanofiller Aspect Ratio on the Properties of Polymer Nanocomposites", *Proc. 21st Annual Meeting of the Polymer Processing Society, PPS 21, Paper SL12.10,* Leipzig, Germany June 19-23, 2005.

G. Chouzouri and M. Xanthos, "Bioactive Composites for Tissue Regeneration", *Proc. 63rd Annual Technical Conference Society of Plastics Engineers*, SPE, **51**, 1363, (2005).

G. Chouzouri, S. Patel and M. Xanthos, "Biocomposites based on Poly(L-lactic acid) and a Functional Synthetic Filler", *Proc. 62nd Annual Technical Conference Society of Plastics Engineers*, SPE, **50**, 3366, (2004).

G. Chouzouri and M. Xanthos, "Biocomposites Based on a Degradable Polyester and a Novel Functional Filler", *Proc. Polymer Processing Society, PPS 2003* Regional Meeting, p. 211, Athens, Greece, September 14-17, 2003.

M. Xanthos, G. Chouzouri, S. Kim, S.H. Patel and M-W. Young, "Functional Additives as Sensors in Intelligent Polymer Coatings", *Farbe & Lack*, 109, 8, 18-23 (2003). (In German).

M. Xanthos, G. Chouzouri, S. Kim, S.H. Patel and M-W. Young, "Functional Additives as Sensors in Intelligent Polymer Coatings", *Proc. European Coatings Conference, SMART COATINGS II,* June 16th-17th, 2003 Berlin, Germany.

G. Chouzouri and M. Xanthos, "Modification of Biodegradable Polyesters with Inorganic Fillers", *Proc. 61st Annual Technical Conference Society of Plastics Engineers*, SPE, **49**, 2561, (2003).

To my beloved husband for his encouragement, love and unceasing support

ACKNOWLEDGMENTS

First and foremost, I would like to express my deepest gratitude for my thesis advisor, Prof. Marino Xanthos. I could not begin to explain my appreciation for his constructive guidance and invaluable teaching in polymer chemistry and processing, which strengthened and provided a solid basis for my future endeavors in this field. It was a great privilege to have Prof. Marino Xanthos as my mentor. It would be impossible for me to fully express how his moral and emotional support helped me persevere through circumstances that would otherwise be overwhelming.

I would also like to thank Prof. Treena Arinzeh, Prof. Michael Jaffe, Prof. Laurent Simon and Prof. Jing Wu for serving as members of my committee. I appreciate their input, and I thank them for their constructive comments.

I would also like to thank the staff of the Polymer Processing Institute (PPI), Newark, NJ for providing a friendly and productive environment. Their invaluable assistance and cooperation is greatly appreciated.

In addition, I would like to thank Dr. Victor Tan of PPI for his guidance and help with the characterization experiments and Dr. Subhash Patel of PPI for providing guidance in developing my experimental skills. Also, Mr. Dale Conti for his timely support and assistance with experimental equipment in the PPI laboratory. Last, but not least, Mr. Chandrakant Patel of NJIT for his help with solution analysis experiments. I would also like to thank Professor Jing Wu and Mr. Jing Zhang of NJIT for providing the PLLA polymer.

The following undergraduate and high school students, Diya Abdeljabbar, Rina Shah and Rana Abdeljabbar, contributed to this research through their internship in our labs during 2005-2006.

It would be inexcusable not to mention my colleagues and friends Dr. Shalini Gautam, Mr. Amit Goyal, Mr. Kuil Park, Mr. JinUk Ha and Mr. Kuan-Yin Lin for their unconditional help and emotional support they provided. They created a pleasant working environment and made the days at NJIT more enjoyable.

Lastly, I take this opportunity to sincerely thank my family and friends for their love and understanding. Specifically, my mother's advice has encouraged and inspired me to stay focused and head towards the right direction. Last, but not least, I am thankful to my husband for love, patience, understanding and his confidence in me. Without his help I could not have done it. I thank him for always being there for me.

TABLE OF CONTENTS

TABLE OF CONTENTS
(Continued)

TABLE OF CONTENTS
(Continued)

Chapter **Page**

TABLE OF CONTENTS
(Continued)

TABLE OF CONTENTS
(Continued)

Chapter **Page**

TABLE OF CONTENTS
(Continued)

LIST OF TABLES

LIST OF TABLES
(Continued)

Table **Page**

LIST OF FIGURES

LIST OF FIGURES
(Continued)

Figure **Page**

LIST OF FIGURES
(Continued)

LIST OF FIGURES
(Continued)

Figure **Page**

LIST OF FIGURES
(Continued)

Figure **Page**

LIST OF FIGURES
(Continued)

Figure **Page**

LIST OF FIGURES
(Continued)

Figure **Page**

LIST OF FIGURES
(Continued)

Figure **Page**

LIST OF FIGURES
(Continued)

LIST OF FIGURES
(Continued)

Figure **Page**

LIST OF SYMBOLS

C	Concentration
CC_p	Carboxyl content of the pellet
D	Diffusion coefficient
D_0	Polymer diffusion coefficient
D_{comp}	Composite diffusion coefficient
ΔH_{cc}	Heat of cold crystallization
ΔH_f	Heat of fusion
ΔH_{pf}	Heat of fusion for a perfect crystal
h	Thickness
I_b	Bioactivity Index
K	Constant for Mark-Houwink equation
k	Rate constant
M_m	Effective moisture equilibrium
$\overline{M_n}$	Number average molecular weight
M_t	Weight gain from moisture absorption
$\overline{M_v}$	Viscosity average molecular weight
N	Average degree of polymerization
N_A	Avogadro's number
$t_{0.5bb}$	Time taken for more than 50% of the interface to bond to bone
T_{cc}	Cold crystallization temperature

LIST OF SYMBOLS
(Continued)

$t_{diffusion}$	Characteristic time for diffusion
T_g	Glass transition temperature
T_m	Melting temperature
$T_{reaction}$	Characteristic time for reaction
W_0	Weight of the starting dry disc
W_d	Initial weight before water exposure
W_t	Weight of the wet disc at time t
W_w	Weight after water exposure

α	Flake aspect ratio
α	Constant for Mark-Houwink equation
δ	Thickness
Δ	Difference or change
ε	Erosion number
$[\eta]$	Intrinsic viscosity
η_{rel}	Relative viscosity
η_{sp}	Specific viscosity
ρ	Density
ϕ	Flake volume fraction
$<\chi>$	Half thickness of polymer matrix

LIST OF SYMBOLS
(Continued)

subscript

0	Initial condition

LIST OF ACRONYMS

AA	Atomic absorption
ASTM	American Society for Testing and Materials
ATR-IR	Attenuated Total Reflectance Infrared Spectroscopy
AVG	Average
AWGC	Apatite wollastonite glass ceramic
BCP	Biphasic calcium phosphates
Bis-GMA	Bisphenol-α-glycidyl methacrylate
BMP	Bone morphogenic protein
C	Carbon
CAS No.	Chemical Abstract Number
CC	Calcium carbonate
CDHA	Calcium deficient hydroxyapatite
CF	Carbon fibers
c-HA	Calcined hydroxyapatite
CM	Compression molded
CR	Silicone rubber
CS	Calcium silicate
DSC	Differential scanning calorimetry
DW	Distilled water
EDX	Energy dispersive X-ray
EXT	Extruded

LIST OF ACRONYMS
(Continued)

FTIR	Fourier Transform Infrared Spectroscopy
GBR	Guided bone regeneration membrane
GF	Glass fibers
HA	Hydroxyapatite
HAPEX™	Hydroxyapatite polyethylene composite
HDPE	High density polyethelyne
IGF	Insulin growth factor
IV	Intrinsic viscosity
KF	Kevlar fibers
LCP	Liquid crystalline polymer
MFI	Melt flow index
MSC	Marrow stromal cells
MW	Molecular weight
OCP	Octacalcium phosphate
PBS	Phosphate buffer saline
PC	Polycarbonate
PCL	Polycaprolactone
PE	Polyethylene
PEA	Polyethylacrylate
PEEK	Polyetheretherketone
PELA	Poly(ethylene glycol-co-lactic acid)

LIST OF ACRONYMS
(Continued)

PET	Poly(ethylene terephthalate)
PGA	Polyglycolic acid
PHB	Polyhydroxybutyrate
PHEMA	Poly(2-hydroxyethyl methacrylate)
PLA	Polylactic acid
PLDLA	Poly(L-DL-lactide)
PLGA	Poly(lactic-co-glycolic) acid
PLLA	Poly(L-lactic) acid
PMMA	Polymethylmethacrylate
PP	Polypropylene
PST	Poly(1,4-butylene adipate-co-1,4-butylene succinate)
PSU	Polysulfone
PTFE	Polytetrafluoroethylene
PU	Polyurethane
SBF	Simulated body fluid
SCORIM®	Shear controlled orientation injection molding
SEM	Scanning electron microscopy
SEVA-C	Blends of starch with ethylene vinyl alcohol
TCP	Tricalcium phosphate
TEM	Transmission electron microscopy
TTCP	Tetracalcium phosphate

LIST OF ACRONYMS
(Continued)

u-HA	Uncalcined hydroxyapatite
UHMWPE	Ultra-high-molecular weight polyethylene
UV-Vis	Ultraviolet-visible
XRD	X-ray diffraction

CHAPTER 1

INTRODUCTION

1.1 General

According to data reported by the American Academy of Orthopedic Surgeons, each year the need for biomaterials supporting bone growth and regeneration is constantly increasing (American Academy of Orthopedic Surgeons website). There are more than six and a half million cases of bone fracture in the United States, where 15% of the cases are difficult to heal. Over one million orthopedic operations involving bone repair, disease and injury are performed annually in the United States. Although, orthopedic prostheses using bioinert materials have fifteen-year survivability of 75-85%, the demand for greater than thirty-year survivability increases along with the percentage of ageing population (Hench, 1998). Specifically, with life expectancy of more than 80 years, many more patients need prostheses and the quality of bone of the patients deteriorates with age. In order to satisfy this growing demand, research shifts to solutions that deal with regeneration rather than replacement of tissues. Taking into account the dental applications as well as the craniofacial operations performed annually, it is understandable why researchers study systems that can promote bone regeneration and try constantly to find even more improved and precise solutions through the principles of tissue engineering.

The current methodologies used for bone regeneration make use of autografts, allografts and xenografts. When autografts are used, the bone tissue is harvested from and implanted into the same patient. Autografts have a success rate of 80 to 90% and they are considered the gold standard of bone grafts since there is a guaranteed

biocompatibility and no risk of transmitting a disease. In addition, the harvested tissue is biologically intact, possessing the cells, proteins and factors that are necessary for proper healing (Laurencin and Khan, 2006).

In the case of allografts, the bone tissue is harvested from another human body (usually cadavers), processed to minimize potential disease transmission and bio-incompatibility and then implanted into the patient. Despite all the precautions to minimize the immunogenic responses between donor and recipient, allografts are still in risk of disease transmission, and recently (November 2001) they have been implicated to transmit a disease in a patient undergoing knee surgery (Laurencin and Khan, 2006).

Alternatively, in xenografts, transplant of bone tissue takes place from one species to the other (e.g. from one animal to a different animal). However, as mentioned above, all these techniques have certain limitations due to the limited donor supply (there are constraints of the amount of tissue that can be harvested from the site), donor site morbidity including infection, pain, possible mechanical weakening of the donor site and genetic differences along with anatomical and structural differences and high levels of resoption during healing (Wei and Ma, 2006, Wang, 2003, and Leonor et al. 2005).

It is evident that common grafting procedures are not adequate for the current clinical demand. For this reason, researchers are trying to improve these techniques with the help of tissue engineering principles and strategies. An important statement that has provided the foundation for various clinical applications regarding skeletal disorders is Wolff's law that states: "Every change in the form and function of bone or of its function alone is followed by certain definite changes in the bone internal architecture, and equally definite alteration in its external conformation, in accordance with mathematical laws"

(Sikavitsas et al. 2001). Taking all the aforementioned into account, alternative routes that have been proposed and used for bone fixation and regeneration have focused in materials such as metals and ceramics (Wang, 2003). Metals used for internal fixation of fractured bones, although provide the strength and toughness required for load-bearing parts of the body (Wang, 2003), face the biggest disadvantage of second surgery that will be eventually required to remove the corroded material over time. In addition, they demonstrate poor overall integration with the tissue at the site of the implantation, along with infection. Furthermore, metals are too stiff which results in "stress-shielding" induction (Leonor et al. 2005). Specifically, when a stiffer material is placed into a bone, the bone will be subjected to reduced mechanical stresses that will lead to bone resorption according to Wolff's law (Murugan and Ramakrishna, 2005). A typical stress-strain relationship for different biomaterials (abbreviations can be found in the beginning of this thesis) used as bone implants is illustrated in Figure 1.1 in comparison with human bone. It is of great importance to match the stiffness of the implant with that of the host tissue to avoid the stress-shielding effects (Murugan and Ramakrishna, 2005).

On the other hand, many ceramics, although ideal candidates due to their bioactivity, exhibit drawbacks due to lower tensile strength and elasticity, and also brittleness and limited use in sites of significant torsion, bending or shear stress (Leonor et al. 2005). To further improve on these drawbacks, synthetic polymers that are considered biocompatible have been developed and used to correct bone fixation problems. Since polymers alone have not been reported to be bioactive (cannot form a bond with the tissue) and since it is also well known that natural bone is a collagen/hydroxyapatite composite researchers were prompted to investigate composites

of bioactive ceramics in polymer matrices (Chouzouri and Xanthos, 2005). Such materials are the focus of this dissertation. Additionally, the absence of corrosion, patient discomfort and severe allergic reactions are major advantages for polymer composite development (Leonor et al. 2005). Table 1.1 presents several biomaterials, both bioinert and bioactive, used for bone grafting along with their advantages, disadvantages and their intended applications.

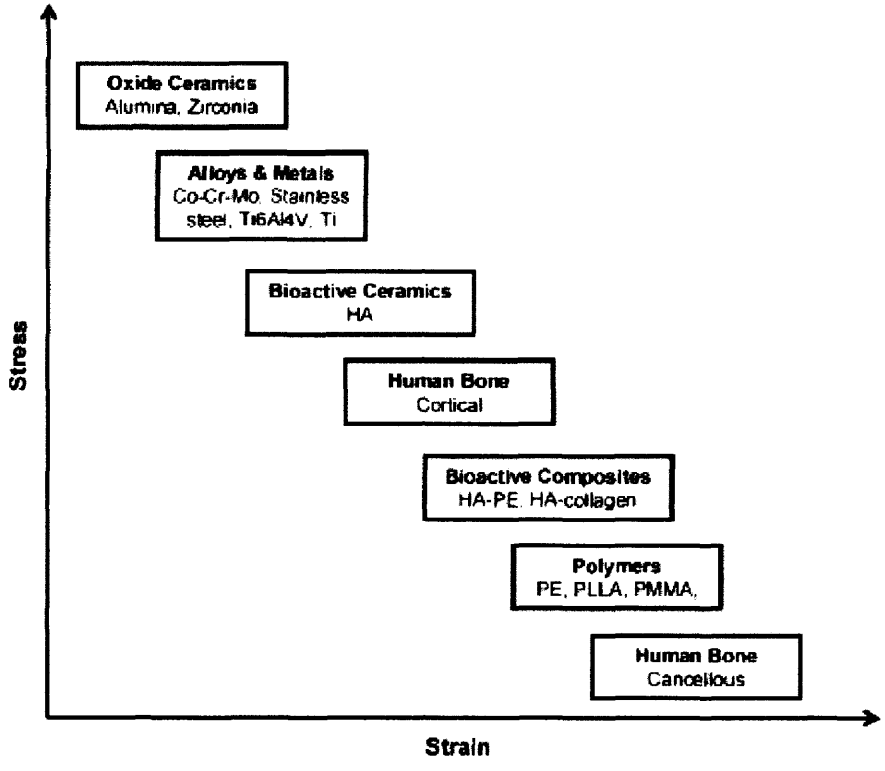

Figure 1.1 A typical stress-strain relationship of a variety of bone implants.
(Source: Murugan and Ramakrishna, 2005)

Table 1.1 Classification of Biomaterials for Bone Grafting

Biomaterials	Advantages[b]	Disadvantages	Applications	Examples
Metal and alloy	Too strong, tough, ductile	Dense, may corrode	Bone plates, load-bearing bone implants, dental arch wire, and dental brackets	Titanium, stainless steel, Co–Cr alloys, and Ti alloys
Ceramic	Bioinert	Brittle, poor tensile, low toughness, lack of resilience	Hip joints and load-bearing bone implants	Alumina, zirconia
	Bioactive Bioresorbable High resistance to wear		Bone filler, coatings on bio-implants, orbital implant, alveolar ridge augmentation, maxillofacial reconstruction, and bone tissue engineering	HA, bioglass TCP
Polymer	Flexible, resilient, surface modifiable, selection of chemical functional groups	Not strong, toxic of a few degraded products	Bone tissue scaffolds, bone screws, pins, bone plates, bone and dental filler, and bone drug delivery	Collagen, gelatin, chitosan, alginate, PLA, PGA, PLGA, PCL, PMMA, PE
Composite	Strong, design flexibility, enhanced mechanical reliability than monolithic	Properties might be varied with respect to fabrication methodology	Bone graft substitutes, middle ear implants, bone tissue scaffolds, guided bone regenerative membranes, and bone drug delivery	HA/collagen, HA/gelatin, HA/chitosan, HA/alginate, HA/PLGA, HA/PLLA, HA/PE
Nanocomposite	Larger surface area, high surface reactivity, relatively strong interfacial-bonding, design flexibility, enhanced mechanical reliability than monolithic and/or microcomposite	No optimized technique for material processing	Major areas of orthopedics, tissue engineering, and drug delivery	Nano-HA/collagen, Nano-HA/gelatin, Nano-HA/chitosan, Nano-HA/PLLA

(Source: Murugan and Ramakrishna, 2005)

In order to achieve a successful bone tissue engineering implant Laurencin and Khan (2006) suggested that one should look to autografts to form a list of requirements, which are described below:

- Biocompatibility: the lack of immunogenic response
- Osteoconductivity: the quality of a structure that is interconnected and permits new cells to attach, proliferate and migrate. This structure also allows nutrient/waste exchange and new vessel penetration.
- Osteoinductivity: the ability to posses the necessary proteins and growth factors that can induce mesenchymal stem cells and other osteoprogenitor cells toward the osteoblast lineage. This is a very important parameter, especially when the defect is of critical size and spontaneous healing cannot be achieved.
- Osteogenicity: the osteoblasts at the site of the new bone formation are able to produce minerals to calcify the collagen matrix that will form the substrate for the new bone.

- Osteointegrity: the bone formation that takes place between the newly formed mineralized tissue and the implant material.
- Mechanical match: the autografts have similar mechanical properties to the surrounding tissue, in order to prevent stress shielding and bone resorption.

Table 1.2 shows the parameters for a successful scaffold (same parameters could be taken into account for any biomaterial used for bone regeneration in tissue engineering) as indicated by autografts.

Table 1.2 Parameters for a Successful Scaffold as Indicated by Autografts

Autograft Quality	Polymers	Ceramics	Composite
Biocompatibility	Yes	Yes	Yes
Osteoconductivity	Yes	Yes	Yes
Osteoinductivity	No (but can add factors)	No (but can add factors)	Yes (with delivered factors)
Osteogenicity	No	Yes	Yes
Osteointegrity	No	Yes	Yes
Mechanical Match	Yes	No	Yes

Neither polymers nor ceramics can accomplish all parameters alone, but this can be achieved when formed into a composite.

(Source: Laurencin and Khan, 2006)

The aforementioned characteristics are very important for a bone tissue engineering biomaterial. There is not one biomaterial that can satisfy all the requirements and for that reason researchers try to combine materials into a composite structure (Laurencin and Khan, 2006).

Following a similar concept for achieving a successful biomaterial for tissue regeneration, Seal et al. (2001) illustrate in Figure 1.2 how some biological and medical requirements of a material should be integrated.

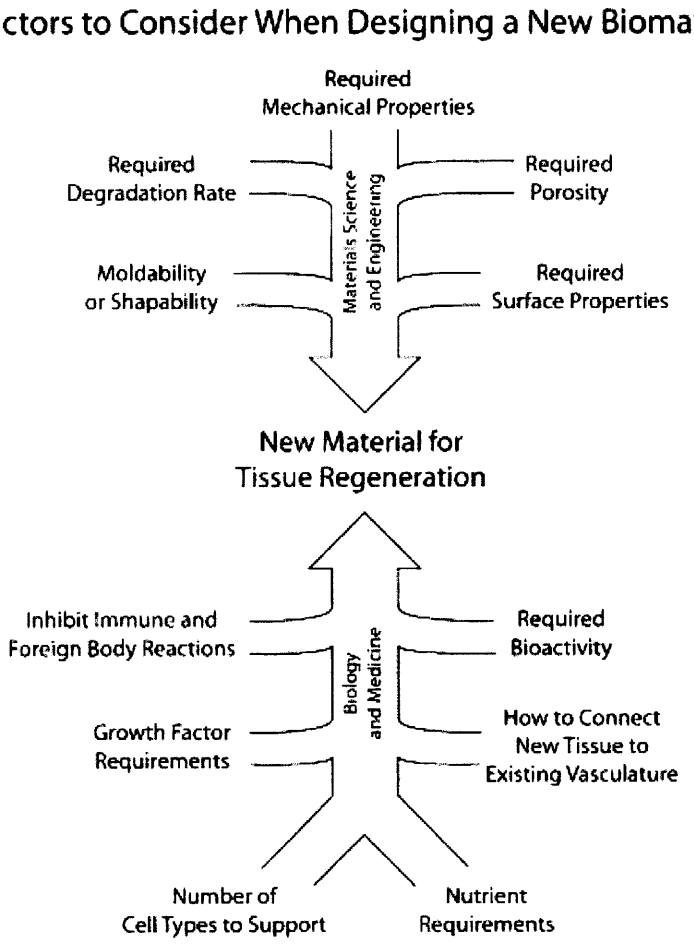

Figure 1.2 Illustration of how some biological and engineering material properties should be integrated in order to achieve successful tissue regeneration biomaterials.
(Source: Seal et al. 2001)

The idea of using composite materials that could combine all the desired properties and characteristics for a successful tissue engineering biomaterial, is not only derived from the parameters used in an autograph and the right medical and engineering properties, but also from the bone structure itself. Bone, as will be discussed in section 1.2, is a composite material consisting of an inorganic and organic phase with a complex structure and several levels of organization.

Over the past decades, several materials have been developed and used as biomaterials for bone regeneration. Figure 1.3 illustrates the evolution of biomaterials used in bone grafting. Abbreviations can be found in the beginning of the thesis.

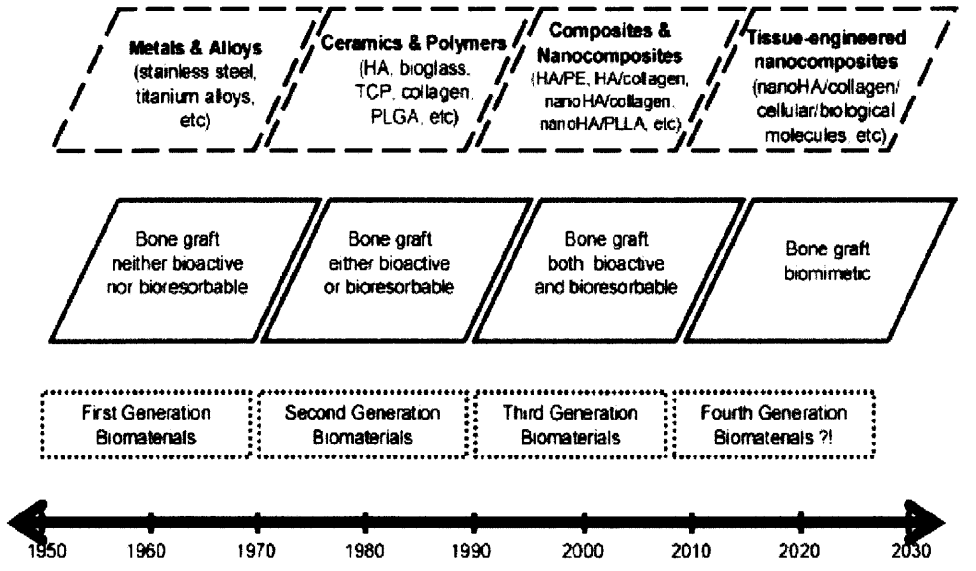

Figure 1.3 Evolution of biomaterials in bone grafting applications.
(Source: Murugan and Ramakrishna, 2005)

1.2 Human Bone

It is essential to understand the structure and organization levels of the human bone and all the biological templates involved, before developing a biomaterial for bone regeneration. Bone must perform multiple, but sometimes quite contrary, functions. It is required to have high strength, but low weight; support remodeling when stresses are applied, but not deform under them; have a certain porosity to allow oxygen and nutrients to reach the cells, but these pores should not result in fractures; and, finally, act as a reservoir for minerals, but not demineralize and hence weaken (Braun, 2003).

Bone is a natural composite material whose major components are type I collagen, calcium phosphate minerals (hydroxyapatite is the predominant one), carbonate substituted apatite and water (Lutton et al. 2001, Chouzouri and Xanthos 2005). Bone also has non-collagenous proteins, lipids, vascular elements and cells in its composition. An overall composition of the bone can be seen in Table 1.3 (Murugan and Ramakrishna, 2005). The mineralized collagen fibril is the basic building block of the bone family of materials. It is composed of fibrous protein collagen in a structural form present also in skin, tendon, and a variety of soft tissues (Weiner and Wagner, 1998). The collagen represents the main component of a three dimensional matrix into which the mineral forms to strengthen the bone. The mineral is dahllite (carbonated apatite with structure $Ca_5(PO_4, CO_3)_3(OH)$) (Weiner and Wagner, 1998). Bone mineral shows a Ca:P ratio ranging from 1.3:1 to 1.9:1. Bone mineralization involves nucleation until a critical size-nucleus is formed. Crystal growth occurs as ions or clusters are added to the critical nucleus. Nucleation may occur again due an increase in ion concentration, increase in temperature or change in solution composition. Heterogeneous nucleation occurs on already formed surfaces facilitated by proteins and lipids. Other growth proteins, except collagen, facilitate mineral formation by nucleation/regulation of the process (Boskey, 2005).

Table 1.3 Bone Composition

Inorganic phase	wt%	Organic phase	wt%
Hydroxyapatite	~60	Collagen	~20
Carbonate	~4	Water	~9
Citrate	~0.9	Non-collagenous proteins (osteocalcin, osteonectin, osteopontin, thrombospondin, morphogenetic proteins, sialoprotein, serum proteins)	~3
Sodium	~0.7		
Magnesium	~0.5		
Other traces: Cl^-, F^-, K^- Sr^{2-}, Ph^{2-}, Zn^{2-}, Cu^{2-}, Fe^{2-}		Other traces: Polysaccharides, lipids, cytokines Primary bone cells: osteoblasts, osteocytes, osteoclasts.	

(Source : Murugan and Ramakrishna, 2005)

The proportions of all the bone major components can vary considerably between bone family members. In addition, the manner in which the building blocks are organized into highly ordered structures can also vary, differentiating the members of the bone family (Weiner and Wagner, 1998). The organization of the bone can be further complicated, since some of the materials are composed of two different organizational patterns, and in return, the whole structure may be folded into even larger substructures. Therefore, there is no term such as bone structure, but rather the hierarchical levels of organization in different bone families (Weiner and Wagner, 1998). The seven hierarchical levels of organization of the bone family of materials according to Weiner and Wagner (1998) can be seen in Figure 1.4.

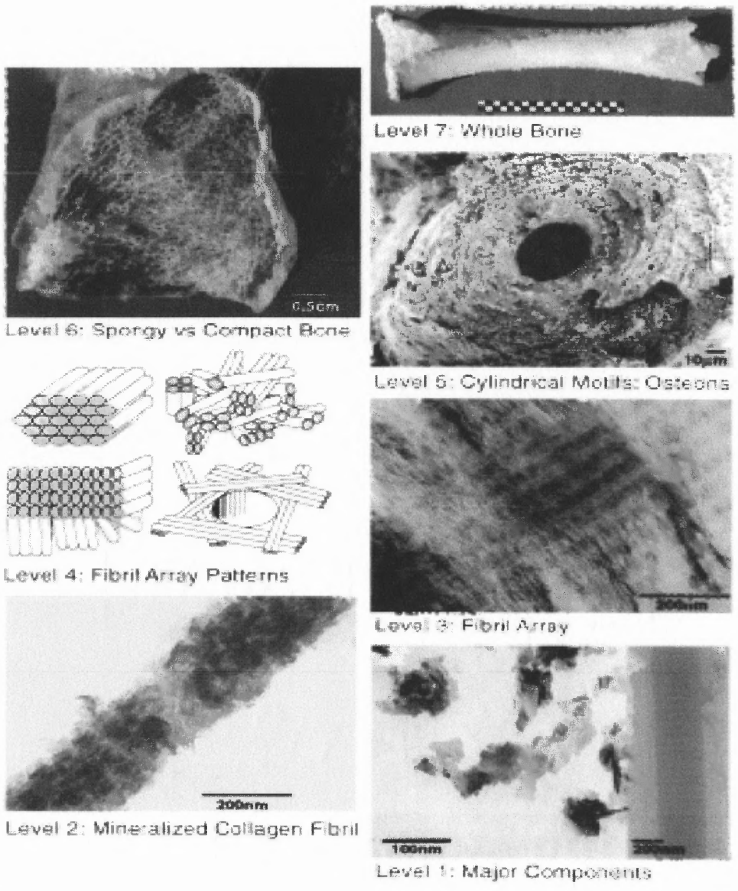

Figure 1.4 The seven hierarchical levels of organization of the bone family of materials according to Weiner and Wagner (1998). Level 1: TEM micrographs of individual mineral crystals from human bone (left side) and a part of an unmineralized and unstained collagen fibril from turkey tendon observed in vitreous ice. Level 2: TEM micrograph of a mineralized collagen fibril from turkey tendon. Level 3: TEM of a thin section of mineralized turkey tendon composed of multiple fibrils. Level 4: Four fibril array organization patterns found in the bone family of materials. Level 5: SEM micrographs of a single human bone osteon. Level 6: Light micrograph of a fractured section through a 5500 year old fossilized human femur. Level 7: Whole bovine bone (scale: 10 cm).
(Source: Weiner and Wagner, 1998)

In view of the fact that bone has such a complex structure with several levels of organization, it is understandable why mimicking a bone structure is so challenging. In developing bone substitutes at a microscopic level, two structural levels are considered. The first one is a bone apatite reinforced collagen that forms lamellae at the nm to μm

scale and the second one is the osteon reinforced interstitial bone at the μm to mm scale. Figure 1.5 represents a form of structural organization of the bone in the human body (Chouzouri and Xanthos 2005, Wang, 2003).

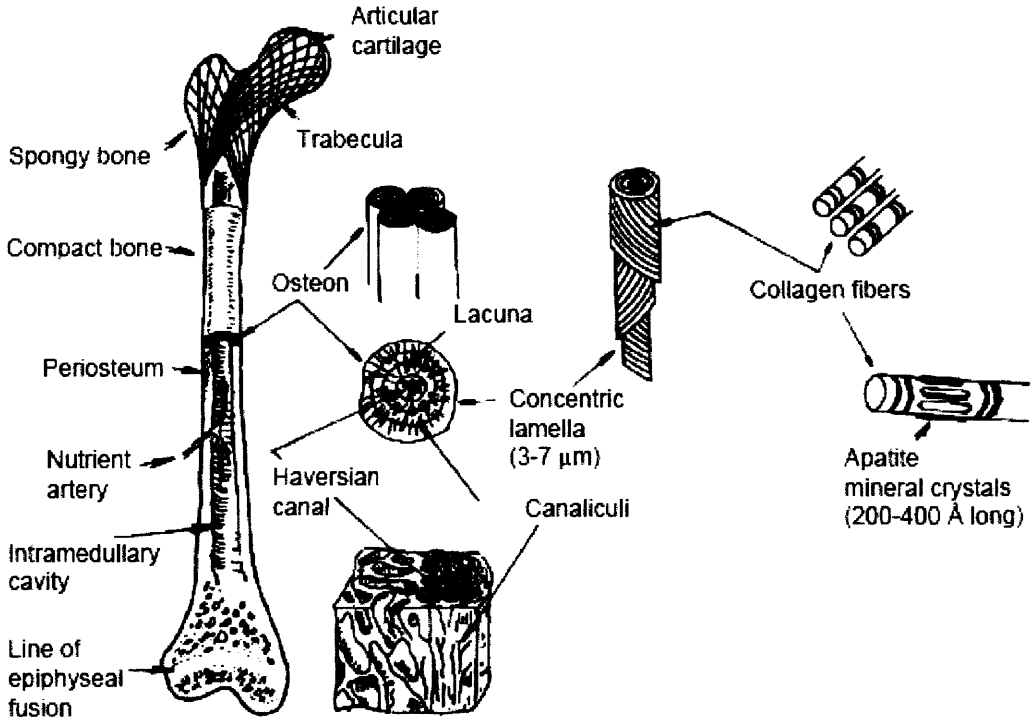

Figure 1.5 Structural organization of the bone in the body.
(Source: Wang 2003)

At the microscopic level, bone has two forms: woven and lamellar. Woven or primary bone is immature bone characterized by coarse fiber arrangement with no orientation and varying mineral content – isotropic properties. It is resorbed by one year of age. Lamellar bone begins forming after 1 month of birth and by age 4 most normal bone is lamellar. It is highly organized and anisotropic, having different mechanical behavior depending on the orientation of applied forces (Doll, 2005).

Bone tissue as shown in Figure 1.5 is arranged in two architectural forms, trabecular, otherwise called cancellous or spongy (around 20% of the total skeleton) and cortical or compact form (the remaining 80% of the skeleton) (Salgado et al. 2005, Sikavitsas et al. 2001). The trabecular bone exhibits high porosity (in the range of 50-90%) and it is arranged as a honeycomb of branching bars, plates and rod called trabeculae. The cortical bone is almost solid (10% porosity). The compact bone functions mechanically in tension, compression and torsion, whereas the spongy bone functions mainly in compression. At the microstructural level, the structural unit that is repeated for compact bone is mostly of osteon or Haversian system. Haversian bone is the most complex type. Vascular channels are surrounded by lamellar bone in arrangements that are called osteons, oriented in the long axis (Doll, 2005). By contrast, the spongy bone contains no such osteon units, but it is made of an interconnected framework of trabeculae (Murugan and Ramakrishna, 2005). An outer bone sheath, called periosteum covers both cortical and cancellous bone (Sikavitsas et al. 2001). Basic types of bones are long, round, irregular-shaped and flat; they can be modeled as beams, columns, rods and cylinders, depending on their mechanical requirements and how are they loaded in vivo (Doll, 2005).

Bone is a brittle anisotropic material with low elongation at fracture (3-4%) whose properties may vary broadly via changes in preferred collagen fiber orientation. The amount of water present in the bone is also an important parameter for its mechanical behavior. Biomechanical properties of the bone are presented in Table 1.4 (Murugan and Ramakrishna, 2005). Specifically, tensile modulus and strength for a human long bone are reported as 17.4 GPa and 135 MPa, respectively, in the axial direction and much

lower in the radial direction: 11.7 GPa and 61.8 MPa , respectively (Xanthos 2005, Callister, 2003). Compressive strength, a property more relevant to actual use of the bone, is higher approaching 196 MPa and 135 MPa in the axial and transverse directions, respectively. Polymer composites for biomedical applications attempt to reach these high modulus/strength levels through the introduction of high volume loadings (as high as 45%) of reinforcing fibers or other fillers in a biocompatible matrix.

Table 1.4 Biomechanical Properties of the Bone

Properties	Measurements	
	Cortical bone	Cancellous bone
Young's modulus (GPa)	14–20	0.05–0.5
Tensile strength (MPa)	50–150	10–20
Compressive strength (MPa)	170–193	7–10
Fracture toughness (MPa $m^{1/2}$)	2–12	0.1
Strain to failure	1–3	5–7
Density (g/cm^3)	1.8–2.2	0.1–1.0
Apparent density (g/cm^3)	1.8–2.0	0.1–1.0
Surface/bone volume (mm^2/mm^3)	2.5	20
Total bone volume (mm^3)	1.4×10^6	0.35×10^6
Total internal surface	3.5×10^6	7.0×10^6

(Source: Murugan and Ramakrishna, 2005)

CHAPTER 2

COMPONENTS OF BIOCOMPOSITES FOR BONE REGENERATION – A REVIEW

2.1 General

In addition to increasing uses of polymer composites for biomedical applications, over the past decade, there is an increasing interest in the development of polymer matrix composites for bone regeneration materials. This interest was triggered by the desire to develop composite materials with the properties of the natural collagen / apatite composite. Polymer composites are mixtures of polymeric matrices with inorganic or organic fillers that have particular geometries (fibers, flakes, spheres, particulates) (Xanthos, 2005). The properties of a polymer composite are affected by the properties of the fillers, the composition, the interaction of components at the interface and the method of fabrication. A composite is designed to result in a combination of the best characteristics of each of its components and the minimum undesirable characteristics. Specifically, a biocomposite for bone regeneration applications should provide distinctive mechanical performance, analogous to the bone one, as well as biocompatibility and biological active response known as bioactivity (Chouzouri and Xanthos, 2005). According to Hench (1996), bioactivity is the ability of a material to elicit a specific biological response at its interface with a living tissue, which results in the formation of a bond between the tissue and the material. Bioactivity in polymer composites is achieved through the addition of specific inorganic additives (fillers) whose bioactivity is independent of the presence of the biocompatible polymer matrix and as such can be used alone.

2.2 Classification of Fillers According to their Functions

Several ceramics, glasses, and glass-ceramics have been used to repair or replace musculoskeletal hard connective tissues. Materials for clinical use can be classified into three categories depending on the relative level of reactivity of an implant and, consequently, of the interfacial layer between the material and the tissue. Firstly, resorbable materials are designed to degrade slowly and replaced by the natural host tissue through a very thin interfacial layer. This is the optimal solution if the requirements of strength and short term performance can be met as the natural tissues can repair and gradually replace themselves throughout life (Hench, 1996, Davis, 2003). Tricalcium phosphates, calcium phosphate salts and calcium carbonate minerals are common bioresorbable ceramics. Secondly, inert and nearly inert materials are the ones where the fibrous tissue at the interface is very thin. In the case of devices implanted with a very tight mechanical fit and loaded in compression, then the implants are very successful. By contrast, when the interface is not chemically or biologically bonded and there is an interfacial movement, then the implant can deteriorate. Common examples are alumina and zirconia. Lastly, bioactive materials are an intermediate between resorbable and nearly inert materials, since they can elicit a specific biological response at the interface, which will lead in the formation of a bond between the tissue and the biomaterial. Typical examples are hydroxyapatite, bioactive glasses and bioactive glass ceramics. Table 2.1 summarizes the most significant ceramics that have been reported to show bioactivity *in vitro* and in most cases *in vivo* (Chouzouri and Xanthos, 2005).

Table 2.1 Bioactive Fillers Used in Tissue Engineering Applications

Chemical Name	Chemical Formula
Hydroxyapatite	$Ca_{10}(PO_4)_6(OH)_2$
Dicalcium Phosphate	$CaHPO_4 \cdot 2H_2O$
β-tricalcium phosphate	$Ca_3(PO_4)_2$
Tetracalcium Phosphate	$Ca_4P_2O_9$
Calcium Carbonate	$CaCO_3$
Wollastonite	$CaSiO_3$
Bioactive Glasses	(see Table 2.5)
A-W Glass Ceramics	$Ca_{10}(PO_4)_6(OH,F)_2 - CaSiO_3$ in $MgO\text{-}CaO\text{-}SiO_2$ matrix

(Source: Chouzouri and Xanthos, 2005)

The level of bioactivity of a material is related to the time taken for more than 50% of the interface to bond to bone ($t_{0.5bb}$), and can be expressed by the following equation:

$$\text{Bioactivity Index, } I_b = 100/ t_{0.5bb} \tag{1.1}$$

Materials with an I_b value greater than 8 (class A) will bond to both soft and hard tissue. Materials with an I_b value less than 8, but greater than 0 (class B) will bond only to hard tissue (Hench, 1996). Table 2.2 includes several implant materials along with their bioactivity index (Hench, 1998).

Table 2.2 Index of Bioactivity of Implant Materials

Biomaterial	I_B	Class of bioactivity	Bone bonding	Soft tissue bonding
4555 bioactive glass	12.5	A	Yes	Yes
5254.6 bioactive glass	10.5	A	Yes	Yes
A/W bioactive glass ceramic	6.0	B	Yes	No
Ceravital glass ceramic	5.6	B	Yes	No
5554.3 bioactive glass	3.7	B	Yes	No
Hydroxyapatite ceramic	3.1	B	Yes	No
Ceravital K6X, K6X'	2.3	B	Yes	No
Alumina	0	0	No	No

(Source: Hench, 1998)

The success of the fillers depends on the type of attachment to connective tissue. The mechanism of tissue attachment is related to the type of tissue response at the biomaterial – tissue interface. There are four different tissue attachment mechanisms for bioceramic implants as shown in Table 2.3 (Hench, 1996, Davis, 2003) depending on type and their porosity. In Figures 2.1 and 2.2, a comparison of the relative chemical activities and a time dependence of formation of bone bonding at the ceramic implant interface can be observed, respectively. In Figure 2.1 the letters refer to class of bioactivity as shown in Table 2.2. In Figure 2.3, a comparison of interfacial thickness of reaction layers for different types of ceramic implants is included. These Tables and Figures facilitate the classification of different types of biomaterials used.

Table 2.3 Tissue Attachment Mechanisms for Bioceramic Implants

Type of attachment	Example
Dense, nonporous, nearly inert ceramics attached by bone growth into surface irregularities by cementing the device into the tissues, by press-fitting into a defect, or attachment via a sewing ring (morphological fixation)	Al_2O_3 (single-crystal and polycrystalline) LTI (low-temperature isotropic carbon)
For porous inert implants, bone ingrowth occurs, which mechanically attaches the bone to the materials (biological fixation)	Al_2O_3 (polycrystalline) Hydroxylapatite-coated porous metals
Dense, nonporous, surface-reactive ceramics, glasses, and glass-ceramics attach directly by chemical bonding with the bone (bioactive fixation)	Bioactive glasses Bioactive glass-ceramics Hydroxylapatite
Dense, nonporous (or porous), resorbable ceramics are designed to be slowly replaced by bone	Calcium sulfate (plaster of paris) Tricalcium phosphate Calcium phosphate salts

(Source: Hench, 1998)

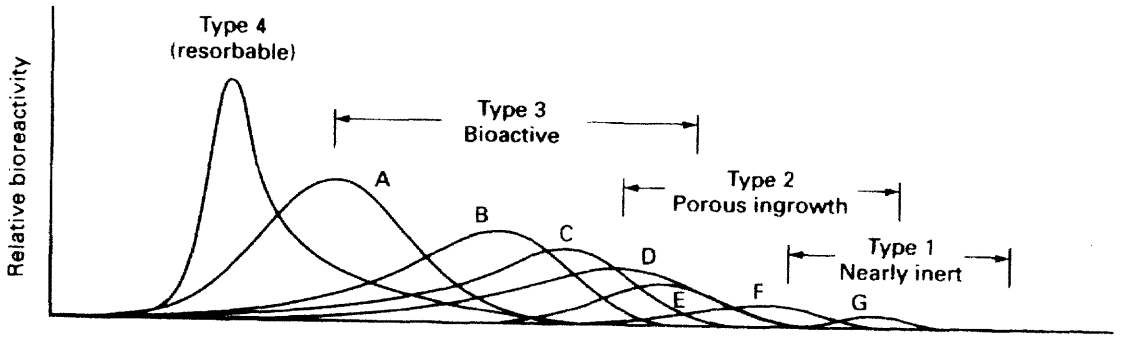

Figure 2.1 Relative rates of bioactivity for various ceramic implants.
(Source: Hench 1998.)

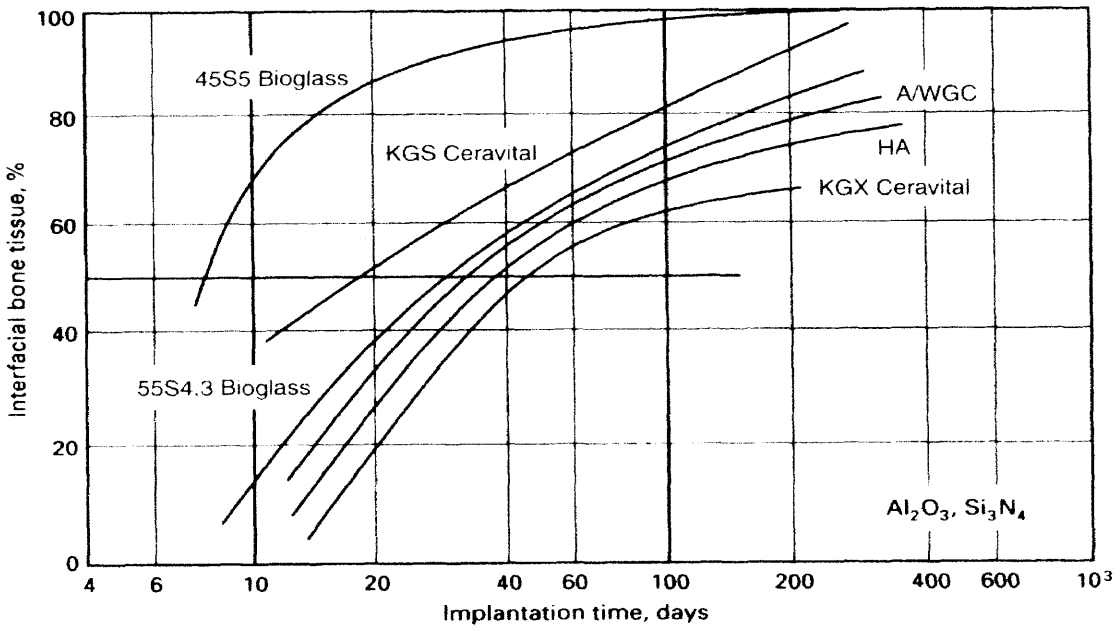

Figure 2.2 Time dependence of formation of bone bonding at an implant interface.
(Source: Hench, 1998)

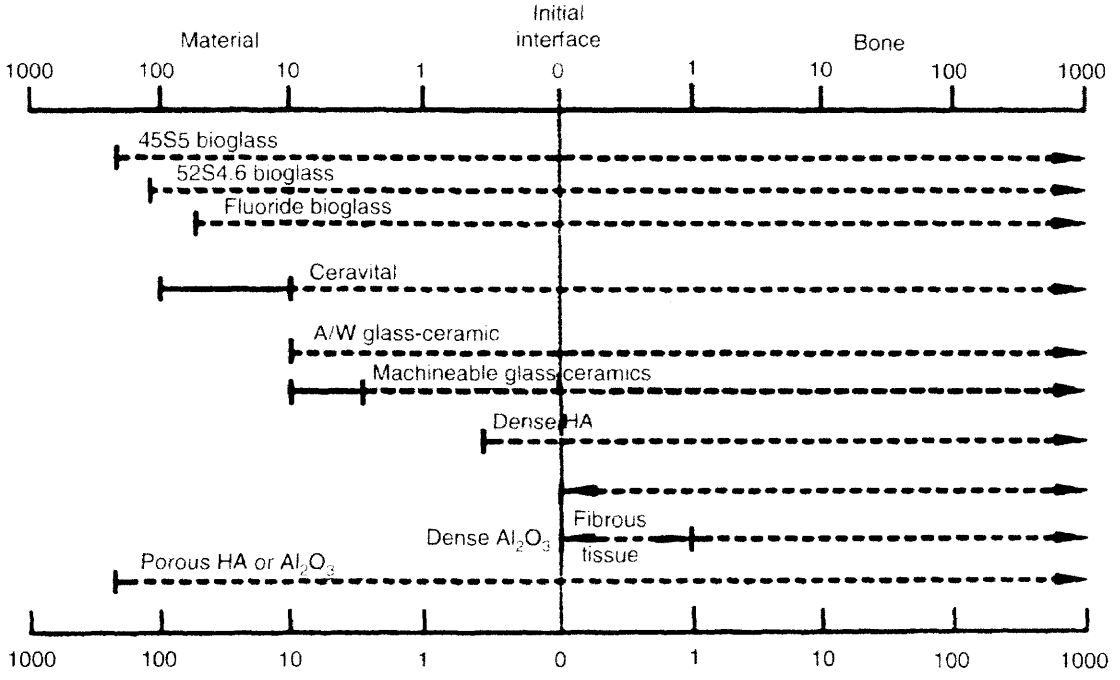

Figure 2.3 Comparison of interfacial thickness (μm) of reaction layers of bioactive implants of fibrous tissue of inactive bioceramics in bone.
(Source: Hench, 1996)

2.3 Types of Bioactive Fillers

2.3.1 Calcium Phosphates

Among bioactive materials, HA is considered to be both biocompatible and osteoconductive, exhibiting only an extracellular response leading to bone growth at the bone –filler interface (Wang, 2003). By contrast, osteoproductive fillers such as bioactive glasses elicit both an extra- and intra-cellular response at the interface (Hench website). None of these fillers are osteoinductive, since the presence of bone morphogenic proteins, BMP, and/or other growth factors (e.g. insulin growth factor IGF-I) are required. Researchers have used several bioceramics along with osteoinductive materials in order to promote faster bone regeneration. One of the main reasons that hydroxyapatite (HA) has been investigated as a bioactive filler is its similarity with the biological hydroxyapatite in impure calcium phosphate form found in the human bone and teeth. HA has a Ca:P ratio of 10:6 and its chemical formula is $Ca_{10}(PO_4)_6(OH)_2$. The biological HA, in addition, contains magnesium, sodium, potassium, and a poorly crystallized carbonate containing apatite phase as well as a second amorphous calcium phosphate phase (Ashman and Gross, 2000).

Different phases of calcium phosphate ceramics have also been used in tissue engineering depending on the application. These differences in forms and phases, along with variations in morphology and stoichiometry introduced by the complexities of different modifications during processing, add to the complexity of calcium phosphate systems (Kumta et al. 2005). Calcium phosphates have many crystallographic features that are similar to the ones of the human bone. Table 2.4 presents the different forms of calcium phosphate along with their molecular formula and their corresponding

Calcium/Phosphorous ratio (Laurencin and Khan, 2006). The stability of these ceramics depends on temperature and the presence of water. In the body ($T=37^0C$ and pH=7.2-7.4) calcium phosphates are converted to HA. At lower pH (< 4.2) dicalcium phosphate ($CaHPO_4 \cdot 2H_2O$) is the stable phase. At higher temperatures other phases of phosphate minerals, such as β-tricalcium phosphate ($Ca_3(PO_4)_2$), chemically similar to HA with Ca:P ratio of 3:2, and tetracalcium phosphate ($Ca_4P_2O_9$) are present. Tricalcium phosphate (TCP) is not a natural bone mineral component, although it can be partly converted to HA in the body according to the following reaction (Hench, 1996):

$$4\ Ca_3(PO_4)_2\ (solid) + 2\ H_2O \rightarrow Ca_{10}(PO_4)_6(OH)_2\ (surface) + 2\ Ca^{2+} + 2\ HPO_4^{2-}$$

TCP is an osteoconductive and resorbable material, with a resoption rate dependent on its chemical structure, porosity and particle size (Ashman and Gross, 2000).

Table 2.4 Different Forms of Calcium Phosphate, their Molecular Formula, and the Corresponding Ca/P Ratio

Calcium Phosphate Form	Molecular Formula	Calcium/Phosphorus Ratio
Tricalcium phosphate (α and β) (TCP)	$Ca_3(PO_4)_2$	1.5
Hydroxyapatite (HA)	$Ca_{10}(PO_4)_6(OH)_2$	1.67
Calcium-deficient hydroxyapatite (CDHA)	$Ca_9(HPO_4)(PO_4)_5(OH)$	1.5
Tetracalcium phosphate (TTCP)	$Ca_4(PO_4)_2O$	2.0
Octacalcium phosphate (OCP)	$Ca_8(HPO_4)_2(PO_4)_4 \cdot 5H_2O$	1.33

(Source: Laurencin and Khan, 2006)

All calcium phosphate ceramics degrade at increasing rate in the following order: α-TCP> β-TCP> HA. Their degradation rate increases as surface area and ionic substitution of CO_3^{2-}, Mg^{2+} and Sr^{2+} in HA increase, and crystallinity, crystal perfection and crystal and grain size decrease.

Biphasic calcium phosphates (BCP: HA/TCP) appear to be even more bioactive and efficient than HA and TCP alone, for the repair of several orthopedic and maxillofacial applications (Toqeut et al. 1999). The degradation rate of BCP can be adapted to the one needed for sufficient bone ingrowth by determining the optimum balance of the HA and TCP phases (Bagot D'Arc and Daculsi, 2003). HA is more similar to natural bone tissue apatite and more stable than TCP. Thus, the incorporation of TCP into BCP ceramics can control the rate of degradation needed for adequate new bone formation (Bagot D'Arc and Daculsi, 2003, Fernedez et al. 1999, Daculsi, 1999). As the material dissolves gradually in the body, it releases calcium and phosphorous ions into the biological medium that consequently transform into carbonated hydroxyapatite that is similar to the biological apatite needed for bone growth. This osteocoalescence process contributes to the strong bone formation at the bone/material interface (Daculsi, 1999, Daculsi et al. 2003).

BCP is obtained by sintering a synthetic or biological calcium deficient apatite at temperatures higher than 700^0C. The degree of calcium deficiency (Ca/P molar ratio less than 1.67) depends strongly on the preparation method used. BCP can be produced by precipitation, hydrolysis or mechanical mixing. The calcium deficiency also depends on the reaction pH, the temperature in the preparation of unsintered apatite and the morphological characteristics. The calcium deficiency affects the HA/TCP ratio in the BCP. This ratio determines the ceramic reactivity, specifically the lower the ratio the higher the reactivity (Daculsi et al. 2003, Manjubala et al. 2001).

BCP ceramics have proven to be useful for clinical applications involving small bone defects or regions that have large contact with bone (Toquet et al. 1999). However,

they exhibit no osteoinductive properties and as a result, cannot be used on their own for the reconstruction and repair of large bone defects. For this reason it is proposed that BCP ceramics should be used along with osteogenic cells to provide solutions for long bone regeneration (Toquet et al. 1999, Bagot D'Arc and Daculsi, 2003, Livingston et al. 2003). When osteogenic cells will be implanted in a BCP ceramic scaffold, the rate of bone formation will increase and as a result, rapid restoration of the long bone defect will take place (Livingston et al. 2003).

2.3.2 Calcium Carbonate

Calcium carbonate ($CaCO_3$) minerals, is another class of bioactive materials that can exist in the forms of vaterite, aragonite and calcite. All forms have the same chemistry, but different crystal structure and symmetries. Aragonite is orthorhombic, vaterite is hexagonal and calcite is trigonal. Calcium carbonate in the form of aragonite (>98% $CaCO_3$) is the natural coral. It is a porous, slowly resorbing material with an average pore size of 150μm and very good interconnectivity. When it is necessary to be used for periodontal osseous defects it can be provided with average particle size of 300-400μm. Calcium carbonate's major advantage is that when other bioactive materials such as HA have to go through the formation of carbonate containing structures, calcium carbonate can pass over that step; consequently, this can result to a more rapid bone ingrowth (Ashman and Gross, 2000).

2.3.3 Silicates

Wollastonite, which is a form of calcium silicate (CS), has also been shown to be bioactive and biocompatible. Liu et al. (2004), used commercially available wollastonite to coat Ti-6Al-4V substrates through a plasma-sprayed method. When the substrates were immersed in simulated body fluids (SBF), an apatite layer was formed through surface reactions. Various forms of calcium silicates such as pseudowollastonite ($\alpha - CaSiO_3$) (Sahai and Anseau, 2005, De Aza et al. 2000) tricalcium silicate (Ca_3SiO_5) (Zhao et al. 2005), β-dicalcium silicate (Cheng, 2006), β-wollastonite (β-$CaSiO_3$) (Wan, 2005, Li and Chang, 2005) and commercially available mineral wollastonite (Risbud, 2001) have been shown to exhibit bioactivity.

Special compositions of glasses appear to have the ability of developing a mechanically strong bond to the bone. The so-called bioactive glasses contain SiO_2, Na_2O, CaO and P_2O_5 in specific ratios (Chouzouri and Xanthos, 2005, Hench, 1996, Ashman and Gross, 2000, Hench, 1988). Bioactive glasses differ from the traditional soda-lime-silica glasses, as they need to contain less than 60 mol% SiO_2, high Na_2O and CaO amounts and also a high CaO/ P_2O_5 ratio. As a result, when these glasses are exposed to physiological liquids they can become highly reactive. This feature distinguishes the bioactive glasses from bioactive ceramics, such as HA. When the latter contacts physiological fluids both its composition and physical state remain unchanged, in contrast with the bioactive glass that undergoes a chemical transformation. A slow exchange of ions between the glass and the fluid takes place (Krajewski and Ravaglioli, 2002) resulting in the formation of a biologically active carbonated HA layer that provides bonding to the bone and also to soft connective tissues. Silicon and calcium

slowly dissolved from the glasses activate families of genes in old bone cells that then form new bone cells (Hench website).

Most of the bioactive glasses are based on bioglass designated as 45S5, which implies 45 wt% SiO_2 and CaO/ P_2O_5 molar ratio of 5:1. Glasses with lower CaO/ P_2O_5 ratio will not bond to the bone. Nevertheless, based on modifications of the 45S5 bioglass a series of other bioactive glasses have been investigated by substituting, for instance, 5-15 wt% B_2O_3 for SiO_2 or 12.5 wt% CaF_2 for CaO (Chouzouri and Xanthos, 2005, Hench. 1996, Ashman and Gross, 2000, Krajewski and Ravaglioli, 2002, Fujibayashi et al. 2003, Brink et al. 1997). Table 2.5 provides typical compositions of bioactive glasses (Hench, 1996).

Table 2.5 Bioactive Glasses and their Composition in Weight Percent

Constituent	45S5 Bioglass	45S5F Bioglass	45S5.4F Bioglass	40S5B5 Bioglass	52S4.6 Bioglass	55S4.3 Bioglass
SiO_2	45	45	45	40	52	55
P_2O_5	6	6	6	6	6	6
CaO	24.5	12.25	14.7	24.5	21	19.5
$Ca(PO_3)_2$	...	...	...	...	...	...
CaF_2	...	12.25	9.8	...	...	...
MgO	...	...	...	...	...	...
MgF_2	...	...	...	...	...	...
Na_2O	24.5	24.5	24.5	24.5	21	19.5
K_2O	...	...	...	...	...	...
Al_2O_3	...	...	...	...	...	...
B_2O_3	...	...	...	5	...	...
Ta_2O_5/TiO_2	...	...	...	...	...	...
Structure	Glass	Glass	Glass	Glass	Glass	...

(Source: Hench, 1996)

2.3.4 Complex Glass Ceramics

A-W glass ceramics (AWGC) consist of crystalline fluoroxydroxyapatite [$Ca_{10}(PO_4)_6(OH)F_2$)] and wollastonite ($CaSiO_3$) in a MgO-CaO- SiO_2 glassy matrix. Nominal composition by weight is: MgO, 4.6; CaO, 44.7; SiO_2, 34.0; P_2O_5, 16.2; CaF_2, 0.5, (Shinzato et al. 2000). They have been used as bone replacements due to their high bioactivity and also to their ability of instantaneously bonding to living tissue without forming a fibrous layer. The mechanical properties of AWGCs are better than those of both bioactive glass and HA (Hench 1996, Shinzato et al. 2000, Yamamuro et al. 1998, Juhasz et al. 2004). In addition, AWGCs appear to have long-term mechanical stability i*n vivo*, as they chemically bond with the living bone 8-12 weeks after implantation (Yamamuro et al. 1998, Juhasz et al. 2004). According to Hench (1996), additions of Al_2O_3 or TiO_2 to the AWGC may inhibit bone bonding. Table 2.6 presents the composition and structure of several glass ceramics (Hench, 1996).

Table 2.6 Glass Ceramics and their Composition in Weight Percent

Constituent	KGC Ceravital	KGS Ceravital	KGy213 Ceravital	A/W-GC
SiO_2	46.2	46	38	34.2
P_2O_5	...	...	...	16.3
CaO	20.2	33	31	44.9
$Ca(PO_3)_2$	25.5	16	13.5	...
CaF_2	...	...	...	0.5
MgO	2.9	...	...	4.6
MgF_2	...	...	...	...
Na_2O	4.8	5	4	...
K_2O	0.4	...	...	...
Al_2O_3	...	...	7	...
B_2O_3	...	...	...	...
Ta_2O_5/TiO	...	...	6.5	...
Structure	Glass-ceramic	Glass-ceramic	...	Glass-ceramic

(Source: Hench, 1996)

2.4 Mechanisms of Filler Bioactivity

Along with the development of bioactive ceramics, numerous studies have been conducted in order to understand the mechanisms under which the crystalline carbonated hydroxyapatite layer that indicates bioactivity is being formed. Many complex physiochemical reactions take place at bioceramic – bone tissue interfaces depending on the elemental composition and the surface properties of each ceramic (Jallot, 2005).

In the case of hydroxyapatite or β-TCP ceramics, an acidic attack leads to partial dissolution of the material. Consequently, changes in porosity, density, loss of material and changes in particle diameter and average crystal size occur. This dissolution releases Ca^{2+} and PO_4^{3-} ions in the surrounding environment. By exposing hydroxyl and phosphate units in the crystal structure of HA, negative charges can occur on its surface.

These ions can be combined with ions from the biological fluids to form other calcium phosphate phases (including Ca-rich amorphous calcium phosphate ACP). Thus, there is an increase of calcium and phosphorous concentration in the surrounding fluids that leads to supersaturation and precipitation of other apatite crystals such as brushite, octacalcium phosphate, carbonated hydroxyapatite, etc. at the material interface. The mechanisms of apatite formation upon immersion in the SBF can be observed in Figure 2.4 (Kim et al. 2005). It is apparent, that these apatite crystals may include Ca^{2+}, Mg^{2+}, CO_3^{2-}, PO_4^{3-}, F^- and other organic molecules resulting from the biological fluids. Depending on the ions included on the precipitated apatite, the formation of carbonated apatite that is needed for bone growth may be inhibited or induced. In the case of Mg^{2+}, the forms of brushite and octacalcium phosphate are predominant, whereas in the case of CO_3^{2-} and F^-, there is mainly apatite formation which leads to the formation of a 200-800 nm thick layer (Jallot, 2005).

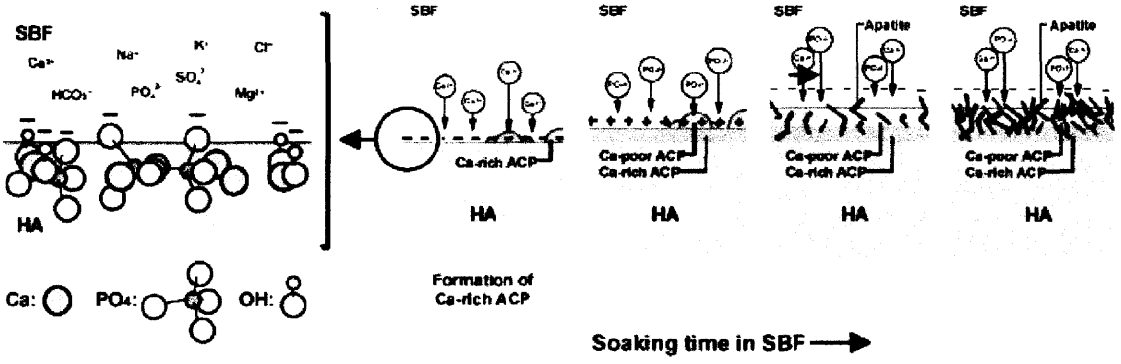

Figure 2.4 Schematic representation of the origin of negative charge on the surface of HA and the process of apatite formation in SBF.
(Source: Kim et al. 2005)

In the case of bioactive glasses, Hench (1998) describes five reaction stages (1-5 in Figure 2.5) and also a sequence of cellular events that are also related to forming a bioactive bond (reaction stages 6-11). Although there are details in molecular biology as well as in genetic level that still need to be established, the physiochemical reactions include dissolution, diffusion, ionic exchange and precipitation (Jallot, 2005).

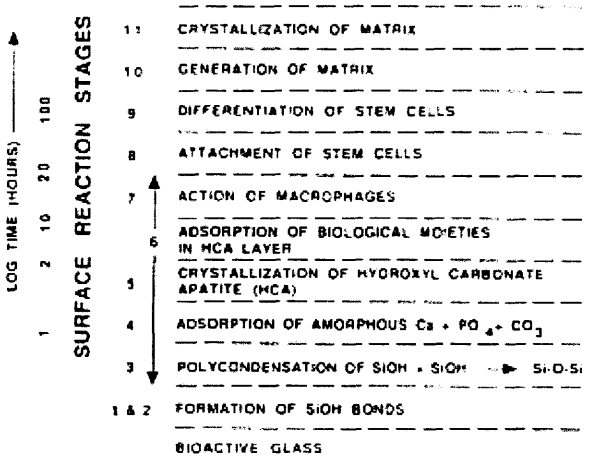

Figure 2.5 Sequence of interfacial reactions involved in forming a bond between tissue and bioactive ceramics.
(Source: Hench, 1998)

Specifically, the surface reactions stages 1-5 are described (Jallot, 2005, Peitl et al. 2001, Filgueiras et al. 1993) as follows:

Stage 1: Rapid exchange of alkali ions (Na^+ or K^+) with H^+ or H_3O^+ from biological fluids through an exchange layer with 200 nm thickness.

$$-Si\text{-}O\text{-}\ Na^+ + H^+ + OH^- \rightarrow -Si\text{-}OH + Na^+_{(solution)} + OH^-$$

Stage 2: Loss of soluble silica in the form of $Si(OH)_4$ to the solution resulting from breaking Si-O-Si bonds and forming silanols Si-OH at the glass/solution interface

$$-Si\text{-}O\text{-}Si- + H_2O \rightarrow -Si\text{-}OH + OH\text{-}Si-$$

Stage 3: Condensation and repolymerization of a hydrated SiO_2 rich layer depleted of alkalis and alkaline earth cations.

$$\text{-Si-OH + OH-Si-} \rightarrow \text{-Si-O-Si- + } H_2O$$

Stage 4: Ca^{2+} and PO_4^{3-} groups migrate from a SiO_2 rich layer to the surface forming $CaO\text{-}P_2O_5$ on the top of a SiO_2 rich layer followed by the growth of an amorphous $CaO\text{-}P_2O_5$ film by incorporation of soluble calcium and phosphate ions from the bulk material as well as from the biological fluids.

Stage 5: The amorphous $CaO\text{-}P_2O_5$ film crystallizes by incorporation of OH^-, CO_3^{2-} or F^- anions from the solution to form a mixed hydroxyl (HCA), carbonate fluoropatite layer (HCFA).

The above *in vitro* reactions are shown schematically in Fig. 2.6 (Peitl et al. 2001).

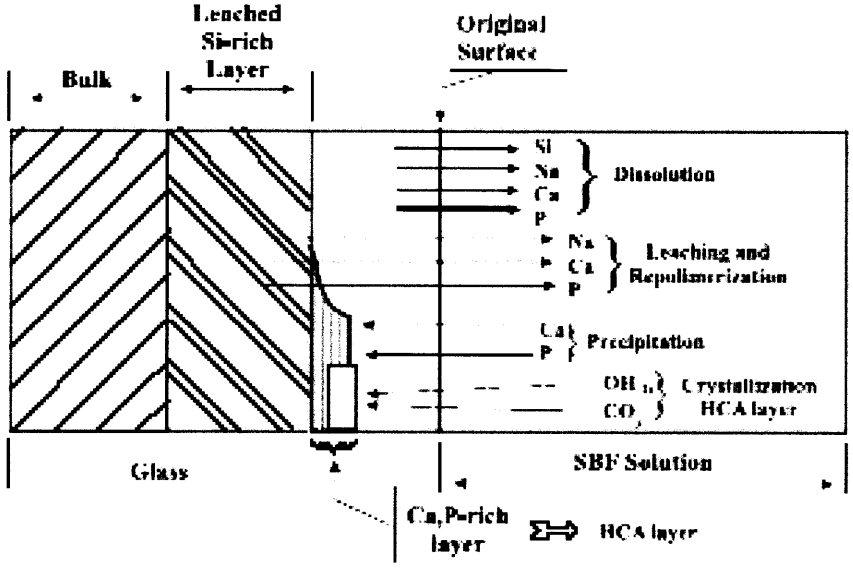

Figure 2.6 Schematic illustration of the surface reactions (1-5) on bioactive glasses, forming double SiO_2 – rich and Ca, P – rich layers.
(Source:Peitl et al. 2001)

The *in vivo* stages that involve the sequence of cellular events to form the bioactive bond are as follows (Jallot, 2005):

Stage 6: Adsorption and desorption of biological growth factors in the HCA layer from the surrounding tissues. Biochemical growth factors facilitate the differentiation of stem cells.

Stage 7: Macrophages help to remove debris from the site, in order for cells to occupy the space.

Stage 8: Stem cells are attaching to the bioactive glass surface.

Stage 9: Stem cells differentiate to form osteoblasts (known as bone growing cells).

Stage 10: Osteoblasts generate the extacellular matrix to form bone.

Stage 11: The inorganic calcium phosphate matrix crystallizes to enclose bone cells in a living composite structure.

It is essential to control the solubility of bioactive materials. If an implant is required to last for a long time period, then low solubility is an important parameter. In the case of bioactive glasses, other elements could be added in order to improve the long term stability by reducing the dissolution of the glass network. Optimization of the bioactive glass properties requires a compromise between bioactivity and solubility. The addition of Al_2O_3 could control the dissolution of the glass, but as mentioned earlier it could also inhibit bone bonding (Jallot, 2005, Hench. 1996).

Given the similarities in composition between bioglass and CS many authors (Liu et al. 2004, De Aza et al. 2000, Zhao et al. 2005, Li and Chang, 2005)] suggested that the formation of apatite on the CS surface may follow a similar mechanism. De Aza (2000),

as well as Sahai and Anseau (2005), reported that in the case of pseudowollastonite immersed in SBF, there is a rapid increase in the concentration of dissolved Ca and Si that leads to a pH increase for the first few days followed by steady state values. They suggest that Ca and Si are leached out from surface layers with protonation of the ceramic. This transforms the pseudowollastonite crystals into an amorphous silica phase. The reaction proceeds and further leaching of calcium leads to an increase of the surrounding fluid pH that creates optimal conditions for partial dissolution of the amorphous silica and further nucleation and precipitation of the calcium phosphate phase.

Filgueiras et al. (1993) studied the *in vitro* surface reactions the take place in the bioactive glass 45S5 in simulated body fluid (SBF) with different compositions. A simulated body fluid is a solution that has been proposed by Kokubo et al. (1990) and has the same ion concentration as in the human blood plasma. After intentionally changing the ion composition in the SBF, Filgueiras et al. (1993) observed that calcium and phosphate ions in SBF accelerate to a small extent the stage 3 reaction that involves the repolymerization of silica and the formation of an amorphous calcium phosphate layer (stage 4) on the bioglass surface. The higher the calcium and phosphorous concentration in the SBF, the more rapidly the amorphous calcium phosphate layer crystallizes to form hydroxy-carbonate apatite. This is in agreement with Kokubo (1998) who states that the silanol groups can induce apatite nucleation and the calcium ions can accelerate this nucleation. Similarly to the case of calcium phosphate materials (Jallot, 2005), the Mg^{2+} ions slow down the formation of the amorphous layer and retard the crystallization of hydroxy-carbonate apatite on the glass surface (Filgueiras et al. 1993).

2.5 Polymers Used as Biomaterials

Polymers have been widely used as biomaterials for permanent and temporary applications during the last decades. Permanent applications make use of biostable polymers that are not subject to degradation in the body. By contrast, temporary applications will eventually degrade in the body, with a life expectancy close to the required healing time. Table 2.7 shows several examples of biostable and biodegradable polymers. Figure 2.7 illustrates the use of polymeric biomaterials in the form of composites for a variety of clinical applications.

Table 2.7 Examples of Polymers Used in Tissue Engineering Applications

Biostable Polymers	Biodegradable Polymers
Polyethylene (PE, HDPE)	Polylactic acid (PLLA)
Polyetheretherketone (PEEK)	Polyglycolic acid (PGA)
Polysulfone (PSU)	Poly-ε-caprolactone (PCL)
Polyurethane (PU)	Poly-β-hydroxybutyrate (PHB)
Polymethylmethacrylate (PMMA)	Polyorthoesters
Bisphenol-α-glycidyl methacrylate (bis-GMA)	Poly-δ-valerolactone
	Blends of starch with ethylene vinyl alcohol (SEVA)

(Source: Chouzouri and Xanthos, 2005)

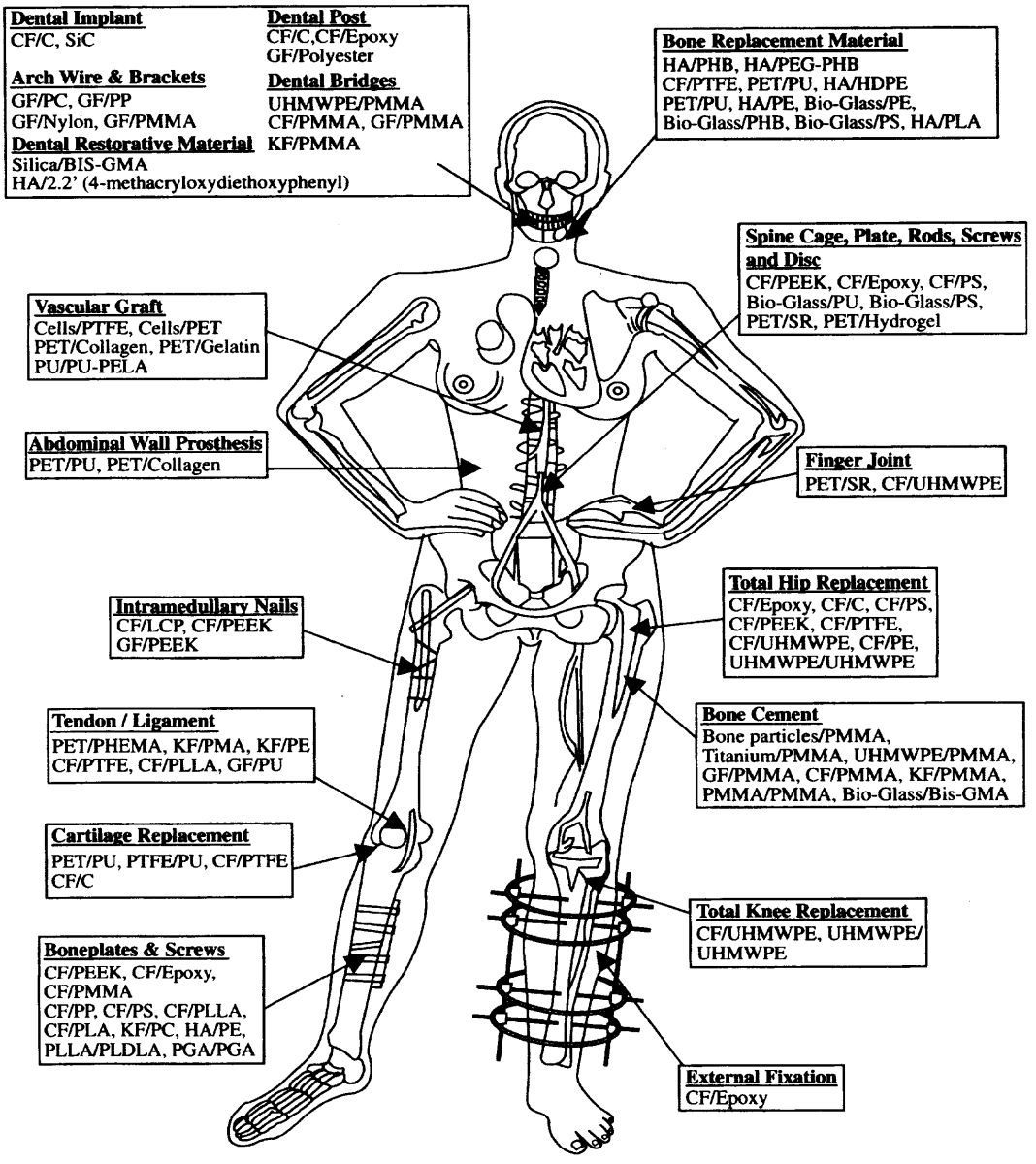

CF: Carbon fibers, C: Carbon, GF: Glass fibers, KF: Kevlar fibers, PMMA: Polymethymethacrylate,
PS: Polysulfone, PP: Polypropylene, UHMWPE: Ultra-high-molecular weight polyethylene,
PLDLA: Poly(L-DL-lactide), PLLA: Poly (L-lactic acid), PGA: Polyglycolic acid, PC: Polycarbonate,
PEEK: Polyetheretheketone; HA: Hydroxyapatite, PMA: Polymethylacrylate,
BIS-GMA: bis-phenol A glycidyl methacrylate, PU: Polyurethane, PTFE: polytetrafluoroethylene,
PET: polyethyleneterephthalate, PEA: poltethylacrylate, SR: silicone rubber,
PELA: Block co-polymer of lactic acid and polyethylene glycol, LCP: liquid crystalline polymer,
PHB: Polyhydroxybutyrate, PEG: polyethyleneglycol,
PHEMA: poly(20hydroxyethyl methacrylate)

Figure 2.7 Common clinical applications and polymers used.
(Source: Ramakrishma et al. 2004)

In the case of biodegradable polymers, hydrolysable linkages, namely ester, orthoester, anhydride, carbonate, amide, urea and urethane are present in their backbones. Aliphatic polyesters are commonly used as biomaterials because of their biocompatibility and their variable physical, chemical and biological properties (Li, 2006). Table 2.8 lists the structures of the most important aliphatic polyesters used as biomaterials. Asymmetric carbon atoms are shown by asterisks.

Table 2.8 Aliphatic Polyesters

Polymer	Acronym	Structure
Poly(glycolic acid)	PGA	$-[-O-CH_2-CO-]_n-$
Poly(lactic acid)	PLA	$-[-O-{}^{*}C(H)(CH_3)-CO-]_n-$
Poly(ε-caprolactone)	PCL	$-[-O-(CH_2)_5-CO-]_n-$
Poly(valerolactone)	PVL	$-[-O-(CH_2)_4-CO-]_n-$
Poly(ε-decalactone)	PDL	$-[-O-{}^{*}C(H)(CH_2)_3CH_3-(CH_2)_4-CO-]_n-$
Poly(1,4-dioxane-2,3-one)		$-[-O-(CH_2)_2-O-CO-CO-]_n-$
Poly(1,3-dioxane-2-one)		$-[-O-(CH_2)_3-O-CO-]_n-$
Poly(*para*-dioxanone)	PDO	$-[-O-(CH_2)_2-O-CH_2-CO-]_n-$
Poly(hydroxy butyrate)	PHB	$-[-O-{}^{*}C(H)(CH_3)-CH_2-CO-]_n-$
Poly(hydroxy valerate)	PHV	$-[-O-{}^{*}C(H)(CH_2-CH_3)-CH_2-CO-]_n-$
Poly(β-malic acid)	PMLA	$-[-O-{}^{*}C(H)(COOH)-CH_2-CO-]_n-$

The standard requirements, as described by Neves et al. (2005), for a polymer to be used as a biomaterial include resistance to aging in saline aqueous media, dimensional stability, biocompatibility, absence of harmful additives that could migrate to the body, fatigue resistance and the ability for the material to be sterilized without significant loss of its properties. A polymer is defined as biocompatible when the material itself or its degradation fragments do not elicit any toxic, inflammatory or allergic reactions in the surrounding tissue. The challenging part in using biodegradable polymers is the ability to control their degradation characteristics, by modifying the polymer hydrophobicity and crystallinity, in order to tailor the properties of the final device. Although polymers have great advantages due to their characteristics, they also exhibit drawbacks due to their low stiffness. Table 2.9 shows the mechanical properties for some polymers used as biomaterials.

Table 2.9 Mechanical Properties of Polymers

Polymers	Young's modulus (GPa)	Tensile strength (MPa)
Biodegradable		
Poly(L-lactic acid)	2.7	50
Poly(DL-lactic acid)	1.9	29
Poly(caprolactone)	0.4	16
Poly(β-hydroxybutyrate)	2.5	36
Non-biodegradable		
Poly(ethylene)	0.88	35
Poly(urethane)	0.02	35
Poly(tetrafluoroethylene)	0.5	27.5
Poly(methyl methacrylate)	2.55	59
Poly(ethylene terephthalate)	2.85	61

(Source: Murugan and Ramakrishna, 2005)

2.6 Polymer Degradation Mechanisms

Although, many studies have been conducted on the synthesis and hydrolytic degradation of these polyesters, the role of the low molecular weight fragments in the degradation process is still unknown. Schliecker et al. (2003), proposed that the hydrolytic degradation process is affected by four parameters; specifically, the degradation rate constant, the amount of water that has been absorbed, the diffusion coefficient of the chain fragments and the solubility of degradation byproducts in the aqueous media.

In addition, Göpferich and Lang (1993) suggested that since hydrolysis is the most important part of degradation, factors that influence the rate of this reaction, as the type of the chemical bond, the pH, the copolymer composition and the water uptake play an essential role. The molecular weight changes and the loss of mechanical strength are important parameters for monitoring degradation. The reactivities that are based either on hydrolysis kinetics data or are extrapolated from low molecular weight fragments that have the same functionality can most times successfully predict the rate of degradation. Anhydride- and ortho-ester bonds are the most reactive ones followed by esters and amides (Göpferich and Lang 1993). Changes of the chemical neighborhood of the functional group through steric and electronic effects may in turn influence the degradation rates. Changes in pH may change the reaction rates of esters by some orders of magnitude due to catalysis. Also, by introducing a second monomer into the chain, properties such as crystallinity and glass transition temperature may be altered, which in turn will influence degradation rates. Specifically, Tserki et al. (2006) synthesized and tested a series of aliphatic homopolyesters and copolyesters from 1,4 butanediol and dimethylesters of succinic and adipic acids. They showed that the lower the crystallinity,

the higher the degradation rates; also by incorporating the secondary comonomer in the polymer structure, mechanical and other physical properties decreased.

Molecular weight, as mentioned earlier, is considered to be the most sensitive parameter for modeling polymer degradation. Particularly, with the M_n (number average molecular weight) directly related to the scission of polymer chains, several relationships have been derived relating the changes in M_n with time and the hydrolysis rate of ester linkages. Specifically, Anderson (1995) and Chu (1995) proposed a statistical method for relating M_n and hydrolysis rate. Assuming that the extent of degradation was not large they suggested the following relationship:

$$1/\overline{M_n} = 1/\overline{M_{no}} + kt \tag{2.2}$$

where $\overline{M_{no}}$ is $\overline{M_n}$ at time t=0 and k is the rate constant. Under this assumption, a linear relationship should exist between $1/\overline{M_n}$ versus time, up until mass loss takes place (Weir et al. 2004). A disadvantage of this mechanism is that it does not take into account the possibility of autocatalysis that would significantly influence the degradation rate.

Pitt and Gu (1987) derived an equation based on the kinetics of the ester-hydrolysis reaction and taking into account the autocatalytic effect.

$$d(E)/dt = -d\,(COOH)/dt = -\,k\,(COOH)\,(H_2O)\,(E) \tag{2.3}$$

where (COOH), (H_2O) and (E) represent the concentration of the carboxyl end groups, water and ester groups, respectively.

By assuming that the ester and water concentrations remain constant and the concentration of acid groups is equal to 1/Mn it can be shown that

$$\overline{M_n} = \overline{M_{no}} e^{-kt} \tag{2.4}$$

If this relationship holds true, a linear relationship should exist between the $\ln \overline{M_n}$ versus time up until mass loss occurs (Weir et al. 2004).

$$\ln \overline{M_n} = -kt + \ln \overline{M_{no}} \tag{2.5}$$

The degradation of a polymer matrix could proceed through the following mechanisms (Proikakis et al. 2006): i) surface or heterogeneous erosion and ii) bulk or homogeneous erosion. In the first case (Schliecker et al. 2003), water is being absorbed by the polymer and hydrolytic ester cleavage occurs at the polymer surface. This generates chain fragments that have acidic end groups. Initially, polymer degradation is faster than water intrusion into the bulk polymer; this results in degradation mainly at the outermost and not in the inner part of the matrix. Thus, a decrease in molecular weight, along with an increase in polydispersity without polymer mass loss occur. After an elapsed short time, water diffusion is relatively rapid in comparison to polymer degradation. Reaction / diffusion phenomena, that involve water soluble low molecular weight degradation products at the surface and the inner part of the polymer, are thought to govern polymer degradation (Schliecker et al. 2003). In small size devices soluble oligomers can escape before the devices are totally degraded. By contrast, in large devices, only soluble oligomers that are located close to the outer surface can escape, whereas the ones inside the device remain entrapped as a result of their relatively small diffusion coefficients. Consequently, carboxyl end groups are more concentrated in the center, and the degradation rate increases due to the autocatalytic effect of carboxyl groups on the ester hydrolysis (Schliecker et al. 2003, Proikakis et al. 2006).

In the second case of homogeneous erosion, polymers degrade slowly and the rate of water diffusion into the system is faster than that of polymer degradation. As a result,

the whole system hydrates rapidly and the polymers when changed, are cleaved throughout. It should be noted that degradable polymers could erode via both pathways depending on the erosion conditions, the geometry of the samples and the hydrophilic/hydrophobic characteristics of the polymer (Proikakis et al. 2006, Xu et al. 2006).

A parameter that indicates which way a degradable polymer will erode is the ratio of the rate of bulk to surface erosions. Applying penetration theory, it can be shown that the thickness (δ) associated with each mechanism is related to a characteristic time, by the following equations:

$$\delta = \sqrt{\frac{4Dt_{diff}}{\pi}} \quad \text{in the case of bulk erosion} \tag{2.6}$$

and

$$\delta = \sqrt{Dt_{reaction}} \quad \text{in the case of surface erosion} \tag{2.7}$$

where $t_{diffusion}$ and $t_{reaction}$ are characteristic times of the two processes and D is the diffusion coefficient.

In order to identify parameters that determine surface or bulk erosion pathways, Burkersroda et al. (2002) proposed a model in which the two characteristic times of Eqns. 2.6 and 2.7 are expressed in terms of a dimensionless number (can be considered as a Deborah number) named "erosion number" to predict surface or bulk erosion.

In the case of amorphous polylactic acid, material degradation proceeds through surface erosion and is faster in the inner part than at the surface due to the autocatalysis phenomena. On the contrary, the degradation of semi-crystalline polylactic acid proceeds in a more complex way. Initially, degradation proceeds though the amorphous regions,

since these have higher water uptake ability than the crystalline ones. The degraded fragments diffuse and then recrystallize. Degree of crystallinity could increase along with degradation. After the major part of the amorphous area degrades, hydrolysis proceeds from the edge to the center of the crystalline domains (Proikakis et al. 2006, Mano et al. 2004).

Polycaprolactone is also a semi-crystalline aliphatic polyester but with higher crystallinity and hydrophobicity than polylactic acid, and as a result, it exhibits a different degradation behavior. The hydrophobicity of polycaprolactone could lead to a surface erosion/degradation behavior as shown by Xu et al. (2006). Polycaprolactone has lower degradation rates than polylactic acid, but being highly compatible with osteoblasts is used for long term implant applications (Mano et al. 2004).

CHAPTER 3

PREPARATION AND PROPERTIES OF POLYMER BIOCOMPOSITES – A REVIEW

3.1 General

Similarly to other fillers in conventional composites, shape, size, size distribution, pH, and volume percentage of the bioactive filler and filler distribution in the matrix and, in addition, type and level of bioactivity play important roles on the properties of the biocomposites. In addition, the matrix properties, the filler-matrix interfacial state as well as the processing parameters are of great importance in the performance of the final biomaterial (Wang, 2003). The majority of such composites are prepared by conventional melt processing methods (extrusion compounding followed by injection or compression molding) although some composites are prepared by solution casting techniques. The state of the art and recent developments in bioinert, biodegradable and injectable polymer composites for hard tissue replacement have been recently reviewed by Mano et al. (2004). Attempts have been made to simulate bone structure and properties through specialized forming technologies including shear controlled orientation injection molding (SCORIM®) (Mano et al. 2004), and hydrostatic extrusion (Wang, 2003).

Also, the biocompatibility of the composite could be enhanced with the addition of the bioactive fillers (Neves et al. 2005). In addition, foreign body reaction due to acidic degradation fragments could be minimized by the neutralizing capacity of some ceramics. Specifically, Li and Chang (2005) have demonstrated that when wollastonite and bioglass are incorporated in poly (lactic-co-glycolic acid) (PLGA) they maintained

the pH of the soaking media during degradation and ultimate release of acidic byproducts in the physiological range. In the case of hydroxyapatite, there was no pH compensation since the pH exhibited an almost linear decrease from 7.4 to 5.6. Similarly, Schiller and Epple (2003), demonstrated that carbonated calcium phosphates are also suitable as pH-stabilizing fillers for polyester degradation whereas hydroxyapatite and β-TCP are not capable of buffering at pH 7.4. In addition, the polymer degradation characteristics can also be affected by the incorporation of the ceramic phase, since the ceramic can act as hydrolysis barrier, delaying the polymer degradation (Neves et al. 2005). This was demonstrated by Li and Chang (2005), for the case of wollastonite and bioglass that delay the degradation of the PLGA. When hydroxyapatite was incorporated in the PLGA matrix degradation was accelerated which makes evident the complexity of each composite system.

A major breakthrough in biocomposites occurred when Bonfield et al. (Wang 2003) filled high density polyethylene (HDPE), a biocompatible and biostable polymer broadly used in orthopedics, with hydroxyapatite. The composite known as HAPEX™, firstly introduced by Smith & Nephew Richards in 1995, (Wang, 2003, Chouzouri and Xanthos, 2005) was the result of pilot studies, laboratory testing, clinical trials and pilot plant production efforts spanning a period of about 15 years until regulatory approval was attained. A range of 0.2 to 0.4 volume fraction HA was determined to be the optimum. HAPEX™ was the first composite designed to mimic the structure and retain the properties of the bone, and is mainly used for middle ear implants. It has mechanical properties similar to the bone and it is easy to trim, which allows the surgeons to precisely fit it at the time of implantation. By varying the type, amount and particle size

of HA and the polyethylene type, a range of mechanical properties approaching those of bones at different parts of the body, and different degrees of bioactivity can be obtained depending on the application (Wang, 2003). As an example, in order to produce composite materials that could carry higher loads, Wang et al. (2000), hydrostatically extruded HAPEX™ at different extrusion ratios after compression molding. Tensile and flexural properties were considerably increased. The higher the extrusion ratio, the stronger and the stiffer the extruded rods appeared. The composites produced through hydrostatic extrusion exhibit mechanical properties similar to the human cortical bone, which make them a potential candidates for load-bearing implant applications. The *in vitro* and *in vivo* responses have also been assessed extensively. In human osteoblast cell primary cultures used for *in vitro* experiments the osteoblast cells appeared to attach to HA; cell proliferation followed, thus confirming the bioactivity of the composites. In *in vivo* experiments with adult rabbits the composite implant surface was covered by newly formed bone.

Sousa et al. (2001) investigated HDPE filled with 25% wt commercially available HA with average particle size of 10 μm, produced by melt mixing and followed by shear controlled orientation injection molding (SCORIM®) to simulate the bone structure. Sousa et al. (2002) also produced composites of blends of starch with ethylene vinyl alcohol (SEVA-C) with 10, 30 and 50% wt hydroxyapatite by twin screw extrusion compounding followed by SCORIM®, as well as conventional injection molding. SCORIM® processing appeared to improve the stiffness of the composites, compared to conventional injection molding. No data were reported regarding the bioactivity of these composites. Similarly, (SEVA-C) filled with 30% wt commercially available HA was

produced by Leonor et al. (2003) by melt mixing followed by injection molding to create circular samples used to study the formation of a calcium phosphate layer in SBF.

Biocomposites of polysulfone (PSU) filled with 40 vol % HA have also been produced for hard tissue replacement (Wang, 2003). Polysulfone is a better matrix candidate for load bearing applications than HDPE due to its higher strength and modulus. The PSU/HA composites were produced by conventional compounding methods, followed by compression or injection molding. By increasing the HA content, the stiffness of the composite was increased to levels close to the lower bounds for human bone. Of particular importance in this and other composites containing HA and bioactive glass is the control of the polymer/filler interfacial strength, a complex problem as bioactivity is also an interface related phenomenon.

Yu et al. (2005) produced HA-reinforced polyetheretherketone (PEEK) composites by mixing HA and PEEK powders, compaction and pressureless sintering. Filler loadings from 10 to 40 vol % were used and the composites were evaluated for bioactivity in SBF. The surface of the 40 vol % composite was covered by an apatite layer in a short immersion period of 3 days, whereas the surface of the 10 vol % composite required 28 days to be fully covered with apatite. Thus, growth rate constant and, thus, bioactivity of the composite increase with increasing HA volume fraction.

In another study, Ni and Wang (2002) introduced different loadings (10, 20 and 30 vol %) HA particles into polyhydroxybutyrate (PHB) matrix and conducted *in vitro* studies. After a short period of time (within 1 day in SBF) formation of apatite was observed. The number of nucleation sites of apatite crystals was proportional to the HA content, and the composite with the higher loading had a faster apatite layer growth as

expected. Dynamic mechanical analysis (DMA) showed that the storage modulus of the composite increased initially, due to apatite formation, and eventually after prolonged immersion periods decreased due to polymer degradation.

Chen and Wang (2002) introduced HA and TCP into polyhydroxybutyrate-polyhydroxyvalerate (PHB-PHV). In composites containing up to 30 vol % of fillers, well distributed in the polymeric matrix, the degradation temperature of the composite was significantly reduced, the melting temperature was slightly affected and the matrix crystallinity varied. Both storage and loss moduli increased with increasing bioceramic content. Finally, a preliminary *in vitro* study showed bioactivity through the formation of bone-like apatite.

Shinzato et al. (2000) evaluated an AWGC filler with an average particle size of 4 μm in bisphenol-A-glycidyl methacrylate (bis-GMA) composites at 70 wt%. The composite had both an uncured and cured surface on each side in order to evaluate the differences in bone bonding strength. Such composites were implanted into the tibiae of male white rabbits. Direct bone formation through a Ca-P rich layer was observed histologically only for the uncured surfaces, presumably due to enhanced diffusion in the uncrosslinked state and faster exposure to the filler surface.

In another study, Juhasz et al. (2004) investigated composites of HDPE filled with AWGC of average particle size from 4.4 to 6.7 μm at filler content ranging from 10 to 50 vol %. With an increase in AWGC volume fraction, increases in Young's modulus, yield strength and bending strength were achieved while the fracture strain decreased. Specifically, a transition in fracture behavior from ductile to brittle was observed at

certain filler concentrations. Based on mechanical and bioactivity test data, composites with 50 vol% AWGC appear to have potential as implants for maxillofacial applications.

3.2 Polylactic Acid and Polycaprolactone Composites

PLA and PCL are common matrices for biocomposites. Hasegawa et al. (2005) have evaluated *in vivo* the biocompatibility, osteoconductivity and biodegradability of a porous composite consisting of HA and PDLLA by implantation into rabbit femoral condyles. They compared the composite with porous HA and concluded that the composite resorbed faster than HA alone. The porous HA was made by sintering HA whereas the HA in the composite was noncalcined and nonsintered, and thus was considered to have lower crystallinity. As a result, not only the degradability of the PDLLA, but also the degradability of HA plays an important role in the final performance of the material. The HA/PDLLA composite showed excellent osteoconductivity and faster resoption than HA alone.

In an *in vivo* study that lasted 5-7 years, Hasegawa et al. (2006) investigated the biocompatibility and biodegradation of HA/PLLA composite bone rods using uncalcined-HA (u-HA) and calcined HA (c-HA) that were implanted into the distal femurs of 25 rabbits. After the implantation, 4 rabbits lived for more than five years whereas 1 rabbit lived for 7 years and 4 months. For the rabbits that died naturally, samples were retrieved and specimens were examined by light microscopy and SEM. The u-HA/PLLA composites showed excellent biodegradability and osteoconductivity. Newly formed bone surrounded the residual material and trabecular bone bonded to the rod was

observed towards the center of the implant. As expected, the mechanical properties of the rods decreased due to polymer degradation.

Kasuga et al. (2003), prepared PLA/calcium carbonate (vaterite) composites by solution mixing and hot pressing of the dried mixture. The weight ratios of vaterite/PLA varied from 10/90 to 7/30. The 10% vaterite composite showed no apatite formation even after 28 days in SBF since the vaterite particle were completely embedded in the PLA matrix and were, thus, unable to dissolve. At 30 wt % vaterite, the modulus of elasticity improved to twice that of the modulus of PLA. The composite exhibited no brittle fracture behavior and a high bending strength of about 50 MPa. In addition, the composite formed a bonelike hydroxy-carbonate apatite layer throughout its surface even after one day in SBF.

Zhang et al. (2004), prepared porous PLLA/bioglass composites by phase separation of polymer solutions containing bioactive glass particles. Silane pretreatment of the glass resulted in better incorporation in the matrix. Increasing the glass content, increased the elastic modulus of the composites, but decreased their tensile strength and break at strain. The silane pretreated glass particles in composites delayed the *in vitro* apatite formation since fewer glass surfaces were exposed and the intervening layer of PLLA decreased the ion release rate from the bioactive glass with untreated glass composites soaked in SBF at body temperature formed bone like apatite layer inside and on their surfaces.

In a similar study, Boccaccini and Maquet (2003), developed porous PLGA/bioglass composites and examined the *in vitro* bioactivity and degradability in PBS. Solution mixing of PLGA was used to incorporate 10, 25 and 50 wt % of bioglass

and a thermally induced phase separation method was developed to produce porous samples. Weight loss, water absorption and molecular weight measurements were taken to monitor the degradation characteristics after a period of up to seven weeks in PBS. The study concluded that the degradation of PLGA was retarded by the presence of bioactive glass. In terms of bioactivity, rapid formation of carbonated hydroxy apatite crystals was confirmed by SEM, XRD and Raman spectroscopy.

In an analogous study, Yao et al. (2005), reported on the optimal synthesis parameters and the kinetics of formation of calcium phosphate layer at the surface of PLGA/bioglass composites. Apatite formation was studied through SEM and energy dispersive X-ray analysis on 30 wt % porous composites. The porous structure supported marrow stromal cells (MSC) proliferation and promoted MSC differentiation into osteoblast phenotype cells. The porous composite was found to be bioactive and demonstrated a significant potential as a bone substitute.

Kazarian et al. (2004) produced bioglass/PDLLA in the form of foams. The formation, size and distribution of 10μm average size apatite after immersion in a PBS solution after 14 and 28 was observed by FTIR imaging on the composite surface. Longer immersion periods (e.g. 63 days) resulted in the formation of a broader apatite layer. The composite scaffolds investigated in this study exhibited a combination of bioactive and bioresorbable properties.

In another study, Maeda et al. (2006), fabricated a PLLA/calcium carbonate hybrid membrane that contained polysiloxane prepared using aminopropyltriethoxysilane (APTES); this was coated with a silicon containing hydroxy-carbonate apatite layer using a biomimetic process since the presence of silicon apparently enhances the apatite

forming ability. Specifically, when Porter et al. (2003), incorporated silicates into hydroxyapatite the rate of bone formation significantly increased due to an increase of the number of defects related to the specific sites within the ceramic that are most likely to dissolve. Thus, an increase in the number of defects leads to an increased HA solubility and consequently to an increased rate of osseointergation. At the surface of 1.5 wt % Si-HA, larger needle like crystallites in the deeper regions of the implant were observed, whereas smaller plate like apatite crystallites were observed at the bone-HA interface. This suggests that two different biological processes are taking place. The needle-like crystallites are generated by a loss of material from the grains of Si-HA and are not due the heterogeneous nucleation of the biological apatite (Porter et al. 2003). In another study, Maeda et al. (2006) by incorporating silicon into their membranes showed a hydroxy-carbonate apatite formation after 3 days in SBF. In addition, the silicon containing membrane had higher cell proliferation ability.

With regard to PCL composites, Lowry et al. (1997), developed a composite of phosphate glass fibers embedded in PCL in the form of rods that were implanted in a rabbit humerous structure model and compared with stainless steel pins. Specimens were removed at 0, 6 and 12 weeks. Histological results revealed minimal inflammation around the PCL pin. Although, mechanical testing showed that PCL pins were weaker than stainless steel pins, there was a significant stress shielding effect for the stainless steel pins.

In another study, Jiang et al. (2005) prepared PCL/continuous bioglass fiber composites by a monomer transfer moulding technique coupled with surface initiated polymerization. The fibers were surface treated with an aminofunctional silane in order

to initiate polymerization. The surface initiated polymerization improved the Young modulus, the flexural strength and also the water resistance of the interface. As a result, rapid degradation of the composite mechanical properties was prevented.

Fujihara et al. (2005), designed a new type of guided bone regeneration membrane (GBR) using PCL/$CaCO_3$ composite nanofibers, produced by the electrospinning method. Composites with two different PCL: $CaCO_3$ ratios (75:25 wt% and 25:75 wt%) were produced. The GBR membranes showed good cell attachment and proliferation when observed under SEM.

Composites of PCL with HA were also produced by Causa et al (2006) and Hao et al. (2002). In the former case, phase inversion and casting were used to prepare porous scaffolds with different vol. % of HA. At 20 vol. % of HA the composite exhibited mechanical properties close to those of the human bone. In the latter case, solid PCL composites with HA nanocrystals were prepared by a solvent casting method and analyzed for thermal and mechanical properties.

Azevedo et al. (2003), also prepared PCL/HA composites by two different methods. Composites were either melt mixed in an extruder, or PCL was grafted on the surface of HA particles by ring opening polymerization of caprolactone in the presence of HA where OH groups acted as initiators. Different percentages of filler were used to obtain composites whose mechanical properties as well as degradation characteristics were investigated. Higher amounts of filler lead, as expected, to an increase in the modulus. The mechanical properties of the materials in the wet state were considerably lower than in the dry state. This was more significant for composites obtained by extrusion rather than the ones obtained by grafting. Degradation results agreed with this

observation since the grafted composites appeared to have slower water uptake and, thus, degrade at a slower rate.

Researchers have also used copolymers of PCL with other biodegradable polymers in order to tailor their degradation characteristics. Ural et al. (2000), synthesized poly(D,L lactide/ε-caprolactone) with two different molecular weights and then incorporated HA by solution mixing. The percent elongation decreased, where as both Young's modulus and yield point increased with increasing HA content. The presence of HA resulted in a reduction in the composite degradation rate.

In another study, Prabhakar et al. (2005), examined degradation properties and the ion release characteristics of PCL containing calcium phosphate glasses. Analytical techniques such as dynamic mechanical analysis and ion chromatography were utilized to investigate the behavior of these composites. It was shown that a modification of the calcium content of the glass structure significantly affected the stiffness, weight loss and pH behavior.

Similarly, Rich et al. (2002) and Jaakkola et al. (2004), synthesized a copolymer of poly(ε-caprolactone-co-DL-lactide) (96/4 molar ratio) and produced composites with two different ranges of granule size (<45μm and 90-315μm) of bioglass in a batch mixer at concentrations ranging from 40-70 wt%. They concluded that the higher the glass content and the glass surface/volume ratio in the matrix, the faster the apatite formation. Narhi et al. (2003), explored the biological behavior of a composite filled with glass S53P4 in experimental bone defects in rabbits. The size of the glass granules varied from less than 45 μm to 90-315 μm. Bone ingrowth was mainly observed in the superficial layers of the composites containing larger particle size filler and higher concentrations.

Using a biomimetic approach, Oliveira and Reis (2004), produced bioactive coatings on the surface of starch/PCL scaffolds. The scaffolds were pre-incubated in a calcium chloride supersaturated solution, and then impregnated with a sodium silicate gel. The water uptake ability of the samples, as well as the apatite layer formation were investigated. After 12 hours of immersion in SBF, an apatite layer, with Ca/P ratios in the range of stoichiometric HA, was observed.

In another study of Rhee (2003), silanol groups appear to provide nucleation sites to favor the formation of apatite crystals in organic polymer/silica hybrids of low and high molecular weight polycaprolactone (PCL) prepared through the sol-gel method. In a SBF solution fast and uniform nucleation and growth occured for the low molecular weight hybrid, due to increased interaction points with the silica and decreased size of the silica domain. Additionally, the lower molecular weight of PCL meant faster degradation and faster exposure of the silica phase in the SBF solution.

CHAPTER 4

SCOPE OF THE THESIS

There is a significant amount of work that has been conducted in the tissue engineering field to produce materials capable of bone regeneration. It is apparent that the number of parameters that affect both bioactivity and degradation is very large and can be very specific for each material. Composites for bone regeneration could be used in different parts of the human body where load-bearing may or may not be essential. This makes every biomaterial unique in terms, not only of properties, but also composition and processing characteristics. Taking all these into account, it is understandable why research in the field is so demanding but also so challenging.

In spite of numerous publications on the potential use of combinations of polymer / bioactive fillers for bone regeneration, little information exists on the assessment of solid, non porous composites prepared via solventless routes and consisting of unmodified, slowly degrading homopolymers with relatively low amounts of reactive fillers.

The scope of this thesis was to fabricate such composites, consisting of degradable polymers and a variety of inorganic fillers, and investigate them in terms of *in vitro* bioactivity, degradability and mechanical properties. A comparison between these composites containing a semicrystalline or an amorphous polymer, along with phosphate and silicate fillers would provide an understanding of the degradation rates and the different reactions between polymers and fillers leading to bone regeneration. Results would allow further optimization of filler properties, such as surface/volume ratio, surface chemistry and size range at the required filler volume fractions. The work

described in the following pages would be expected to contribute to the establishment of a relationship between process conditions, degradability and bioactivity.

CHAPTER 5

EXPERIMENTAL

5.1 Materials

5.1.1 Fillers

A variety of fillers were chosen and used in this experimental study. One of the objectives was to screen these fillers for bioactivity, in terms of apatite formation, and then incorporate them in biodegradable polymers to form biocomposites that could eventually be used for tissue regeneration applications. Table 5.1 shows the properties and characteristics of the fillers used for the initial screening.

Table 5.1 Characteristics of Fillers

Fillers	Chemical Composition**	Density (g/cc)*	Shape	Size	Source
Calcium Phosphate Tribasic (HA)	$Ca_{10}(OH)_2(PO_4)_6$	3.14	Irregular Particles	N/A*	Sigma Aldrich
β-Tricalcium Phosphate	$Ca_3(PO_4)_2$	2.3	Irregular Particles	N/A*	Fluka
Calcium Carbonate	$CaCO_3$	2.93	Irregular Particles	N/A*	Sigma Aldrich
Calcium Silicate	$CaSiO_3$	2.9	Irregular Particles	‹ 75μm	Sigma Aldrich
Bioactive Glass 45S5	SiO_2(45wt%), Na_2O(24.5wt%), CaO(24.5wt%), P_2O_5(6wt%)	About 2.5	Plate-like	90-212μm**	Mo-Sci Health Care L.C.C.
Bioactive Glass 1393	SiO_2(53wt%), Na_2O(6wt%), K_2O(12wt%), CaO(20wt%), P_2O_5(4wt%), MgO(5 wt%)	About 2.5	Plate-like	90-212μm**	Mo-Sci Health Care L.C.C.

*Non – Available
** Suppliers information

The pH of the calcium silicate (CS) and the bioactive glass 45S5 (bioglass) of 5 wt% aqueous slurry solution is 9.6 and 10.8, respectively. SEM micrographs of CS and bioglass powders are shown in Appendix A.

5.1.2 Polymers

Several aliphatic polyesters were chosen and used for the experimental study. All of them are reported to be biodegradable and can be processed as conventional thermoplastic polyesters. They are as follows:

1. Poly (1, 4-butylene adipate-co-1,4-butylene succinate) [PST], extended with 1,6-diisocyanatohexane, a biodegradable thermoplastic polyester (CAS No. 119553672) obtained from Sigma-Aldrich. The measured carboxyl content CC_p of the pellets was 0.0535 eq./10^6g, corresponding to an acid number of 3.0.

2. Poly-L-lactic acid [PLLA] (trade name Biomer L9000) (CAS No. 26680-10-4), a semicrystalline polyester, obtained from Biomer. Polylactic acid is derived from naturally occurring lactic acid, which has two isomers as shown in Figure 5.1. The (S) L(+) isomer was used in this work. The measured carboxyl content CC_p of the pellets was 0.0247 eq./10^6g, corresponding to an acid number of 1.4.

3. Polylactic acid [PLA] (trade name PLA4060D) obtained from NatureWorks®. This resin is amorphous and was used for comparison with other semicrystalline polyesters with regard to degradation and the resulting bioactivity of the composites.

4. Poly-ε-caprolactone [PCL] (trade name TONE P767) recommended among others for compostable applications, with density of 1.145 g/cc, number average molecular weight

of 50,000 and melt flow index (MFI) of 1.9g/10min were supplied by Dow Chemicals. Reported melting temperature was 60^0C.

The properties and characteristics of the polyesters are summarized in Table 5.2.

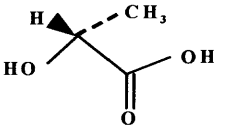

(R) D (-) Lactic Acid

(Levorotatory)

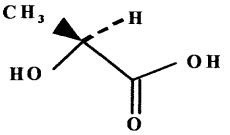

(S) L (+) Lactic Acid

(Dextrorotatory)

Figure 5.1 Isomers of lactic acid.

Table 5.2 Characteristics of Polyesters (Suppliers information)

Polymers	Chemical Structure	Density	Melting Temperature (^{0}C)	Molecular Weight (M_n)	Source
PST	$[-CO(CH_2)_nCO_2(CH_2)_4O-]_x$ $[-CONH(CH_2)_6NHCO-]$ $[-O(CH_2)]$	N/A	95	N/A	Sigma Aldrich
PLLA	$H[-O-CH(CH_3)COO-]_nOH$	1.25	160	130,000	Biomer
PLA	$H[-O-CH(CH_3)COO-]_nOH$	1.25	-	N/A	NatureWorks®
PCL	$\left(-OCH_2\ (CH_2)_3\ CH_2-\overset{O}{\overset{\|}{C}}-\right)_n$	1.145	60	50000	Dow Chemicals

5.1.3 Degradation and Bioactivity Media

5.1.3.1 Phosphate Buffer Saline Solution (PBS). In order to follow the degradation behavior of the aliphatic polyesters and their composites, pouches of phosphate buffer saline (PBS) were obtained from Sigma Aldrich. Contents of one pouch, when dissolved in one liter of distilled or deionized water, yielded 0.01 M phosphate buffered saline solution (NaCl 0.138 M; KCl 0.0027 M) with a pH 7.4, at 25 °C. The composition of the PBS aqueous solution is 1.38 mM NaCl, 1.15 mM Na_2HPO_4, 1.2 mM KH_2PO_4 and 2.7 mM KCl. PBS is a buffer solution that is commonly used by researchers for hydrolytic degradation and *in vitro* controlled release experiments.

5.1.3.2 Simulated Body Fluid (SBF). Kokubo (1990, 2006) developed a simulated body fluid that has inorganic ion concentrations similar to those of human extracellular fluid in order to study the formation of apatite on bioactive materials *in vitro*. The simulated body fluid is often abbreviated as SBF. Its ion concentrations are given on Table 5.3. It was prepared by dissolving appropriate amounts of NaCl, $NaHCO_3$, KCl, $K_2HPO_4 \cdot 3H_2O$, $MgCl_2 \cdot 6H_2O$, $CaCl_2$ and Na_2SO_4 in distilled water and buffering to pH 7.4 at 36.5^0C with tris(hydroxymethyl)aminomethane and 1M HCl solution. The complete procedure and the reagents used for the preparation of SBF can be found in Appendix B. The SBF is known to be a metastable solution and it was kept refrigerated throughout the course of these experiments.

Table 5.3 Ion Concentrations of the Simulated Body Fluid and Human Blood Plasma

Ion	Concentration ($mmol/dm^3$)	
	Simulated body fluid (SBF)	Human blood plasma
Na^+	142.0	142.0
K^+	5.0	5.0
Mg^{2+}	1.5	1.5
Ca^{2+}	2.5	2.5
Cl^-	147.8	103.0
HCO_3^-	4.2	27.0
HPO_4^{2-}	1.0	1.0
SO_4^{2-}	0.5	0.5

(Source: Kokubo, 1990).

5.2 Processing

5.2.1 Preparation of Filler Samples

Fillers were compression molded to form tablets (in the absence of binders) in a 13mm diameter mold used to prepare KBr samples for FTIR analysis. Fillers were also used in their original powder form for screening bioactivity.

5.2.2 Preparation of Polymer Samples

Polymers used in this study underwent different processing steps depending on the testing method that followed. Polymers used as controls for degradation and bioactivity experiments underwent the same processing and shaping procedures as their composites, discussed in 5.2.3.

Neat PLLA, PST and PCL polymers were fed in a 15mm twin-screw extruder (APV MP-2015) at 200^0C, 130^0C and 80^0C barrel temperatures respectively in order to obtain control samples. Neat PLA was fed in a Brabender Plasticorder PL2000 at 190^0C and 60 rpm for 10 minutes under a nitrogen blanket in order to obtain a control sample.

Extruded and batch processed unfilled polymers were then compression molded in a PHI press at their processing temperatures using a 44kN force for 5 minutes;

standard test disc specimens with nominal thickness of 0.75 mm and diameter ranging from 20 to 33mm were prepared for the degradation and bioactivity studies. Similarly, compression molded samples of unprocessed polymers in a film form were prepared and used for degradation studies that followed intrinsic viscosity changes.

PLA pellets were predried and extruded through a Brabender single screw extruder (D=1.9cm and L/D=15), equipped with a 10 cm flat sheet die to obtain film samples (0.15 mm in thickness) for mechanical testing.

Cylindrical samples of unfilled PLA, after being processed in the batch mixer, were used for testing their compressive properties. The samples were 5.96 mm in diameter and 27 mm in length and were produced using a 15 – cavity transfer mold by compression molding.

5.2.3 Preparation of Composite Samples

Composite samples were prepared by solution mixing as well as melt mixing. PCL was dissolved in 40 cc dichloromethane at room temperature and each filler was added at a PCL / filler weight ratio of 7:3. The samples were left in the fumehood overnight at room temperature. After most of the dichloromethane had evaporated, the remaining solids were transferred into Pyrex dishes and dried under vacuum.

Neat polymers (PLLA, PCL) were predried and ground to a fine powder under liquid nitrogen (when possible) and then premixed with powdered fillers at a 7:3 polymer : filler weight ratio, before feeding the mixture in a co-rotating 15 mm twin screw extruder (APV MP-2015) at each polymer's processing temperature. In the case of the

PLA composites, mixing took place in a Brabender Plasticorder (PL2000) at 190^{0}C and 60 rpm for 10 minutes under a nitrogen blanket.

Composite samples were ground into powders and compression molded in a PHI press at processing temperatures using a 44 kN force for 5 minutes to form standard test disc specimens with nominal thickness of 0.75 mm and diameter ranging from 20 to 33 mm for the degradation and bioactivity studies.

PLA composite samples used for testing of their compressive properties were produced in a cylindrical shape in a 15 – cavity transfer mold, as their unfilled counterparts.

5.3 Testing and Characterization of Fillers for Bioactivity

5.3.1 Immersion in Simulated Body Fluid (SBF)

In order to test the bioactivity of the neat fillers, 1 g of each filler was dispersed in 100ml of SBF solution. The flasks containing the dispersion were then immersed in a water bath and shaken at 36.5^{0}C for predetermined time periods (6h, 9h, 1d and 1 week) (Kim et al. 2005). After removing the samples by decanting the SBF, the powders were washed with ethanol and dried under vacuum at room temperature overnight. Distilled water (DW) instead of SBF was also used as a control. Compression molded samples in the form of tablets (in the absence of binders) were also immersed in SBF at 36.5^{0}C.

5.3.2 Analysis of Surface Structure and Morphology

5.3.2.1 Scanning Electron Microscopy. The surface of the neat filler samples in powder and tablet form, before and after exposure to the SBF solution (or distilled water for the powder fillers), was examined by SEM (LEO Field Emission Gun 1530-VP Digital SEM). The specimens were carbon coated using a Bal-Tec Med 020 Sputter Coater and then viewed by varying the working voltage (from 1 to 10 kV).

5.3.2.2 Energy Dispersive X-Ray Analysis. Elemental analysis was performed on all filler samples before and after immersion in the SBF solution or distilled water. In addition to apatite growth, bioactivity was investigated by analyzing for elements like Ca and P that could be part of an apatite type layer formed at the surface. The Ca/P ratio was calculated and compared with the Ca/P ratio of 1.67 which according to Clifford et al. (2001) is equivalent to the one in the carbonated hydroxyapatite needed for bone ingrowth.

5.3.2.3 X-Ray Diffraction. The powdered fillers before and after immersion in the SBF were analyzed using a Philips PW 3040MPD DY715 X-ray diffractometer in order to detect and analyze the precipitated apatite layer. The specimens were scanned through the 2θ range between 15^{o} and 60^{o}.

5.4 Testing and Characterization of Composites and Unfilled Polymers for Bioactivity

5.4.1 Immersion in Simulated Body Fluid

The compression molded composites and unfilled polymer samples were immersed in duplicates in the SBF solution at a surface area/volume ratio of 0.1 and a temperature of

36.5^{0}C. After predetermined time periods (1, 4 and 8 weeks), the samples were removed, rinsed with PBS followed by ethanol, and then dried under vacuum at room temperature overnight.

5.4.2 Analysis of Surface Structure and Morphology

5.4.2.1 Scanning Electron Microscopy. The surface of the composites and unfilled polymers before and after exposure to the SBF solution was examined by SEM as described in Section 5.3.2.1.

5.4.2.2 Energy Dispersive X-Ray Analysis. Elemental analysis was performed on all samples before and after immersion in the SBF solution. Bioactivity was investigated, similarly to the neat fillers, by analyzing for elements like Ca and P that could be part of an apatite type layer formed at the surface.

5.4.2.3 X-Ray Diffraction. The composite and unfilled polymer discs before and after immersion in the SBF were analyzed as described in Section 5.3.2.3.

5.4.3 SBF Solution Analysis

5.4.3.1 Atomic Absorption Spectroscopy. Atomic Absorption (AA) Spectroscopy was used to evaluate changes in the concentration of Ca^{2+} ions in the SBF solution at different immersion times. A Perkin Elmer AAnalyst 400 with detection limit of less than 1 ppm was used. Standards and samples were prepared according to the Direct Air-Acetylene Flame method that is described in Appendix C. Average values are reported from measurements on duplicate samples that showed good reproducibility.

5.4.3.2 UV – Visible Spectroscopy. An HP 8453 UV-Vis spectrophotometer was used to detect changes in the concentration of phosphorous in the SBF solution at different immersion times. Standards and samples for UV-Visible analysis were prepared according to the Ascorbic Acid method described in Appendix C. Average values are reported from measurements on duplicate samples that showed good reproducibility.

5.5 Hydrolytic Degradation of Composites and Unfilled Polymers

5.5.1 Weight and pH Changes as a Function of Time

Degradation experiments for the composites and unfilled polymers were conducted by immersing the specimens in triplicate in a PBS solution of pH 7.4 at 36.5^0C. Weight changes were monitored after predetermined time periods by removing the samples from the solution and wiping the excess liquid. Weight changes were calculated at each time period using the following equation:

$$\% \text{ Weight Change} = 100 \times (W_t - W_0) / W_0 \qquad (5.1)$$

where W_t and W_0, respectively are weights of the wet and starting dry discs at time t.

The pH of the buffer solution at different degradation periods, after sample removal, was measured to monitor changes that could be a combination of acidic degradation byproducts resulting from the polymer and any neutralization effects resulting from the fillers. When the tests were completed, the specimens were washed with distilled water and dried under vacuum at room temperature for further characterization.

5.5.2 Intrinsic Viscosity as a Function of Time

The intrinsic viscosity [η] of 1% w/v solutions of PCL in dichloromethane and PLLA, PLA and PST in chloroform, before and after several immersion periods of their discs or films in PBS was measured at 25^{0}C in a constant temperature bath using an Ubbelohde viscometer (Kannon K879) by using the Solomon-Ciuta Eqn. 5.2 (Xanthos et al. 2001) for a single point measurement:

$$[\eta] = [(\eta_{sp} - \ln \eta_{rel})]^{0.5} / C \tag{5.2}$$

where η_{sp} and η_{rel} are the specific and relative viscosity respectively, and C is the concentration.

The solvents were filtered three times using disposable Teflon filters (CR syringe filter Acrodisc® PTFE, 25 mm diameter, 1.0 μm pore size, Luer fitting). In the case of the composite samples, the filler was removed by dissolving the polymer in the filtered solvent, centrifuging and decanting the polymer solution. The polymer solution was then filtered and dried in order to obtain the neat polymer that was redissolved to 1% w/v solution.

5.5.3 Thermal Properties as a Function of Time

Information on glass transition temperature (T_g), melting temperature (T_m), cold crystallization temperature (T_{cc}) as well as heat of fusion (ΔH) and % crystallinity was obtained by Differential Scanning Calorimetry, DSC (TA Instruments, QA100). For all samples, heating and cooling rates were 20^{0}C/min.

5.5.4 Mechanical Properties as a Function of Time

Tensile stress at yield and break and elongation at yield and break of PLA films (Type 5) were measured by a Tinius-Olsen (Lo Cap Universal) testing machine as per ASTM method D882, at a rate of testing of 12.7 mm/min. The average of five determinations per sample is reported along with standard deviations.

Compressive stress and strain at yield and break and compressive modulus were measured by a Tinius-Olsen (Lo Cap Universal) testing machine as per ASTM method D1621, at a rate of testing of 1.27 mm/min. The average of five determinations per sample is reported along with standard deviations.

CHAPTER 6

RESULTS AND DISCUSSION

6.1 Bioactivity of Neat Fillers

6.1.1 Fillers in the Form of Powders and Tablets

Biocomposites capable of stimulating bone regeneration require a combination of properties such as bioactivity, biocompatibility and degradation characteristics with adequate mechanical properties. Material selection and proper combination of the selected materials are critical parameters in order to achieve the above requirements. The rate and the uniformity at which the apatite layer is forming on the surface of the bioactive filler are very important and need to be coupled with the right polymer degradation characteristics in order to support bone formation with the desirable mechanical properties. This is the main reason that initial experiments in this study involved SEM with EDX elemental analysis and XRD characterization of the neat fillers in the form of powders or tablets after immersion in SBF.

A variety of fillers were tested for bioactivity, in terms of apatite growth, after immersion in SBF. In this section results with CS and bioglass will be reported. Results with other fillers are included in Appendix D. Formation of carbonated apatite, which is a characteristic of bioactive materials, is reproduced *in vitro* upon immersion in SBF that has the same ion concentration as human blood plasma. Literature has suggested that materials with high ionic solubility readily form apatite precipitates on their surface. This takes place through a chain of reactions including dissolution, precipitation and ion exchange accompanied by absorption and incorporation of biological molecules (Ducheyne and Qiu, 1999). Specifically, in the case of silicon containing bioactive

materials, dissolution of calcium ions and simultaneous formation of a silica-rich layer at the material interface is the proposed mechanism for HA formation (Siriphannon et al. 2002). The dissolution of the calcium ion increases the degree of supersaturation of the surrounding fluid with respect to HA and the silica-rich layer supplies the needed nucleation sites by dissolving silicate ions. The nucleation and growth of the HA layer proceeds by reaction with the calcium, phosphate and hydroxide ions from the SBF; sometimes, ions such as carbonate or fluoride are also incorporated in the final structure.

The method that was followed in this work gives only an indication of bioactivity. In the case of powders, the results are more complicated than in the case of tablets, since different particles may show different nucleation activity and the area of interest in SEM images is highly localized. An additional drawback is that the materials used in this study are commercially available and not in-house synthesized. Several researchers have synthesized and used bioactive fillers in order to control purity and, at the same time, the amorphous and crystalline phases which exhibit different microtextures and specific surface areas (Siriphannon et al. 2002, De Aza et al. 2000, Zhao et al. 2005, Wan et al. 2005, Lin et al. 2005, Peitl et al. 2001). Although some powders have been used by researchers ((Siriphannon et al. 2002, Kim et al. 2005), the majority uses scaffolds or bioactive materials in pellet form.

6.1.1.1 Calcium Silicate. Figure 6.1 shows SEM micrographs of calcium silicate (CS) in powder form before and after one week immersion in DW and SBF. No obvious changes are observed on the surface of the particles even after a week. Calcium silicate in the form of wollastonite has been shown in the literature (Liu et al. 2004) to have a bioactive and biocompatible response. Various forms of calcium silicate such as

pseudowollastonite (α – $CaSiO_3$) (Sahai and Anseau, 2005, De Aza et al. 2000) tricalcium silicate (Ca_3SiO_5) (Zhao et al. 2005), β-dicalcium silicate (Cheng, 2006), β-wollastonite (β-$CaSiO_3$) (Wan et al. 2005, Li and Chang, 2005), amorphous calcium silicate, β-calcium silicate and α-calcium silicate (Siriphannon et al. 2002), and commercially available mineral wollastonite (Risbud et al. 2001) have been shown to exhibit different degrees of bioactivity.

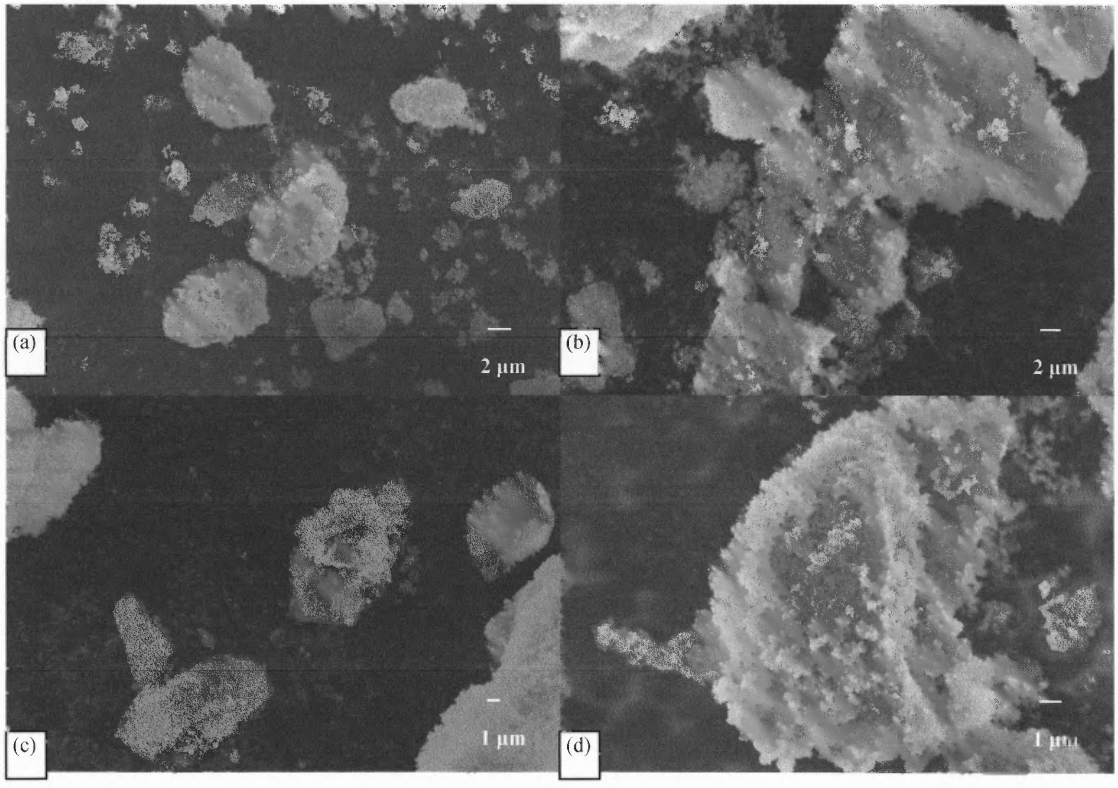

Figure 6.1 CS powder before and after immersion in DW and SBF. (a) Before immersion. (b) After six hours immersion in DW. (c) After 6 hrs immersion in SBF. (d) After 24 hrs immersion in SBF. (e) After 168 hrs (one week) immersion in SBF.

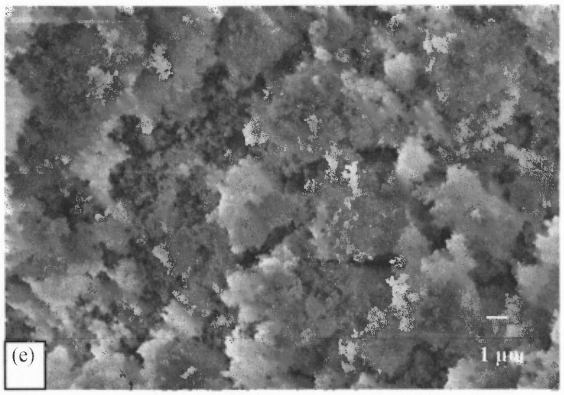

Figure 6.1 CS powder before and after immersion in DW and SBF. (a) Before immersion. (b) After six hours immersion in DW. (c) After 6 hrs immersion in SBF. (d) After 24 hrs immersion in SBF. (e) After 168 hrs (one week) immersion in SBF. (Continued).

Figure 6.2(a) represents the molded surface of a CS tablet before SBF immersion. Globules of mineral precipitates appeared on the exposed CS surface after one week (Fig. 6.2(b)) whereas at higher magnification (Fig. 6.2(c)) the precipitates appear as needle-like deposits. It is evident that the pressed sample shows mineral growth that could not be observed for the sample in powder form. This could be due to the formation of additional active nucleation sites as a result of the sample manufacturing method.

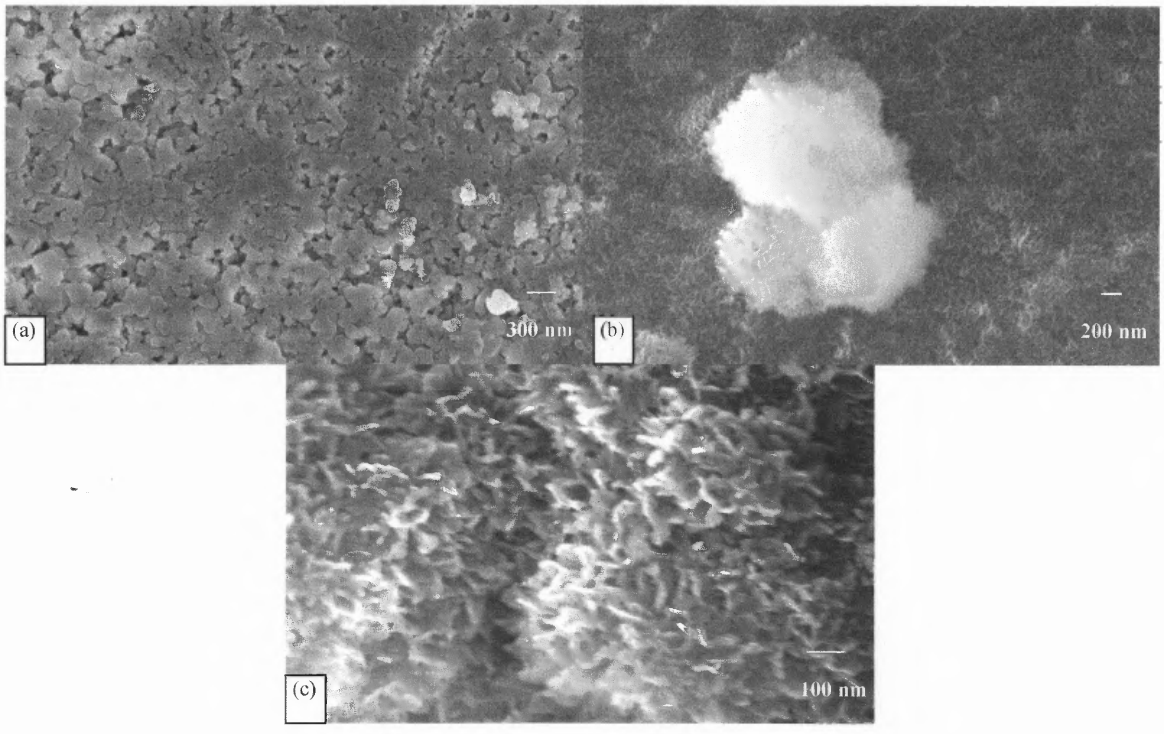

Figure 6.2 SEM micrographs of calcium silicate molded surface showing growth of mineral precipitates. (a) Before immersion in SBF. (b) After one week immersion; globules of mineral precipitates are shown on the exposed surface. (c) Higher magnification of the globular structure shows needle like deposits.

Figure 6.3 shows XRD spectra of CS before and after immersion in DW and SBF. The intensities of the 31.7° [211] and 40° peaks of apatite increased with immersion time. Activity can be seen as early as after 6 hours immersion in SBF. After 168 hours (one week) immersion, apatite formation at 31.7° was observed. In addition, a peak at 29.3° can be observed in the CS as early as six hours immersion in SBF. This is in agreement with results of Siriphannon et al. (2002) who observed this peak as early as after two hours and attributed it to the crystallization of an amorphous $CaCO_3$ constituent in the original CS. Similarly to our study, Siriphannon et al. (2002) clearly observed by the XRD pattern the formation of crystalline HA that seemed to cover the bioactive material surface as early as 24 hours after immersion. A residual calcite peak at 29.3° and at 40°

was also strong in both Siriphannon et al. (2002) and our own studies. Formation of apatite structures in our work is also confirmed by EDX data (not shown) that showed differences in the Ca/P ratios ranging from 8.09 after 9 hrs, to 5.3 after 168 hours in SBF. Although the Ca/P ratio does not appear to be the one of biological apatite (1.67), it certainly shows a tendency towards that value. Note that the different crystalline and amorphous phases of the material are important for its bioactivity behavior as shown by Siriphannon et al. (2002) in the case of β-CS and α-CS for apatite layers with different formation behavior, microstructure and particle size. Based on data from these authors and our XRD data, it appears that the CS used in the present work is mostly amorphous with an expected different nucleation and growth behavior than that of crystalline CS fillers.

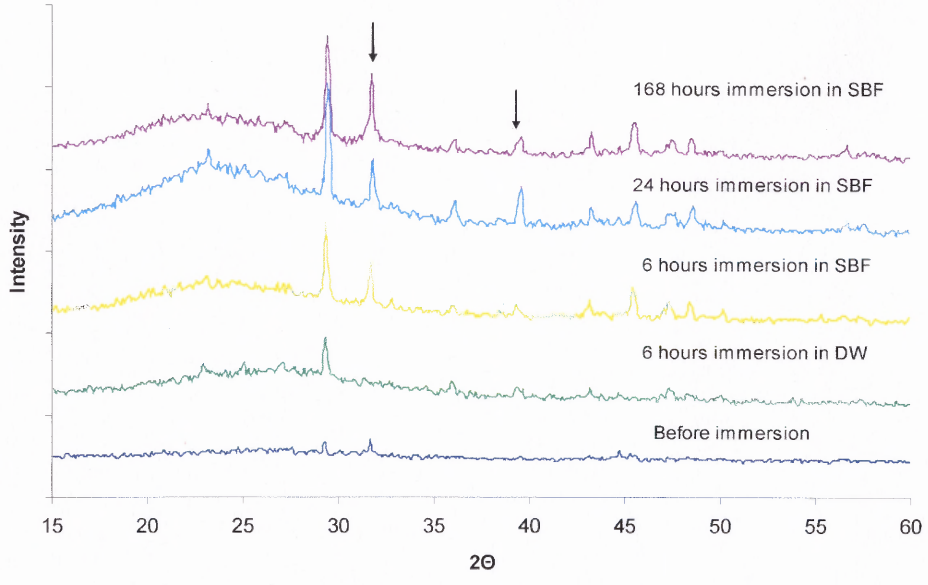

Figure 6.3 XRD spectra of CS before and after immersion in DW and SBF.

6.1.1.2 Bioglass. Figure 6.4 represents SEM micrographs of bioactive glass 45S5 (bioglass) in powder form before and after immersion in SBF and DW. Bioglass has a reported decay rate of 150 μg/ cm^2/day (Mo-Sci, 2007) and appears to be very reactive, since some type of precipitation is noted even after immersion in DW. When bioglass was immersed in SBF, fast mineral precipitation (after 6 hours in SBF) appeared. In Figure 6.4(e), mineral precipitates can be seen in the form of globules that will eventually cover the entire filler surface at longer immersion periods. After only 6 hours the coverage appears to be nearly homogeneous.

Figure 6.5 includes SEM micrographs of the molded bioglass surface before and after one and two weeks immersion periods in SBF. Figure 6.5(a) shows the molded bioglass surface before immersion as free of mineral precipitates. After one week immersion, nucleation and growth have occurred on the exposed surface resulting in clusters of mineral precipitates. These precipitates, at a higher magnification (Fig. 6.5(c)), appeared as needle shaped nanosized crystallites, in agreement with results reported in the literature (Fujibayashi et al. 2003). After two weeks of immersion (Fig. 6.5(d)), the bioglass area appeared to be fully covered with mineral precipitates.

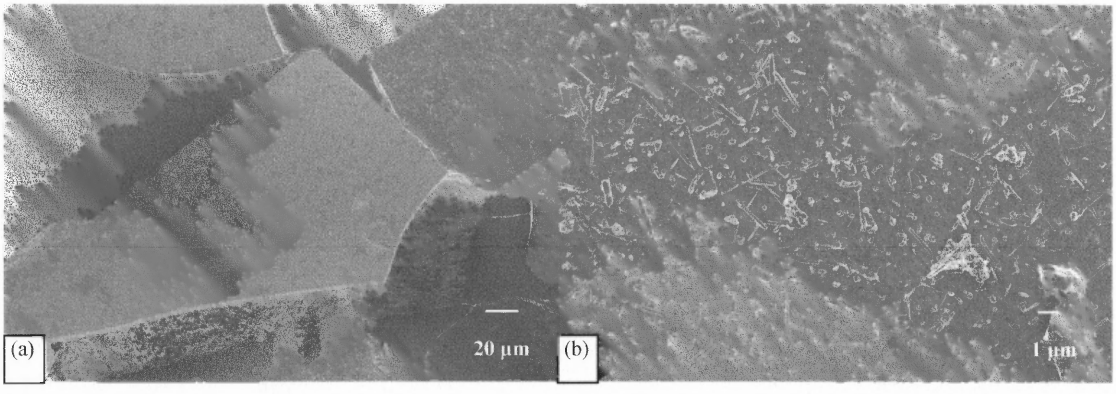

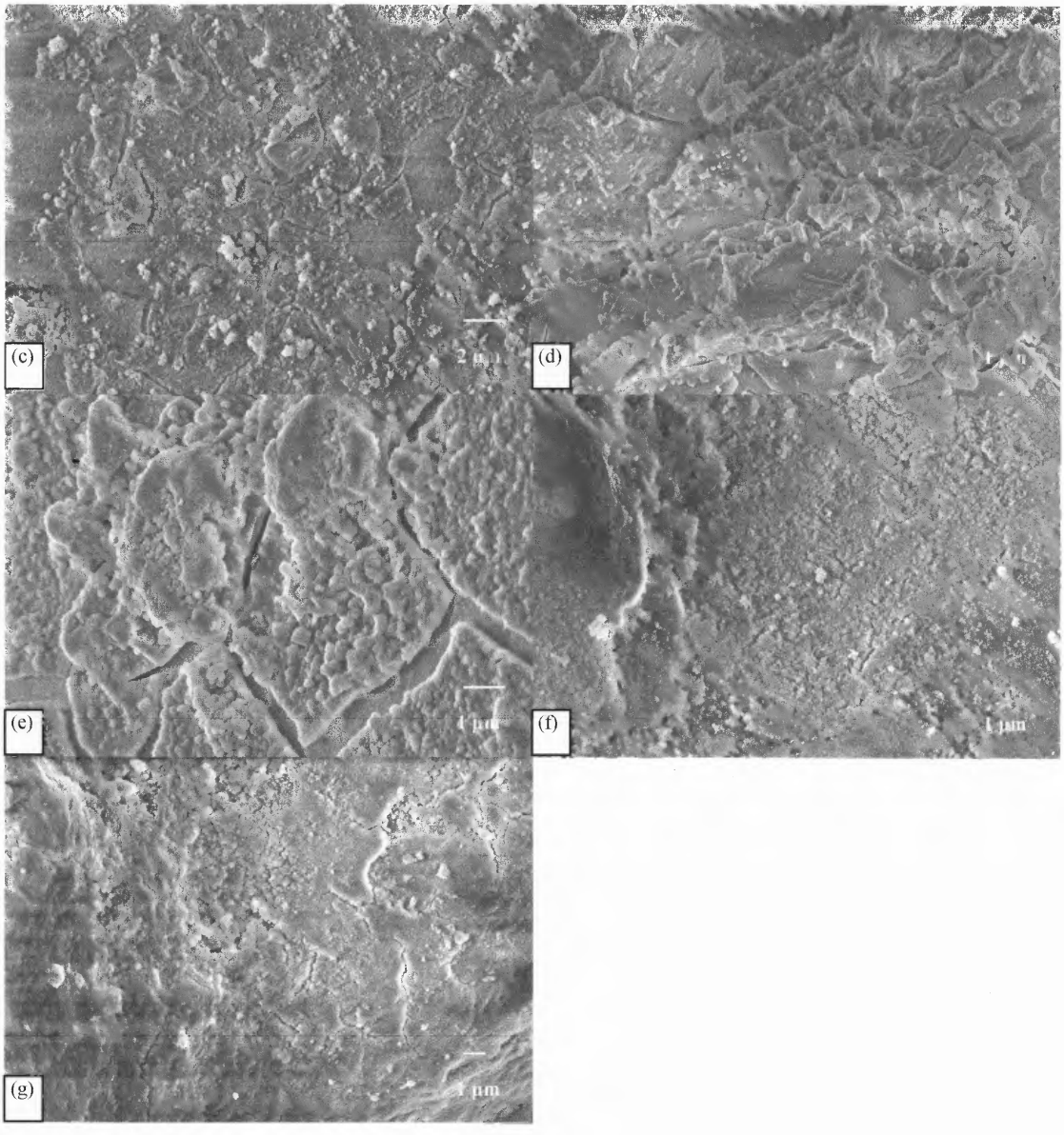

Figure 6.4 Bioglass powder before and after immersion in DW and SBF. (a) Before immersion. (b) Before immersion at higher magnification. (c) After six hours immersion in DW. (d) After six hours immersion in SBF. (e) After six hours immersion in SBF at higher magnification. (f) After 24 hrs immersion in SBF. (g) After 168 hrs (one week) immersion in SBF.

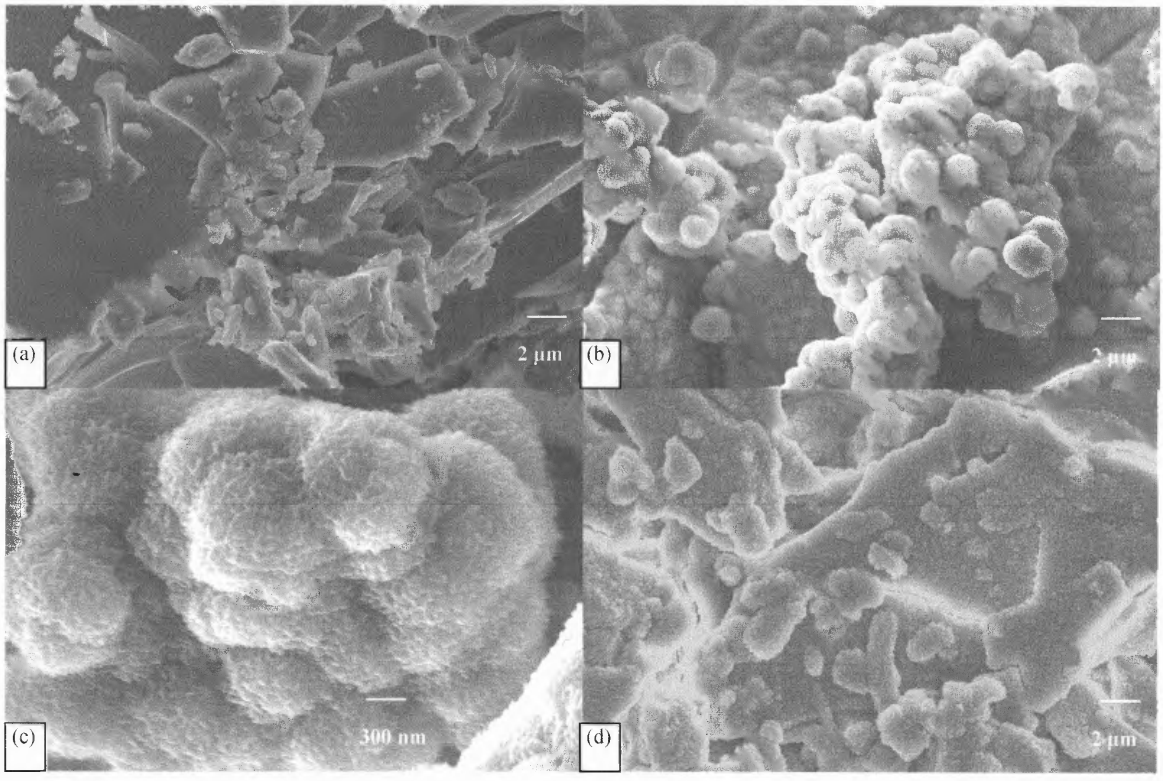

Figure 6.5 SEM micrographs of bioglass molded surface showing mineral growth on the exposed surfaces over one and two weeks periods immersion in SBF. (a) Before immersion. (b) After one week immersion; clusters of mineral precipitates are observed on the surface. (c) Higher magnification of (b); closer view of the clusters reveals needle shaped nanosized crystallites. (d) After two weeks immersion; area appears to be fully covered with mineral precipitates.

EDX results (Fig. 6.6) for the bioglass molded surface showed the changes in Na, Ca, P and Si concentrations at different immersion periods. The ratio of calcium to phosphorus changed towards a 1.67 value as a function of exposure time presumably due to the formation of hydroxyapatite on the bioglass surface.

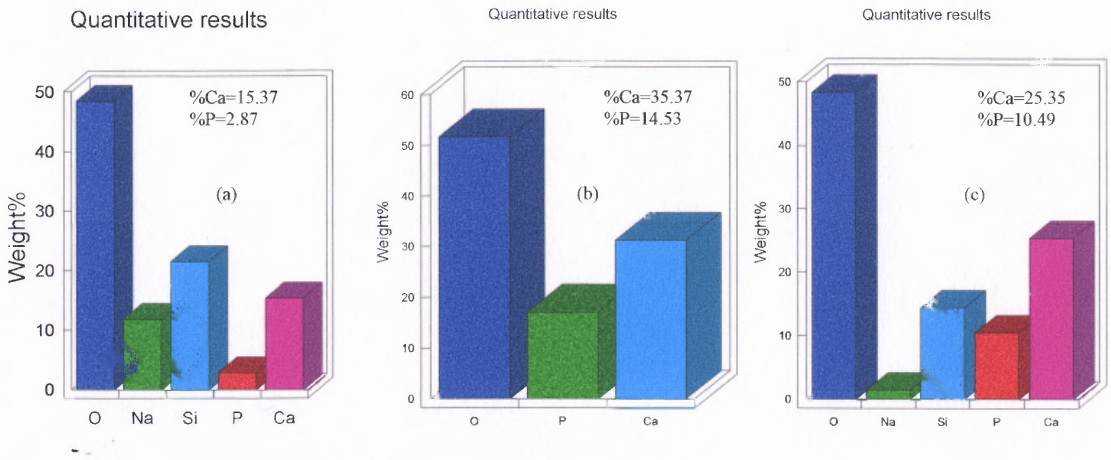

Figure 6.6 EDX elemental analysis of bioglass compressed surface as a function of exposure time showing a Ca/P ratio approaching 1.67. (a) Before immersion; Ca/P ratio equals to 5.36. (b) After one week immersion; Ca/P ratio equals to 2.43. (c) After two weeks immersion; Ca/P ratio equals 2.41.

Figure 6.7 shows XRD spectra for bioglass powder before and after immersion in DW and SBF. For amorphous bioglass, an apatite peak [212] appearing at 32° after six hours immersion became less broad with respect to longer immersion times, suggesting formation of apatite with higher crystallinity. This is in agreement with data of Fulgueiras et al. (1993) showing that the amorphous $CaO-P_2O_5$-rich layer starts forming in as little as 5-10 minutes, whereas the crystalline phase develops after 90-360 minutes on bioglass. Kontonasaki et al (2002) showed that the crystallization of the HA layer for PerioGlass powder (a Bioglass® Synthetic Bone Graft Particulate) appears to be completed after 24 hours immersion in SBF, and the precipitation that could be observed after 18 hours was an amorphous $CaO-P_2O_5$-rich layer. These results are in reasonable agreement with the results of our study for the initial testing periods.

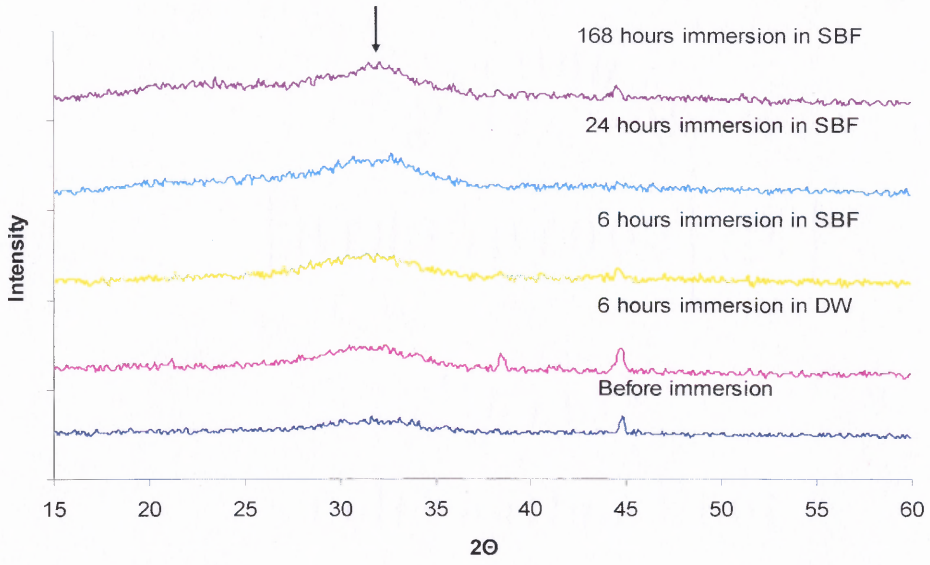

Figure 6.7 XRD spectra of bioglass powder before and after immersion in DW and SBF.

In order to compare the different rates in nucleation and growth for different filler sample preparation procedures, non polished rods of bioglass were cut in discs measuring 12 mm diameter and 2.65 mm thickness and tested in SBF solution. Figure 6.8 shows SEM micrographs of the discs before and after three, five and seven days of SBF immersion. Results in surface morphology are similar to the results for the compression molded samples, as expected. The irregularities on the disc surface appear to have acted as nucleation sites for apatite formation. It should be noted that results with polished discs showed zero nucleation/growth.

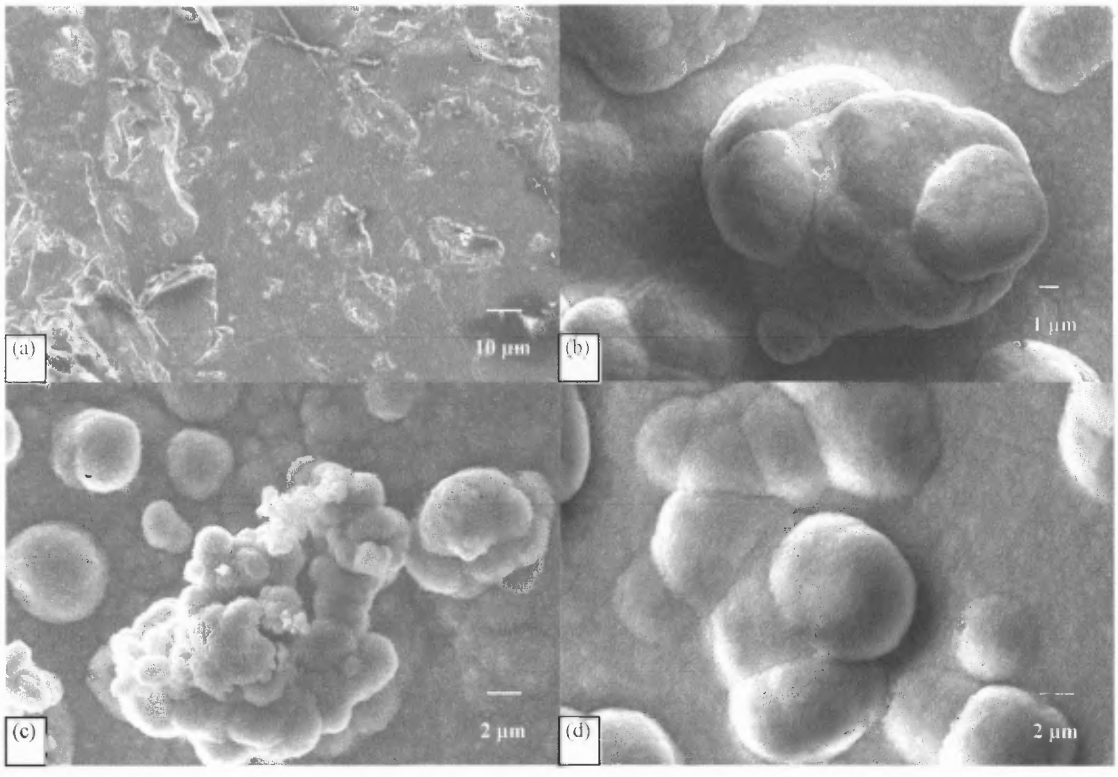

Figure 6.8 SEM micrographs of bioglass disc surface showing mineral growth on the exposed surfaces over three, five and seven day periods immersion in SBF. (a) Before immersion in SBF; surface irregularities are present. (b) After three days immersion; clusters of mineral precipitates are observed on the surface. (c) After five days immersion. (d) After seven days immersion; area appears to be homogeneously covered with mineral precipitates above and beneath the irregularities.

Figure 6.9 represents EDX results for the bioglass disc, showing the changes in Na, Ca, P and Si concentrations with respect to different immersion periods. The ratio of Ca/P changed from 5.36 before immersion to 1.70 after seven days immersion in SBF. This value is very close to the biological apatite (1.67) and confirms the formation of hydroxyapatite on the disc surface. Discs appear to reach terminal Ca/P values earlier than compressed surfaces, which would be due to the different manufacturing processes.

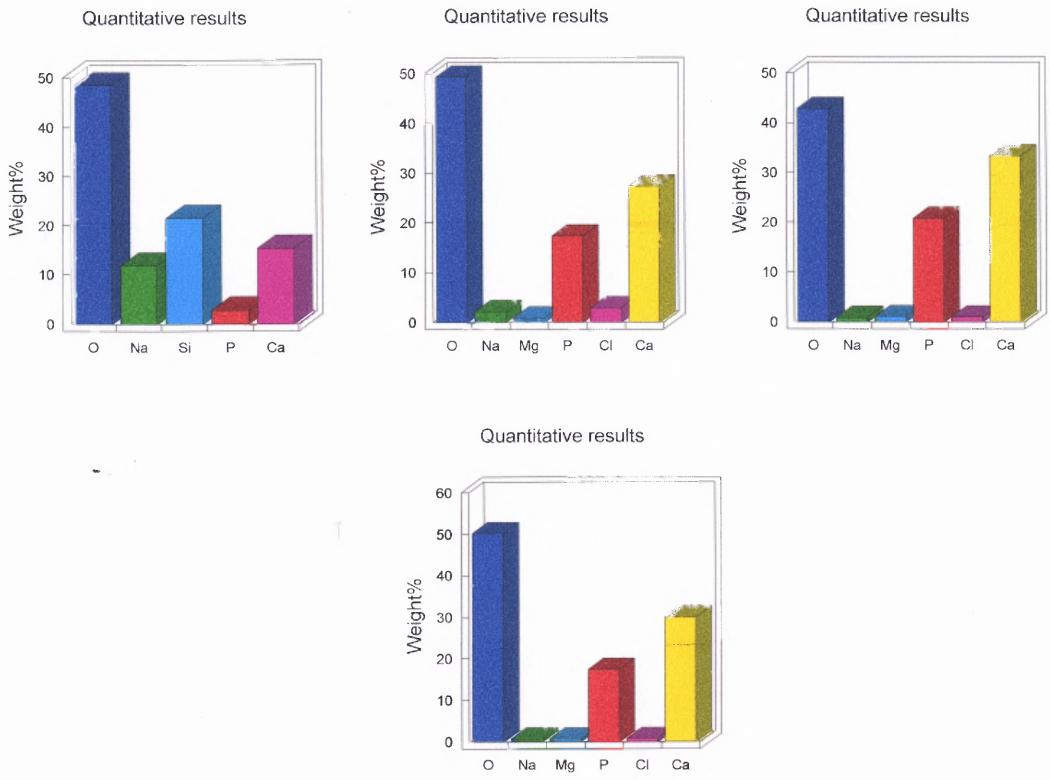

Figure 6.9 EDX elemental analysis of bioglass discs as a function of exposure time showing a Ca/P ratio approaching 1.67. (a) Before immersion; Ca/P ratio equals to 5.36. (b) After three days immersion; Ca/P equals to 1.59. (c) After five days immersion; Ca/P equals to 1.60, (d) After seven days of immersion; Ca/P equals to 1.72.

SEM analysis of data obtained with bioglass powder 1393 (BG1393) after immersion in DW and SBF showed little or no apatite growth. XRD data were very much different that those obtained with bioglass showing peaks at different 2θ locations than those corresponding to apatite. The composition of this glass is significant different than that of bioglass (see Table 5.1); furthermore, no decay rates are available from the manufacturer that would assist in the interpretation of the observed behavior. SEM and XRD data for this particular glass are shown in Appendix D.

6.2 Bioactivity of PCL Composites

In the case of PCL composites five fillers (HA, β-TCP, $CaCO_3$, bioglass, CS) and two different processing methods were used: solution and melt mixing. The results and the effect of both processing methods are presented in a parallel manner for better understanding.

6.2.1 SEM Characterization

Figure 6.10 includes SEM micrographs of extrusion processed unfilled PCL before and after immersion in SBF. Figure 6.10(a) representing the polymer surface before immersion showed some surface roughness and cracks, possibly the result of defects during sample preparation. No obvious changes, as expected, were evident on the polymer surface after immersion (Figs. 6.10(b), 6.12(c)) with no mineral nucleation and growth.

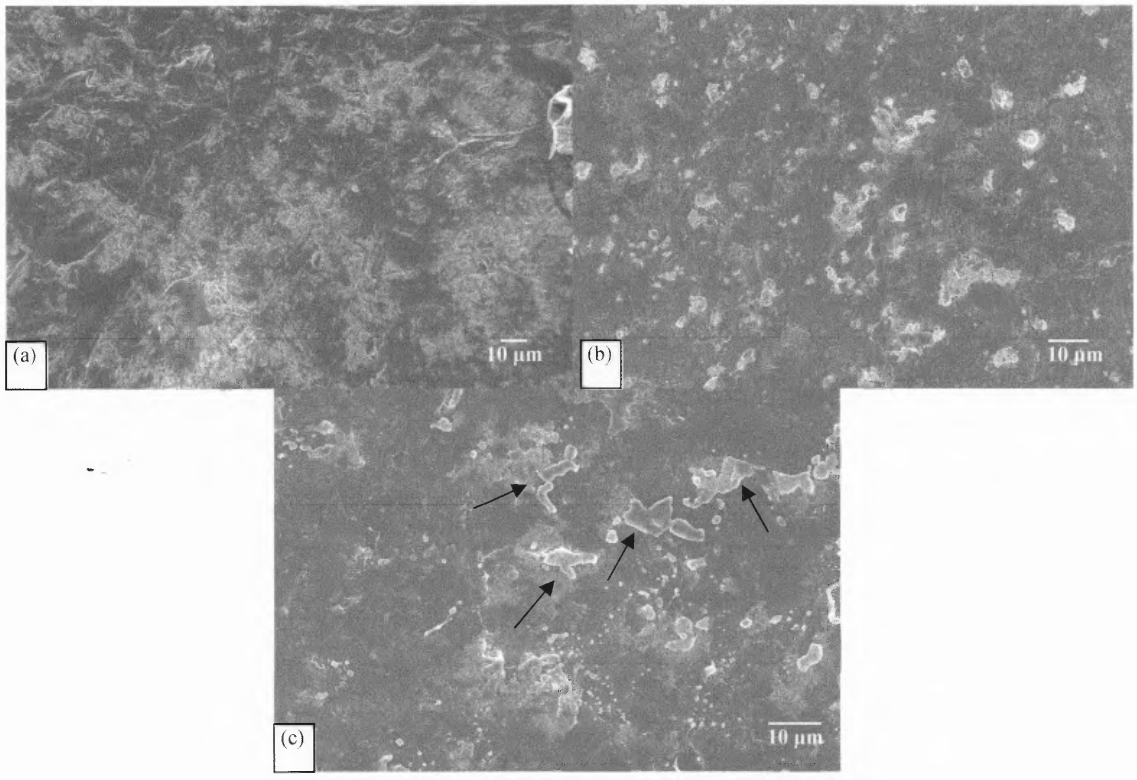

Figure 6.10 SEM micrographs of extrusion processed unfilled PCL samples before and after immersion in SBF solution showing no mineral precipitation. (a) Before immersion; some surface roughness due to processing conditions can be observed. (b) After one week immersion; no obvious changes, only formation of some cracks. (c) After four weeks immersion; no precipitation, just cracks and surface roughness similar to previous time periods.

In the case of composites described below, the diffusion of the SBF through a thin layer of the surface polymer is followed by attack of the bioactive fillers; these will eventually start decaying and partially dissolve, while exhibiting apatite forming ability as per the mechanisms discussed by Kim et al. (2005) for calcium phosphates, Hench (1988) for bioglass and De Aza (2000) and Siriphannon et al. (2002) for calcium silicate. It is generally expected in tissue engineering (Lei et al. 2007) that the degradation rate

should be slower than the bone formation since the biomaterial needs to have sufficient mechanical properties to support the bone regeneration process.

6.2.1.1 PCL/HA Composites. Figure 6.11 represents SEM micrographs of *extrusion processed* PCL/HA surfaces. The non immersed in SBF surface appears to be rough, possibly as a result of the processing conditions. This roughness could result to more nucleation sites for apatite formation. After one week (Figs. 6.11(b), 6.11(c)), degradation of the thin layer of the polymer surface has brought HA particles in contact with the SBF solution and some mineral precipitates in the form of small spherical crystals are evident. According to EDX analysis (results not shown), the Ca/P ratio was 1.67 and 1.52 after one and four weeks respectively. Lei at al. (2007) suggested that a Ca/P ratio of 1.67 is the one of the apatite needed for bone regeneration, whereas the 1.50 ratio implies β-TCP formation that will act as a template for further apatite formation. A possible explanation for this opposite effect could be that apatite has already been formed in one week time period through other calcium phosphates; since SBF was not replenished throughout our experiments calcium reservoirs (for the four week period) were not sufficient for further surface reactions and apatite formation.

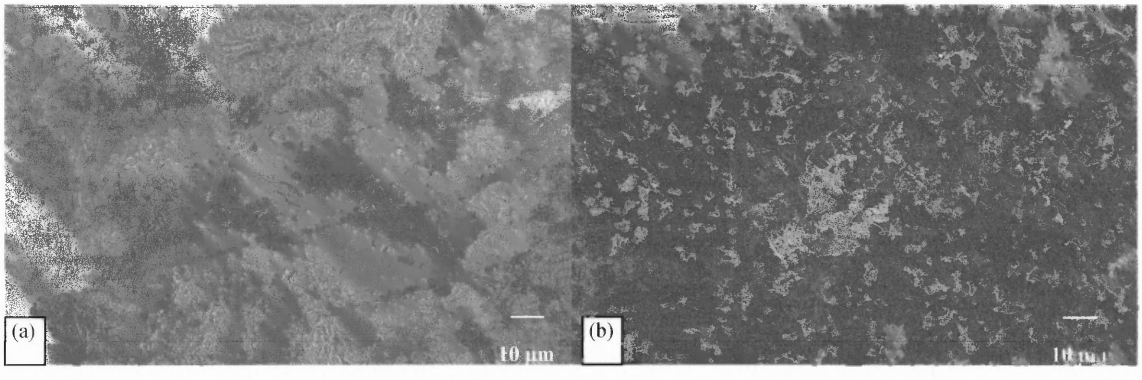

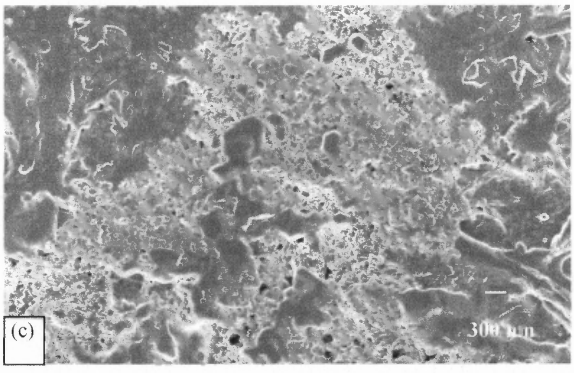

Figure 6.11 SEM micrographs of extrusion processed PCL/HA samples before and after immersion in SBF solution showing some initial mineral precipitation. (a) Before immersion; some surface roughness due to processing conditions can be observed. (b) After one week immersion; formation of some cracks possibly due to polymer degradation and some mineral precipitation is evident on the surface. (c) Higher magnification for after one week immersion samples; clusters of mineral precipitates are detected on the sample surface.

Figure 6.12 shows SEM micrographs of the surfaces of *solution mixed* PCL/HA samples. The surface for the non exposed PCL/HA (Fig. 6.12(a)) appears to be smooth and free of defects. After one week immersion in SBF (Fig. 6.12(b)), cracks have formed and small spherical crystals appear on the composite surface, initiating the formation of apatite layer that would eventually cover the entire surface. Figure 6.12(c) shows a higher magnification of the one week exposed surface. It appears as if mineral precipitation covers an area further inside the sample surface than in the sample prepared by extrusion.

Differences in apatite formation behavior may be related to differences of extrusion vs. solution mixed samples in terms of: a) thermal history and its effects on the stability of the calcium phosphate fillers (Hench, 1998), b) crystallinity and thickness of the outer surface polymer layer and their effects on permeation rate and degradation, and c) distribution of filler particles at/or near this outer layer and its effect on uniformity of

mineral coverage. In addition to the mixing method, differences in chemical structure, impurities, porosity and particle size of the bioactive ceramic (Laurencin and Khan, 2006) play an important role in the behavior of the composite material. Many researchers have synthesized the bioactive HA filler (Yu et al. 2005, Higashi et al. 1986, Hao et al. 2002) in order to control the resorption rate and, thus, the bioactivity.

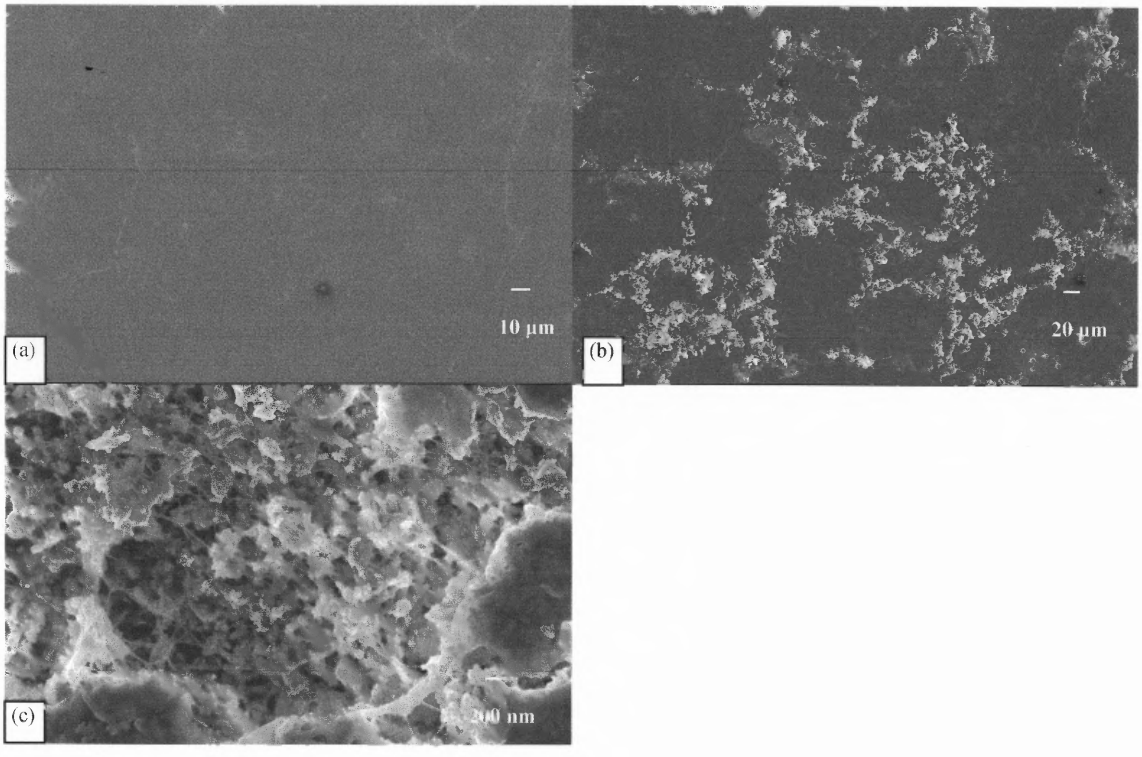

Figure 6.12 SEM micrographs of solution mixed PCL/HA samples before and after immersion in SBF solution showing some mineral precipitation in the form of spherical crystals. (a) Before immersion. (b) After one week immersion; formation of some cracks possibly due to degradation and some mineral precipitation is evident on the surface. (c) Higher magnification for after one week immersion; clusters of mineral precipitates were detected on the sample surface.

6.2.1.2 PCL/β-TCP Composites. Figure 6.13 represents SEM micrographs of *extrusion processed* PCL/β-TCP surfaces. Before immersion (Fig. 6.13(a)) the surface appears to be rough with some cracks. After one week immersion (Fig. 6.13(b)), some precipitation through the formed cracks appears on the surface, similarly to the HA composite. At higher magnification (Fig. 6.13(c)), the structure of the precipitates appears to be spherical crystallites and remains the same even after four weeks immersion (Fig. 6.13(d)).

In a study conducted by Xin et al. (2005), out of all bioactive ceramics (including HA, glass ceramics, bioglass, α-TCP and β-TCP), β-TCP although having a very good ability of osteointegration, shows poor ability of apatite formation both *in vitro* and *in vivo.* In the work of Lei et al. (2007) 20% PCL/TCP composite scaffolds showed the initiation of formation of an apatite layer on the scaffolds surface after 17 days of SBF immersion. Mineral precipitates such as octacalcium phosphate (OCP) and β-TCP were the precursors for the formation of apatite. After four weeks immersion, apatite had formed continuously on the surface of the scaffold. It is important to note the differences between our solid samples and scaffolds. Scaffolds with certain porosities have higher water uptake, which could lead to higher degradation rates, and also more nucleation areas that could be exposed to SBF. In addition, the different crystallographic features of TCP could lead to different apatite formation rates and uniformity.

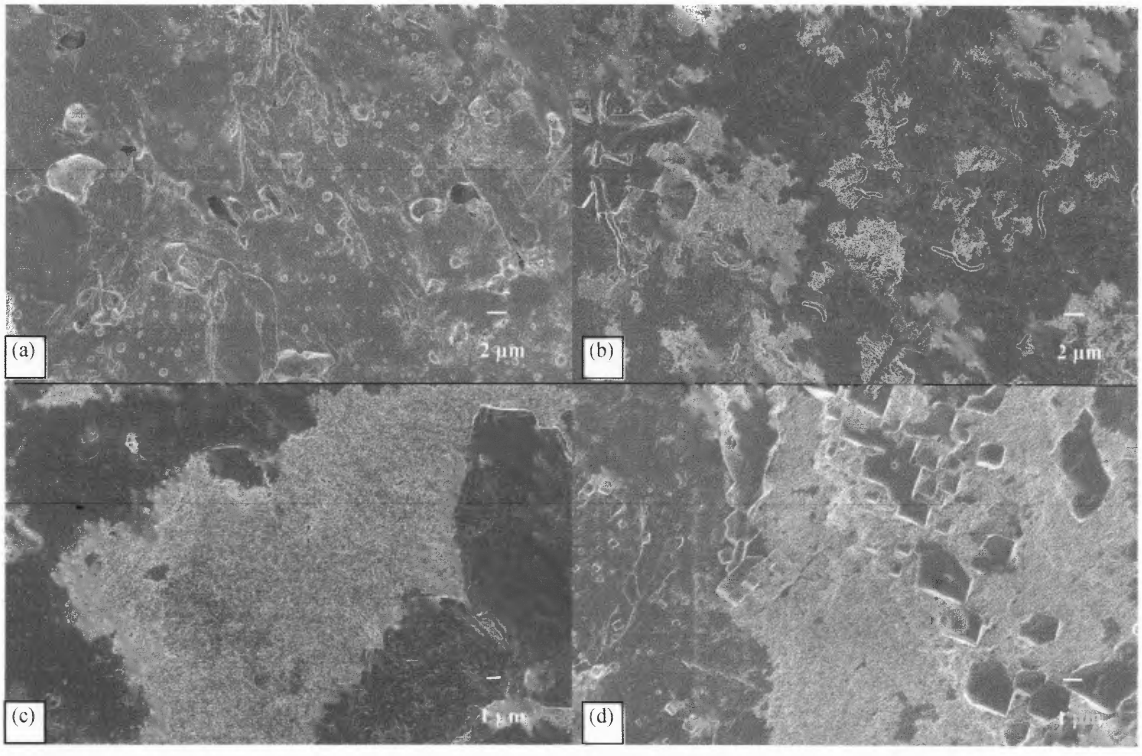

Figure 6.13 SEM micrographs of melt mixed PCL/TCP samples before and after immersion in SBF solution showing some mineral precipitation in the form of spherical crystals. (a) Before immersion. (b) After one week immersion; formation of some cracks possibly due to degradation and some mineral precipitation is evident on the surface. (c) Higher magnification for after one week immersion; clusters of mineral precipitates were detected on the sample surface. (d) After four weeks immersion; Similar structures with the one week exposure. Some salt crystals from the solution are evident on the sample surface.

In the case of *solution mixed* PCL/β-TCP composites, it is evident from Fig. 6.14 that after one week immersion mineral precipitation in the form of small spherical crystals appears on the composite surface. Morphology is different and more pronounced compared to the case of melt mixed composites. Once more the effect of different processing conditions is apparent.

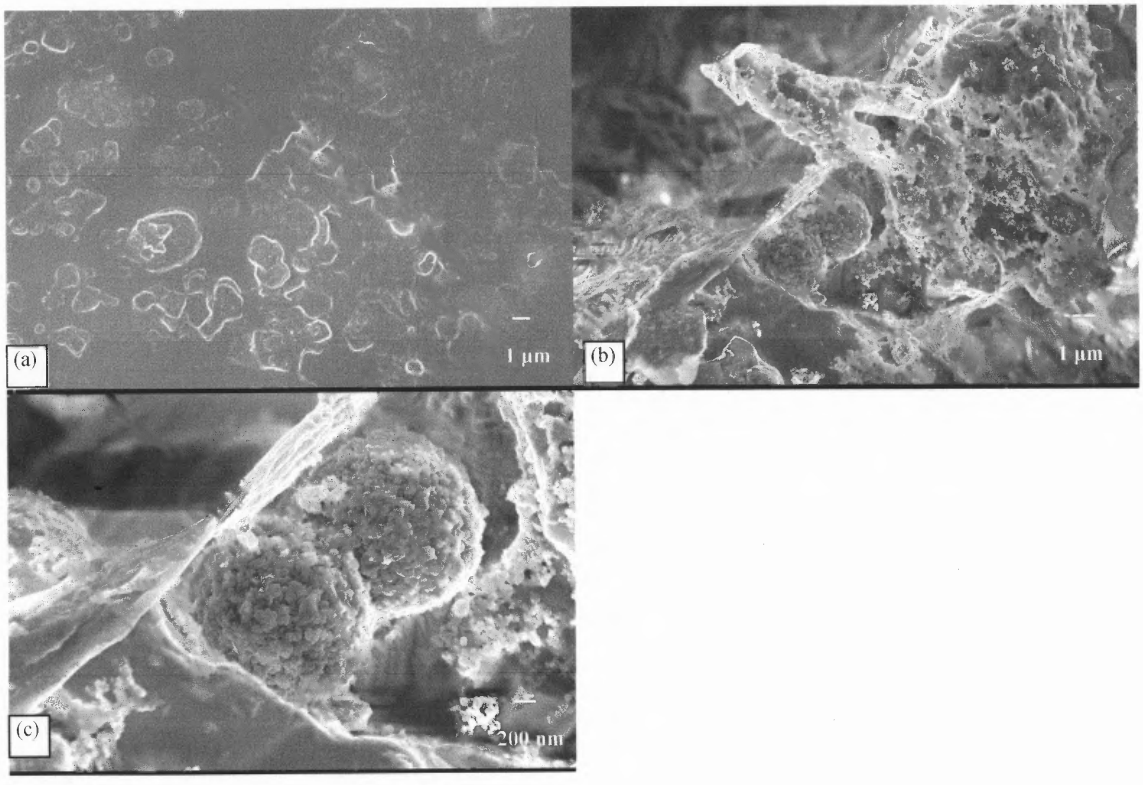

Figure 6.14 SEM micrographs of solution mixed PCL/TCP samples before and after immersion in SBF solution showing some mineral precipitation in the form of spherical crystals. (a) Before immersion. (b) After one week immersion; formation of small spherical crystals appear on the surface (c) Higher magnification for after one week immersion; clusters/globules of mineral precipitates were detected on the sample surface.

6.2.1.3 PCL/$CaCO_3$ Composites. In the case of PCL/$CaCO_3$ *extrusion mixed* composites, SEM micrographs can be seen in Figure 6.15. After only one week immersion (Fig. 6.15(b)), many globules of mineral precipitates can be observed on the composite surface. At higher magnification (Fig. 6.15(c)), the globules seem to have a needle like, presumably apatite, structure that is similar to the one that had been observed in the case of bioglass filler. After four weeks immersion (Fig. 6.15(d)), the growth appears to be limited, possible due to the lack of SBF replenishment.

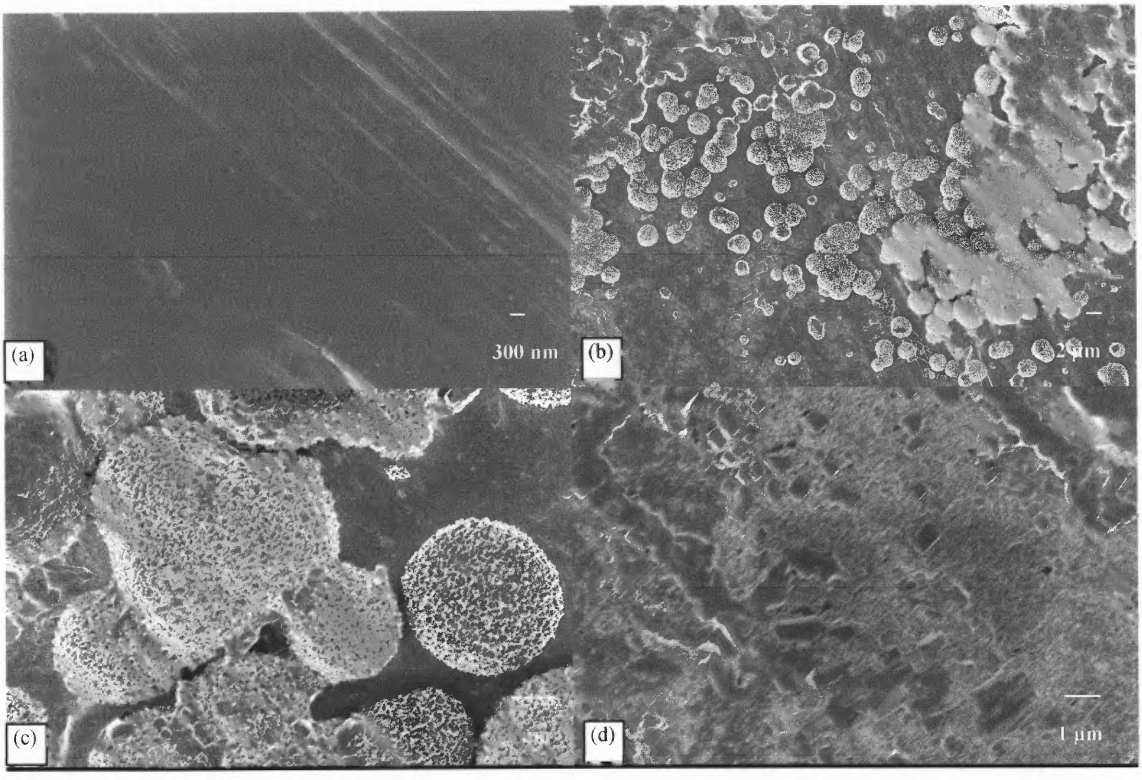

Figure 6.15 SEM micrographs of extrusion mixed PCL/ $CaCO_3$ samples before and after immersion in SBF solution showing some mineral precipitation in the form of spherical crystals. (a) Before immersion; sample surface free of roughness and cracks. (b) After one week immersion; formation of many small mineral globules appear on the surface (c) Higher magnification for after one week immersion; clusters/globules of mineral precipitates have a needle like structure. (d) After four weeks immersion; limited mineral precipitation.

6.2.1.4 PCL/bioglass Composites. Figure 6.16 represents *extrusion mixed* SEM micrographs of PCL/bioglass surfaces. There was mineral precipitation after only one week exposure in SBF (Fig. 6.16(a)). At higher magnification (Fig. 6.16(b)), the small spherical crystals represented a precipitated mineral morphology that was similar to that reported in literature (Lu et al. 2005, Zhang et al. 2004). The crystals would have been expected to grow and form a layer of apatite on the surface that would later crystallize to bonelike apatite. However, this was not evident in our case even after eight weeks of immersion, as shown in Figure 6.16(c) taken at lower magnification, where no significant

differences from the first week were observed. The reason could be that the human body is a constant reservoir of SBF, whereas under the present experimental conditions SBF was not replenished. In addition, the hydrophobic nature and slow degradation kinetics of the PCL may have also affected apatite formation. The sporadic mineral growth that appeared on the examined sample surfaces may also be related to the partial dissolution of the Ca-P deposition during immersion, due to changes in ion saturation, as suggested by Jaakola et al. (2004). The same authors showed considerable bioactivity of bioglass in a 96/4 molar ratio poly(ε-caprolactone-co-DL-lactide) matrix at high filler concentrations (over 40 wt%) and high filler surface area/volume ratio over a six month period. Bioactivity was, in general, assessed through SEM microscopy, FTIR and ion concentration analysis and, in addition, SBF was replenished over the testing period. It is of interest to note that in spite of the presumed higher hydrophilicity of the copolymer matrix vs. our homopolymer and the presence of more nucleation sites due to its easier hydrolysis, comparison of the copolymer composites containing 40 wt% bioglass (particle size 90-315μm) with the present homopolymer composites containing 30 wt% bioglass (particle size 90-212μm) indicated limited apatite growth in both cases up to three months exposure.

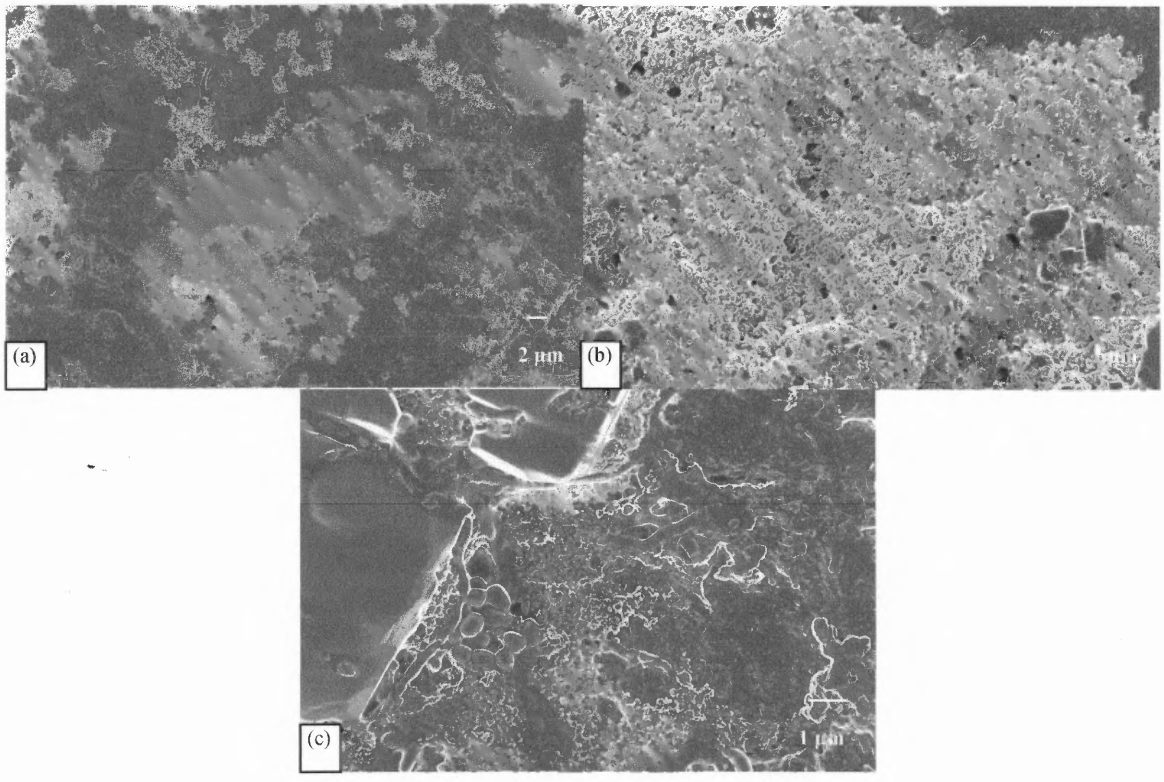

Figure 6.16 SEM micrographs of extrusion mixed PCL/bioglass composites after immersion in SBF solution showing mineral precipitation on the polymer surface. (a) After one week immersion; mineral precipitation can be observed on the surface of the composites. (b) Higher magnification of (a); small spherical crystals appear on the surface of the composite. (c) After eight weeks immersion; similar spherical crystals have precipitated on the surface.

6.2.1.5 PCL/CS Composites. Figure 6.17 includes a series of SEM micrographs of *extrusion mixed* PCL/CS composites as a function of immersion time. Figure 6.17(a) represents a non exposed area free of any precipitates. By contrast to Figure 6.16(b) for PCL/bioglass composites, one week exposure (Fig. 6.17(b)) results in much lower surface coverage. However, significant surface coverage could be observed after four and eight week periods in the form of spherical calcium phosphate crystals. This may be due to the presence of non consumed Ca, Si and P in the SBF as a result of the slower nucleation activity during the first week. Note that the spherical agglomerated texture of the precipitates after four and eight weeks (Figs 6.17(c) and 6.17(d)) are not appreciably

different than that observed by Rhee (2003) after only seven days. The faster and more uniform nucleation and growth of apatite crystals observed by this author may be due to the much lower molecular weight PCLs (MW from 1960 to 4167) and the type and more uniform distribution of the silica nano-hybrid filler used.

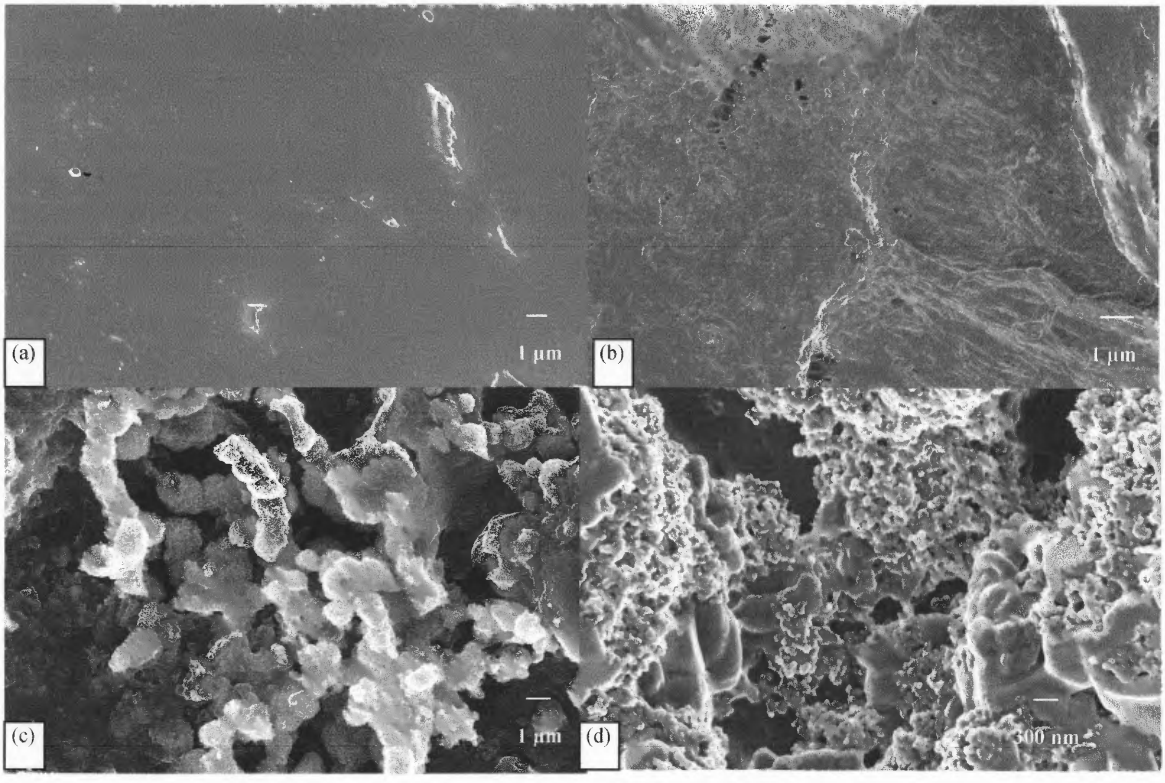

Figure 6.17 SEM micrographs of extrusion mixed PCL / CS composite surface before and after SBF immersion. (a) Before immersion. (b) After one week immersion; some surface roughness can be observed corresponding to slower nucleation and growth than in the bioglass composite. (c) After four weeks immersion; clusters of mineral precipitate on the polymer surface. (d) After eight weeks immersion; mineral formation has uniformly covered the composite surface.

In the case of *solution mixed* PCL/CS composites, Figure 6.18 represents SEM micrographs before and after SBF immersion. There is an apparent growth of nano-feature flake- and needle-shaped microparticles on the exposed surfaces similar to bone-like apatite layer (Liu and Ma (2004)). Nucleation and growth seems to be faster for the

solution mixed PCL/CS composites. As mentioned earlier, this could be due not only to different processing temperatures and history, but also differences in surface morphology (thinner outer layer for the solution mixed composites).

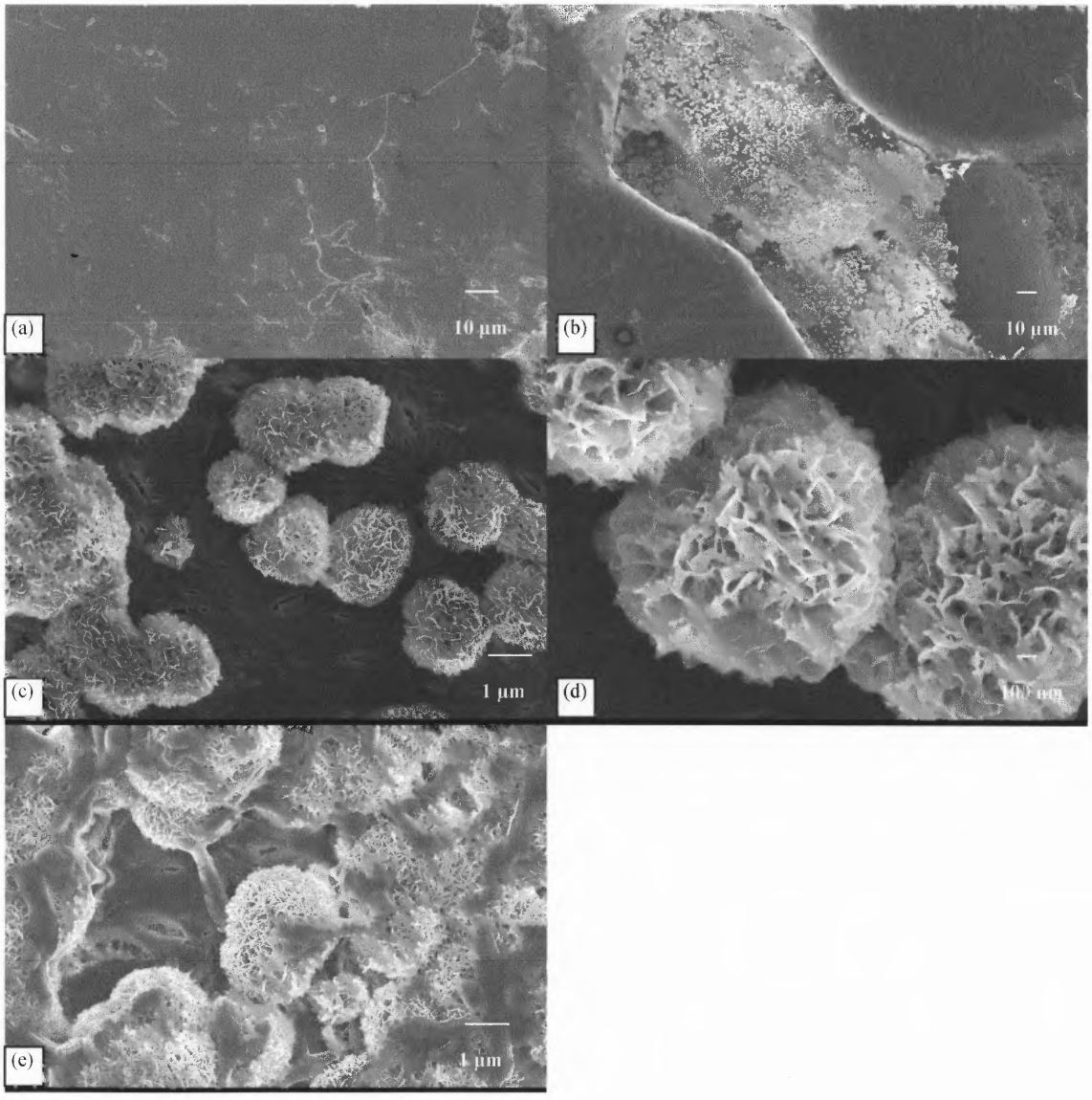

Figure 6.18 SEM micrographs of solution mixed PCL/CS composite surface before and after SBF immersion. (a) Before immersion. (b) After one week immersion; nucleation and growth appears in one of the cracks. Many spherical precipitates are present. (c) Higher magnification of 6.18(b); different sized globules of mineral precipitate on the polymer surface. (d) Higher magnification of 6.18(c); mineral precipitation at higher magnification appears as needle like crystallites. (e) After two weeks immersion; spherical mineral precipitates cover the surface along with degradation residues.

6.2.2 XRD Data and Concentration Changes in SBF

The time for initial formation of apatite crystals on the surface of the composites is shown in the XRD data of Figures 6.21 to 6.25. For the HA composite (Fig. 6.19), the apatite peaks at 25°, 32°, 40° and 49° are attributed to apatite formation (Yu et al. 2005, Ni and Wang, 2002). These peaks are more evident after one week, whereas after four weeks are weaker. For the β-TCP composite, (Fig. 6.20) apatite peaks appear at 25°, 31°, 32° and 49° and are again more pronounced after one week immersion than after four weeks. For the $CaCO_3$ composite (Fig. 6.21), apatite peaks appear after 1 week at around 32^0, 40° and 49° and are weaker after four weeks immersion. For the BIOGLASS composite (Fig. 6.22) the apatite peak at 32° (Fujibayashi et al. 2003, Yu et al. 2005 and Kasuga et al. 2003) appearing first after one week, was more evident after eight weeks, although still very weak. For the CS composites (Fig. 6.23), in addition to a peak at 32°, a second peak attributed to apatite at about 26° could also be observed after one week. Both peaks appeared to be very weak after four and eight weeks immersion suggesting slow and random nucleation and growth of the apatite crystals in the high molecular weight PCL of the present work, in relative agreement with similar findings by Rhee (2003).

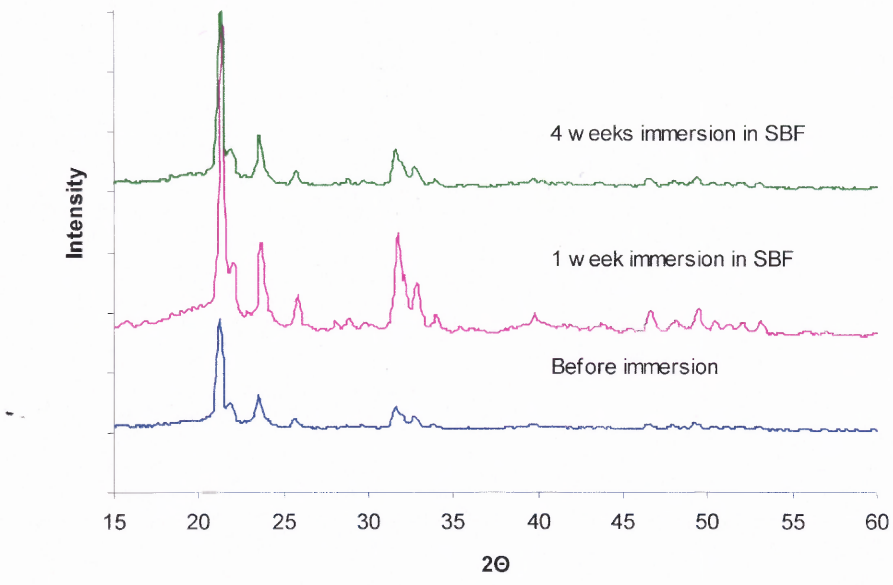

Figure 6.19 XRD spectra of PCL/HA composite before and after immersion in SBF. The peaks at 31^0 and 32^0 that formed after one week exposure in SBF will eventually become a peak at 32^0. This peak, along with the peaks at 25^0, 40^0 and 49^0 correspond to hydroxyapatite.

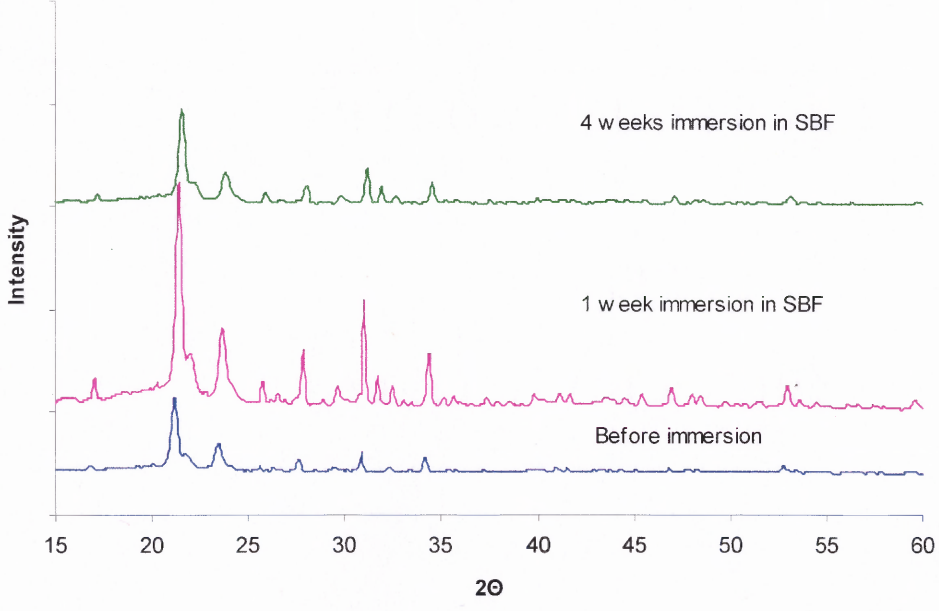

Figure 6.20 XRD spectra of PCL/β-TCP composite before and after immersion in SBF. The peaks at 31^0 and 32^0 that formed after one week exposure in SBF will eventually become a peak at 32^0. This peak, along with the peaks at 25^0 and 49^0 correspond to hydroxyapatite and appear weaker after four weeks immersion.

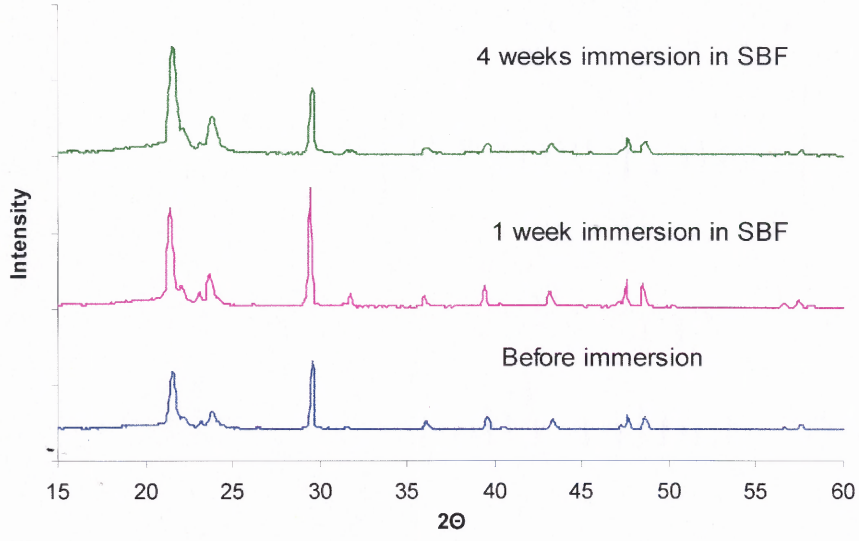

Figure 6.21 XRD spectra of PCL/$CaCO_3$ composite before and after immersion in SBF. The peaks around 32^0, 40^o and 49^o first appear after one week immersion and are weaker after four weeks immersion.

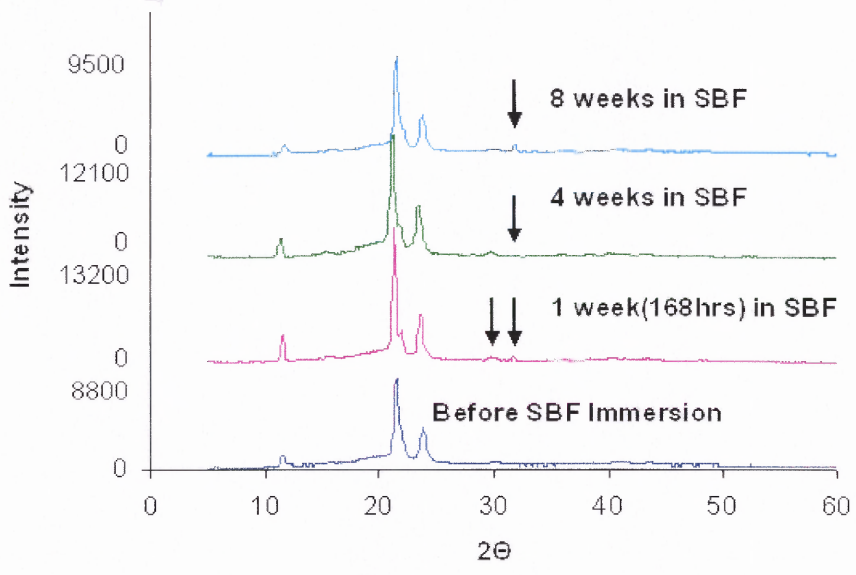

Figure 6.22 XRD spectra of PCL / bioglass composite before and after immersion in SBF. The peaks at 31^0 and 32^0 that formed after one week exposure in SBF eventually became a peak at 32^0 after four weeks. This peak corresponds to hydroxyapatite and becomes even more intense after eight weeks.

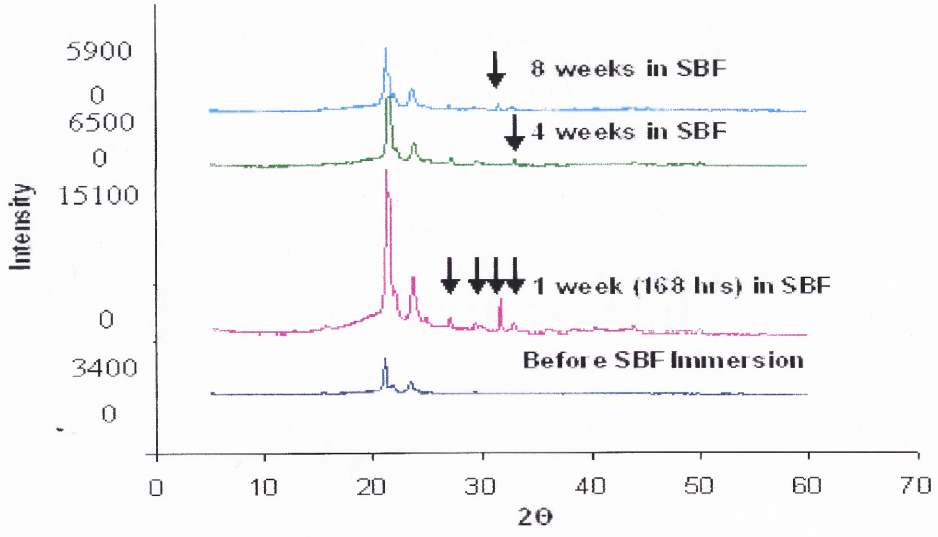

Figure 6.23 XRD spectra of PCL/CS composite before and after immersion in SBF. Peaks at 31^0 and 33^0 appear after one week immersion and will eventually become a peak at 32^0 with longer immersion periods.

The results from AA spectroscopy on SBF used in the immersion of PCL/bioglass and PCL/CS composites (Fig. 6.24) showed that the calcium present in both fillers diffuses out as a function of time. Note that there is a higher rate of release of calcium in the CS composites. In the case of the bioglass composites, initially there was a lack of change in calcium concentration that may be the result of balancing of the release and consumption processes since calcium diffuses out of the fillers but is also consumed from the SBF solution towards the surface of the immersed sample. This may indicate a faster rate of apatite formation for the bioglass composites although this is not corroborated by the previous XRD and SEM results. In Figure 6.24, the slightly abnormal behavior of the unfilled polymer may be related to the presence of precompounded additives/impurities.

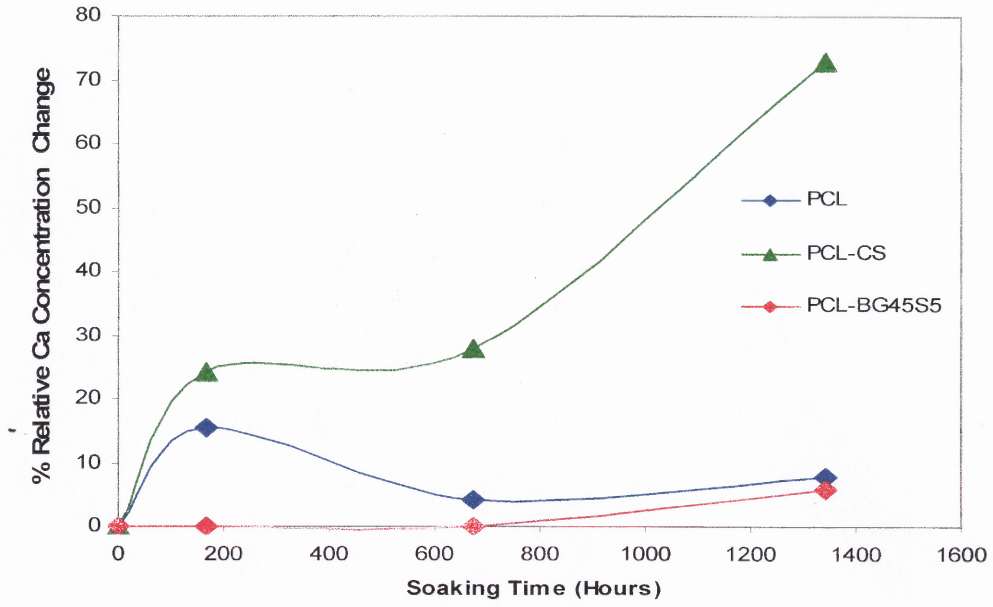

Figure 6.24 Relative changes in calcium concentration for the PCL composites after soaking in SBF. The changes in calcium concentration is a two way process that involves its release by the fillers and also its consumption from SBF to the surface of the bioactive material. Values shown are mean of two samples per group.

Similarly, UV-Vis spectroscopy (Fig. 6.25) revealed that phosphorus is being consumed from the SBF solution towards the surface of the PCL and the surfaces of both composites. However, the PCL/bioglass composite started to release phosphorus to the SBF solution after about four weeks immersion period, whereas the PCL/CS composite continued consuming phosphorus. This may be another indication of the faster rate of apatite formation on the bioglass composites. It should be noted that the calcium and phosphorous ionic concentrations of the SBF solution used in this work was shown to be somewhat higher than the calculated concentrations based on Kokubo's ideal recipe (1990). For example phosphorous concentration in our control SBF prior to immersion

was 44 ppm versus 31 ppm. As a result, Figures 6.24 and 6.25 are using relative ion concentration changes instead of absolute numbers.

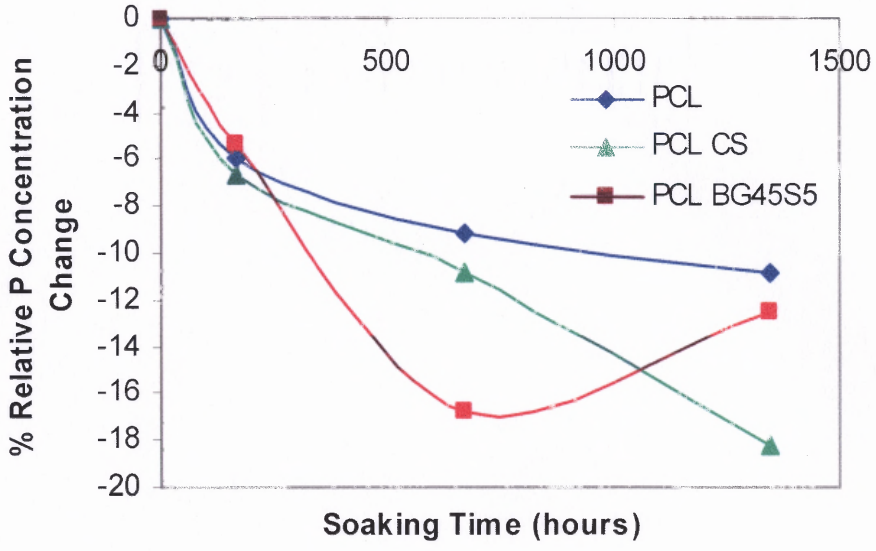

Figure 6.25 Relative changes in phosphorus concentration for the PCL composites after immersion in SBF. In all cases phosphorus is being consumed by the composites. In the case of PCL/bioglass, phosphorus releases only after eight week period. Values shown are mean of two samples per group.

6.2.3 Summary

In summary, SEM images for the melt processed PCL/bioglass composites showed mineral precipitation after the first week of immersion and lack of additional precipitation for the remaining testing period (four and eight weeks). This was not in agreement with the XRD data of the same composites that showed an apatite peak at 32°, which increased in intensity as a function of immersion time up to eight weeks. By comparison, apatite growth from XRD results was evident from the initial experiments (up to one week) with the neat bioglass filler; SEM and EDX data for the neat filler also showed coverage and uniformity of an apatite layer after immersion. The limited

bioactivity in the bioglass composite could be due to the PCL hydrophobicity and the resulting slow degradation rate. The longer immersion periods for the composite samples vs. the neat fillers could explain these differences. In addition, the coverage area examined in SEM and EDX is much more localized compared to the larger testing area of the XRD samples.

Results from AA and UV-Vis spectroscopy on bioglass composites, showed no change in Ca concentration during the first four weeks, possibly due to equilibrium in Ca concentration diffusing in and out of the composite sample, and a continuous consumption of P from the SBF up to four weeks. These results suggest that the bioglass composite could show additional apatite growth after the four week immersion period; this was delayed due to the slow degradation kinetics of the outer PCL layer and since SBF was not replenished throughout the testing period, ion concentrations were insufficient for reactions leading to the apatite layer formation.

In the case of melt processed CS composites SEM data showed mineral surface coverage after the first four week period. Nucleation and growth were slow and as a result Ca, Si and P ions had not been consumed up to four weeks. After four and eight weeks, there was significant coverage. As in the case of PCL/bioglass composites, XRD data were not in agreement with SEM results since the apatite peaks that appeared after one week were weaker after four and eight weeks. Again, these results could be due to the different testing areas used in the experiments.

AA and UV-Vis spectroscopy experiments were in agreement with SEM data since there was a continuous Ca release and P consumption, denoting that reactions could still take place after four weeks. In the case of solution mixed CS composites there was a

faster nucleation and growth that could be due to different processing temperatures and history, but also due to differences in surface morphology. A similar behavior was shown for the neat filler in the case of powder vs. molded surface. It appeared that the molded surface of the filler showed more apatite growth due to the different sample manufacturing method.

6.3 Bioactivity of PLA Composites

6.3.1 SEM Characterization

Figure 6.26 includes SEM micrographs of melt processed PLA before and after SBF immersion. Figure 6.26(a) represents the unfilled polymer surface before immersion in SBF. Figure 6.26(b) and (c) represent the PLA surface after one and eight weeks immersion, respectively. There is no apparent nucleation and growth, only some surface roughness due to degradation and possibly some salt deposition from the SBF solution.

Results with PLA filled with bioglass and CS are discussed below.

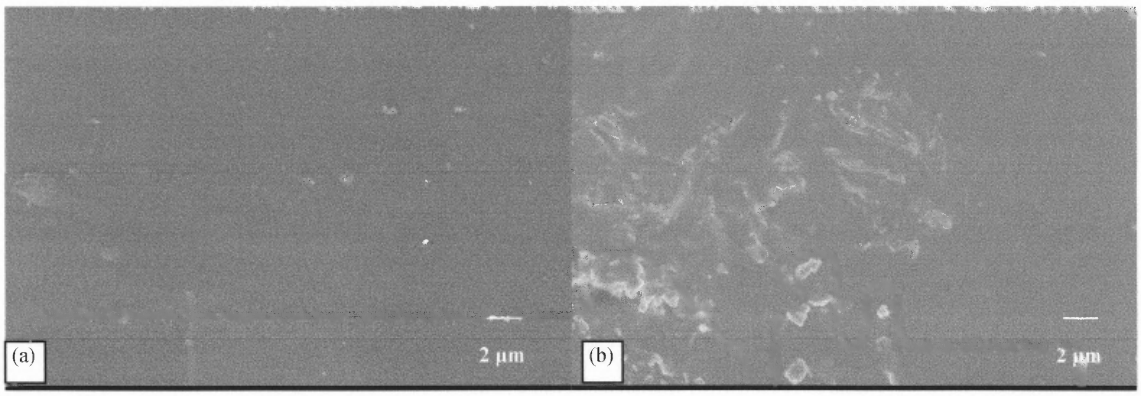

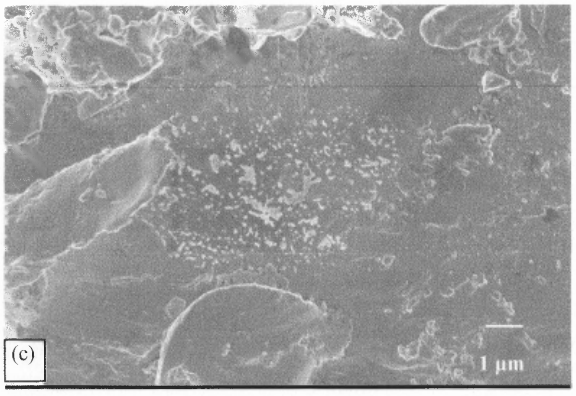

Figure 6.26 SEM micrographs of melt processed unfilled PLA samples before and after immersion in SBF solution showing no nucleation and growth. (a) Before immersion. (b) After one week immersion; no mineral precipitation, only some surface roughness occurs. (c) After eight weeks immersion; no precipitation, just surface roughness and salt deposition from the SBF.

6.3.1.1 PLA/bioglass Composites. Figure 6.27 represents SEM micrographs of melt processed PLA/bioglass surfaces. There was mineral precipitation after only one week exposure to the SBF (Fig. 6.27(b)). After four and eight weeks, the mineral crystals would have been expected to grow and form a crystalline bonelike apatite. However, as for the PCL/bioglass composites, this was not evident as no significant differences from week one were observed. This could again be due to the experimental conditions of this study, i.e. that SBF was not replenished, thus, not allowing more Ca and P ions to react and form the final bonelike apatite. EDX results support this argument, as Ca/P ratios were only 1.19 and 0.502 (results not shown) after one and four weeks, respectively. The mineral morphology of the spherical crystals that appeared after immersion in the SBF were similar to the ones reported in the literature (Zhang et al. 2004, Lu et al. 2005). Specifically, Zhang et al. (2004) reported that the apatite formation in the case of porous PLLA (composite scaffolds) was related to the PLLA hydrolysis, which resulted in a negatively charged PLLA surface. The Ca ions from the solutions were positively

charged and as a result attracted to the hydrolyzed PLLA surface. Apatite formed through the attraction of phosphate groups from the solution and the increase of local apatite ion activity product. According to the authors, the apatite formation on porous PLLA was enhanced by the addition of bioglass particles, similarly to this study. For the lower bioglass content, apatite formation was rapid, whereas this was not the case for the higher content. The delayed apatite formation for the higher bioglass content was, according to the authors, due to the greater bioactivity content, which resulted in more exposed glass surfaces and larger immersion ratio (the ratio of the immersed glass surface to the SBF volume).

In the study of Lu et al. (2005), composites of polylactide-co-glycolide (PLAGA) with bioglass were fabricated using the solvent-casting process. The rate of apatite formation was dependent on the bioglass content. The immersion time required for apatite formation decreased with increasing bioglass content. This is in agreement with the study of Zhang et al. (2004), although the critical parameter for such a comparison is the immersion ratio. Lu et al. (2005) found that the size and the overall surface coverage visibly increased with immersion time. This is not the case in the present study, since as has been already discussed above SBF was not replenished.

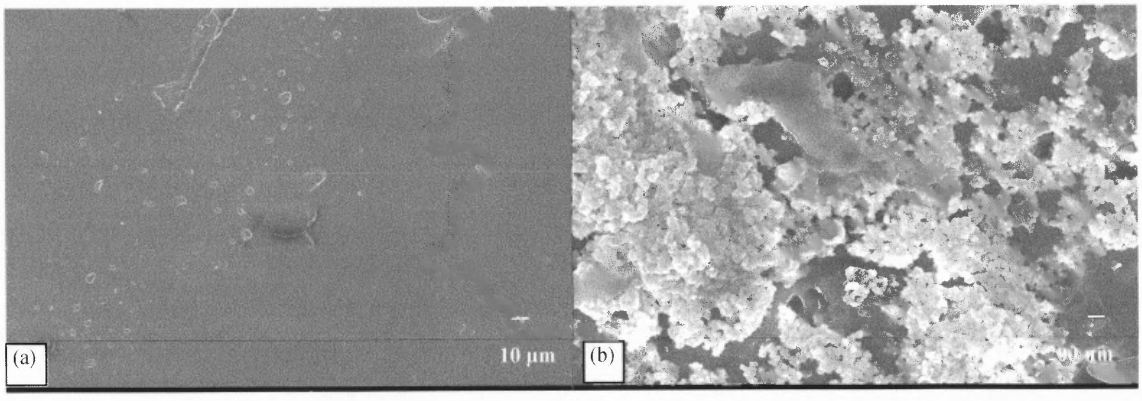

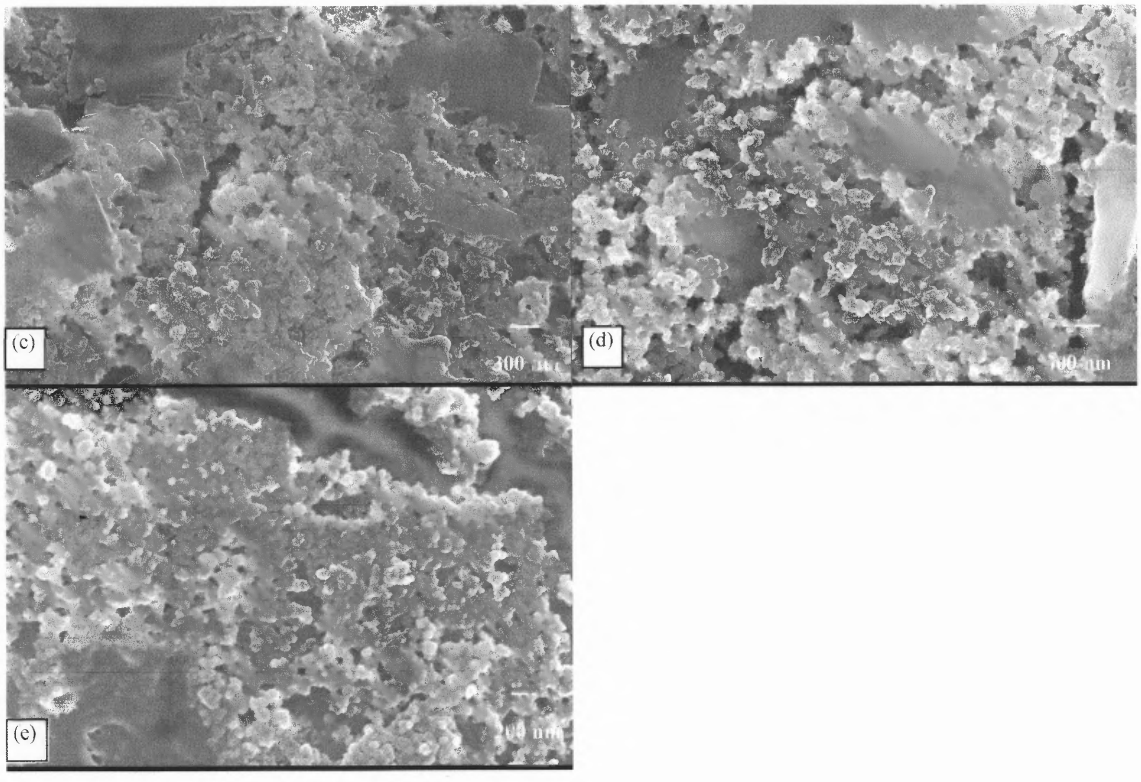

Figure 6.27 SEM micrographs of PLA / bioglass composites before and after immersion in SBF showing mineral precipitation on the polymer surface. (a) Before immersion. (b) After one week immersion; mineral precipitation can be observed on the composite surface. (c) After four weeks; small spherical crystals appear on the surface of the composite. (d) Higher magnification of (c). (e) After eight weeks; mineral growth is still evident on the surface of the composite.

6.3.1.2 PLA/CS Composites. Figure 6.28 includes a series of SEM micrographs of surfaces of melt mixed PLA/CS composites as a function of immersion time. Figures 6.28(a)-(b) are SEM micrographs after one week immersion in SBF. It is evident that globules of mineral precipitates fully cover the exposed area. Figures 6.28(c)-(d) represent higher magnifications of (a) and (b) where globular structures appear in two different forms: needle-like and spherical deposits. This could be due to the different extent of reaction during the various stages of apatite formation. Figures (e-g) are SEM micrographs after four weeks immersion in SBF. Similarly to the earlier time period, globular mineral precipitates are present on the polymer surface. In addition, solid

polymer degradation by-products appear on the surface. Figure 6.28(h) is the higher magnification of (e-g) showing again the needle-like structures. Black spots maybe attributed to polymer degradation by-products. Figure 6.28(i) shows an SEM micrograph after eight weeks immersion in SBF. Mineral precipitation appears to a lesser extent in the form of spherical crystals. Again, a possible reason for the effect of diminishing mineral precipitation after longer periods is that SBF was not replenished and as a result all the Ca, Si and P ions needed to form the apatite layer had already been consumed. Similar mineral precipitation was observed by Li and Chang (2004) for PDLLA/wollastonite composite scaffolds after one week immersion in SBF. Mineral deposits were evident on the scaffold surface. At higher magnification, the crystals had the typical morphology of apatite crystals and their size was 100-200nm in length. In the present study, the precipitates are similar to the apatite crystals of Zhang et al. (2004) and their size is about 10 μm after one week immersion. These results of PLA/CS composites at different time periods are confirmed by EDX results (data not shown) indicating that the Ca/P ratio is 1.67 (equal to that of biological apatite), 1.57 and 1.21 after one, four and eight weeks, respectively.

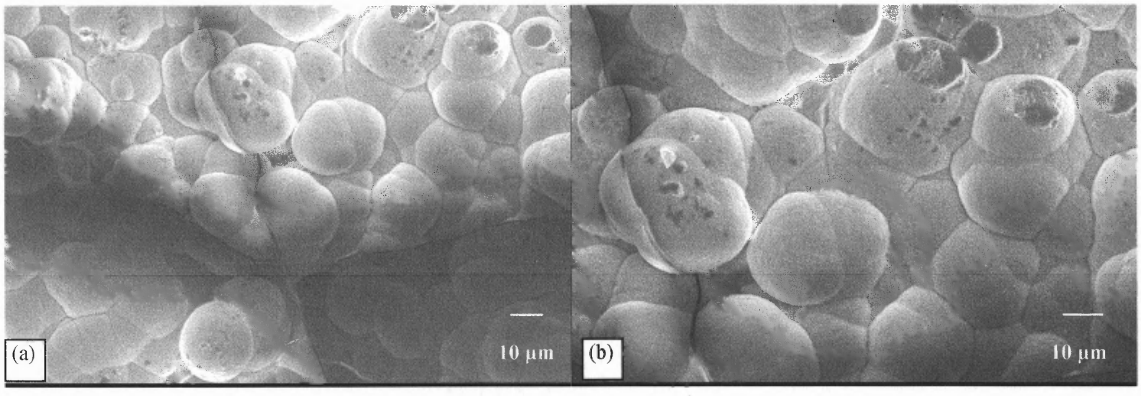

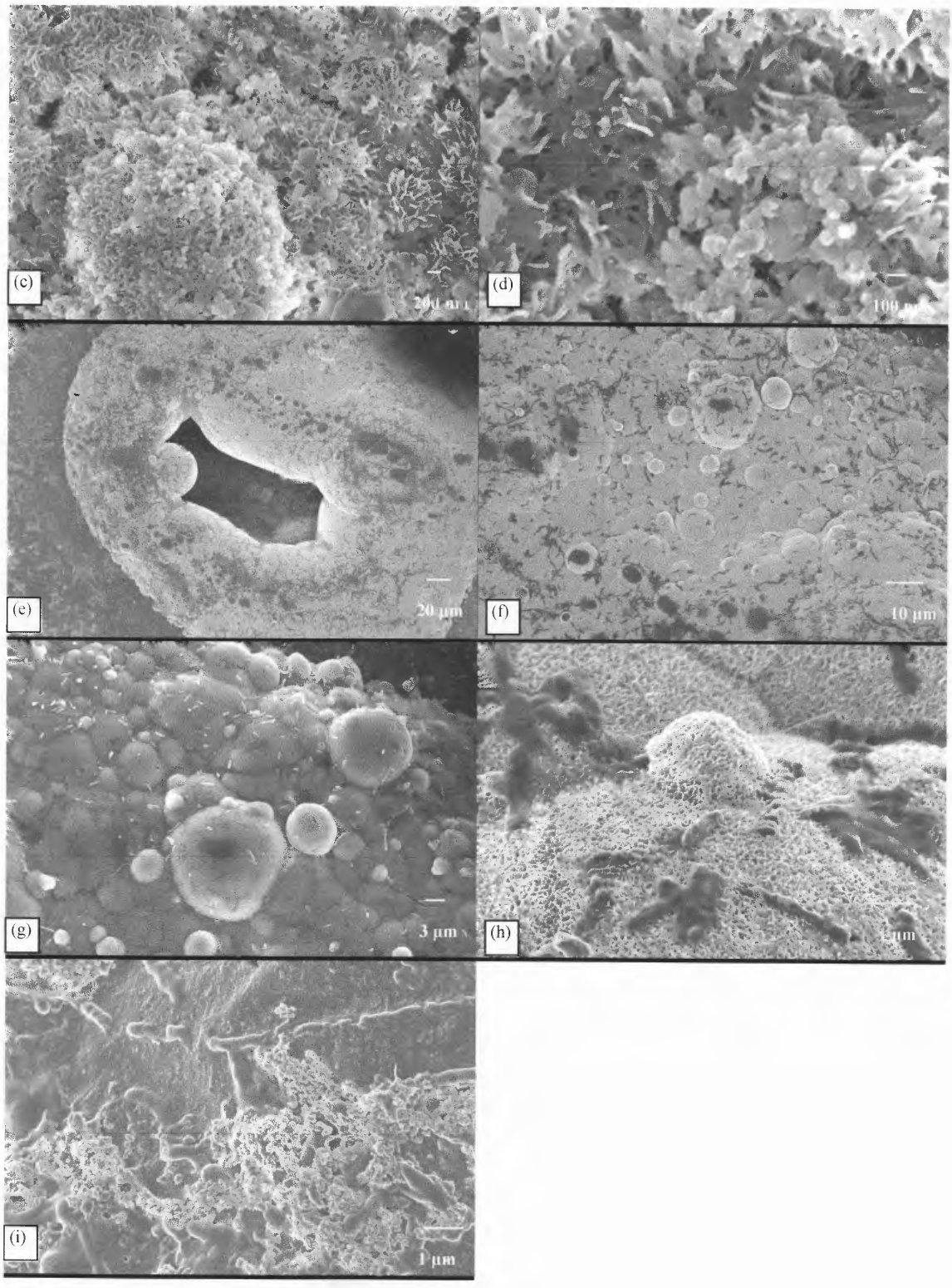

Figure 6.28 SEM micrographs of PLA/CS after immersion in SBF. (a)-(b) After one week immersion in SBF; globules of mineral precipitates are shown to fully cover the exposed area. (c)-(d) Higher magnification of (a) and (b); globular structures appear in

two different forms: needle-like and spherical deposits. (e-g) After four weeks immersion in SBF; globular mineral precipitates and polymer degradation by-products appear on the surface. (h) Higher magnification of (e-g) showing again the needle-like structures. Black spots maybe attributed to polymer degradation by-products. (i) After eight weeks; Mineral precipitation appears to a less extent in the form of spherical crystals.

6.3.2 XRD Data and Concentration Changes in SBF

The time for initial apatite formation on the surface of the composites is shown in the XRD data of Figures 6.29 and 6.30 for the PLA/bioglass and PLA/CS composites, respectively. For the PLA/bioglass composite, there are no peaks before immersion since both compounds are amorphous. After one and four weeks in SBF, the apatite peak is observed at about 32°. This peak is not evident after eight weeks, possibly due to reasons that mentioned above (limited SBF ionic activity due to non replenishment). These results are in agreement with Zhang et al. (2004) who observed apatite peaks at 25° and 32° after one and two weeks immersion.

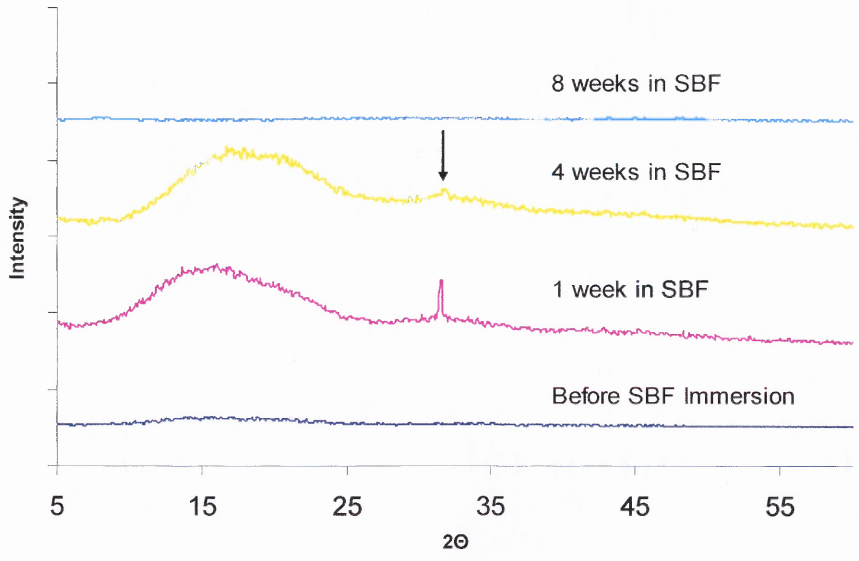

Figure 6.29 XRD spectra of PLA/bioglass composite before and after immersion in SBF. The peak at about 32° that formed after one week exposure in SBF corresponds to hydroxyapatite.

Figure 6.30 is the XRD spectra of PLA/CS composite before and after SBF immersion. After one week immersion two peaks at 29.3° and 32° are present. These peaks are attributed to calcite and hydroxyapatite, respectively (Siriphannon et al. 2002). These peaks are still evident after four weeks, but appear very weak after the eight week period. These results are in agreement with the EDX data that show initially formation of HA that is no longer present after eight weeks. This may be due to the non representative area observed by SEM or EDX vs. the entire sample analyzed by XRD.

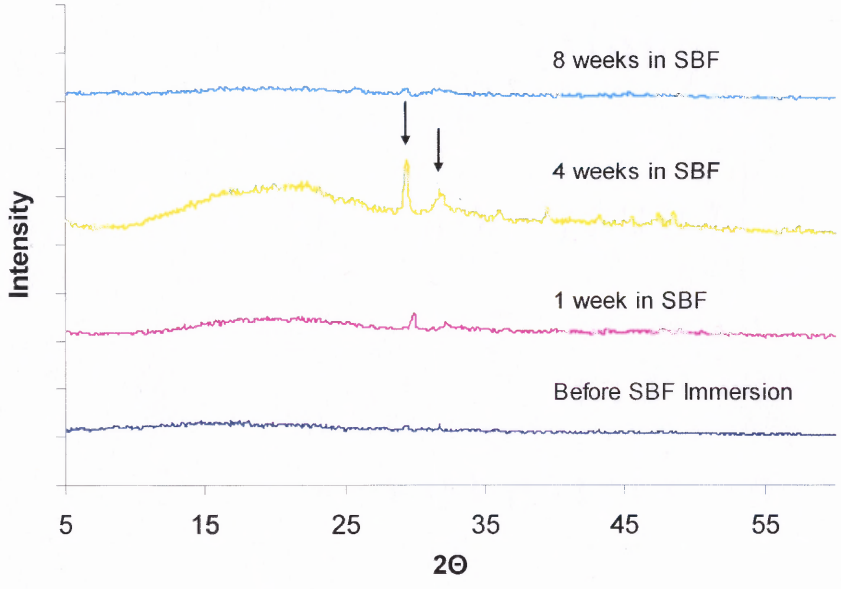

Figure 6.30 XRD spectra of PLA/CS before and after immersion in SBF. Peaks at 29.3° and 32° after one week immersion are attributed to calcite and hydroxyapatite respectively.

The results from AA spectroscopy on SBF used in the immersion of PLA composites (Fig. 6.31) showed that the calcium present in the two fillers diffuses out as a function of immersion time. The changes in the calcium concentration involves a two way process, since the calcium can be released by the fillers and can also be consumed

from SBF to the surface of the bioactive material. For the CS composites there is a higher rate of release of calcium, which after the initial 350 hours starts to decrease denoting consumption from the SBF on the composite surface. This is in partial agreement with Li and Chang's data (2004) showing that Ca ion concentrations increased rapidly for the first three days of immersion, followed by a slower increase up to 21 days. In the case of bioglass composites there is an initial increase in the rate of release of calcium, followed by a decrease after 700 hours. This is in agreement with Lu et al. (2005) who observed an initial burst of Ca release from the substrate followed by Ca precipitation as immersion continued.

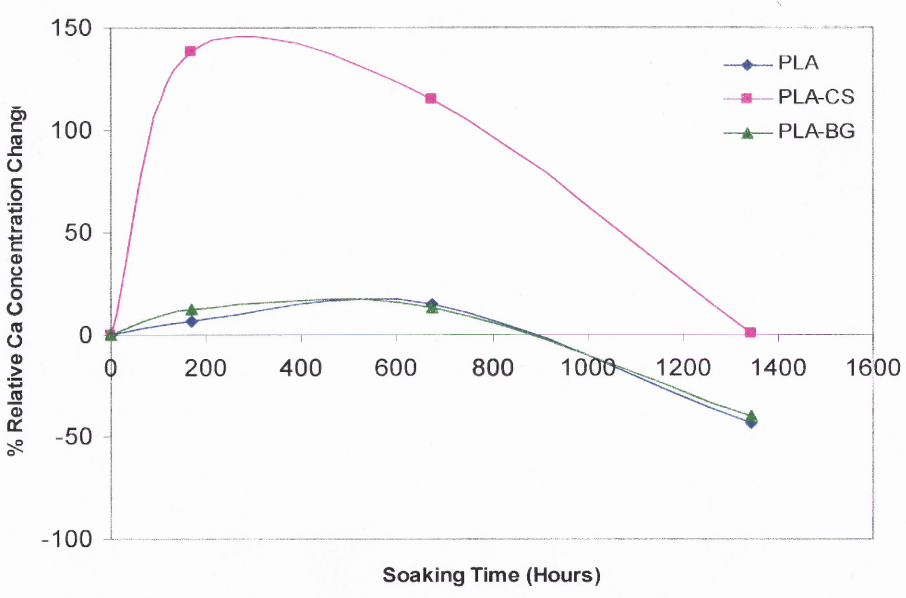

Figure 6.31 Relative changes in calcium concentration for the PLA composites after immersion in SBF. Values shown are mean of two samples per group.

Figure 6.32 presents the results of the UV-Vis spectroscopy. Phosphorus is being consumed from the SBF solution towards the surface of the PLA composites. Both composites appear to consume phosphorus from the SBF fast. The PLA/CS composite

appears to have a faster consumption than the PLA/bioglass composite; this suggests a faster rate of apatite formation on the surface of the CS composites which is in agreement with the SEM and EDX results presented above. In comparison with the PCL composites, the rate of phosphorus consumption is overall higher (70% vs. 18%) for the PLA composites. This could be due to faster degradation rates of the PLA matrix and the hydrophilicity enhancement of the PLA composites due to the presence of fillers. In the case of the unfilled PLA, there is an initial phosphorous consumption that follows a release and consumption again over the total period of the study.

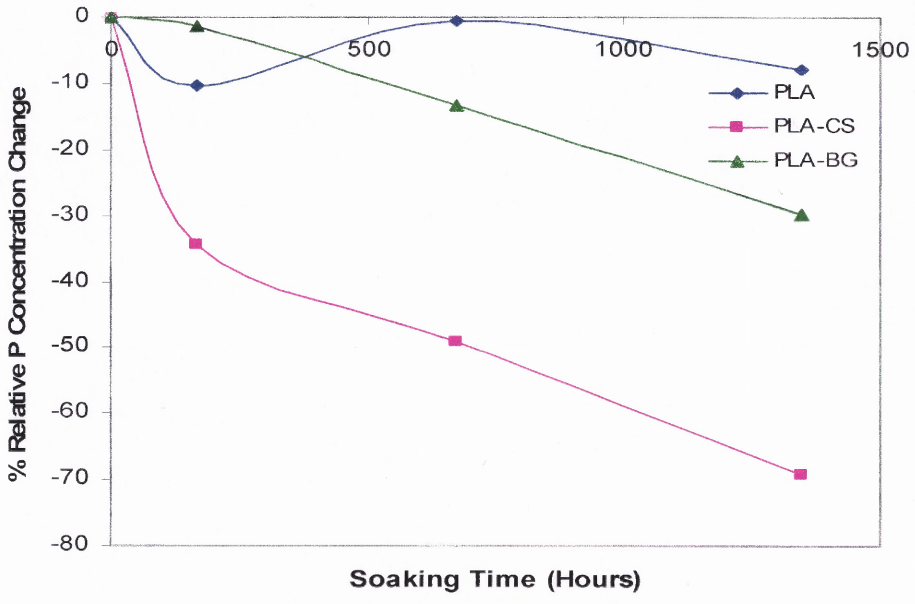

Figure 6.32 Relative changes in phosphorus concentration for the PLA composites after immersion in SBF. Values shown are mean of two samples per group.

6.3.3 Summary

In summary, SEM images of the bioglass composites showed mineral precipitation after one week immersion. For longer time periods, up to eight weeks, lack of additional apatite growth was also shown by EDX data. XRD data were in agreement with SEM

and EDX data, since the peak at 32° was evident after one and four weeks, but no longer visible after eight weeks immersion. Calcium ions appeared to diffuse out of the sample, through an initial burst after one week, followed by a slower release. This could mean that concentration changes may have reached equilibrium since Ca is also consumed by the sample from the SBF. Phosphorous was consumed from the SBF during the entire testing period. AA and UV-Vis results imply that, in the case of PLA composites, faster degradations rates apply, possibly due to the higher polymer hydrophilicity enhanced by the hydrophilic nature of the filler.

In the case of PLA/CS composites the SEM images showed globules of mineral precipitates that fully covered the exposed area after one and four weeks immersion. After eight weeks, and possibly due to limited ionic activity (since SBF was not replenished), mineral precipitation appears to a lesser extent. These data were also supported by EDX analysis. XRD results showed apatite peaks after one week immersion becoming weaker after four weeks and not present at all after eight weeks. Similarly to bioglass composites, Ca diffuses out of the CS composites, but the process reaches equilibrium after eight weeks immersion. In the case of P consumption, a similar trend as for the bioglass composite is observed, but at higher consumption rates implying higher hydrophilicity for the CS composites. It appears that after the eight week period, ionic activity is limited; thus, bioactivity of the composites (as shown by SEM, EDX and XRD data) is also limited.

6.4 Degradation of Unfilled Polymers

6.4.1 Weight Changes as a Function of Time

Figures 6.33-6.35 represent % weight changes of the different polymer and composite samples as a function of time. Figures 6.33 and 6.34 show that for both PLLA and PST polymers, extruded samples show slightly higher water uptake than compression molded samples, although within experimental error only slight differences as a function of time from 1 up to 120 days are observed. This will lead to a faster degradation rate for the extruded samples, since the additional processing step may have lowered the molecular weight of the sample. Figure 6.35 shows slight changes in the degradation behavior of all aliphatic polyesters used in this study over the first 30-day period with the amorphous PLA appearing to have a faster degradation rate.

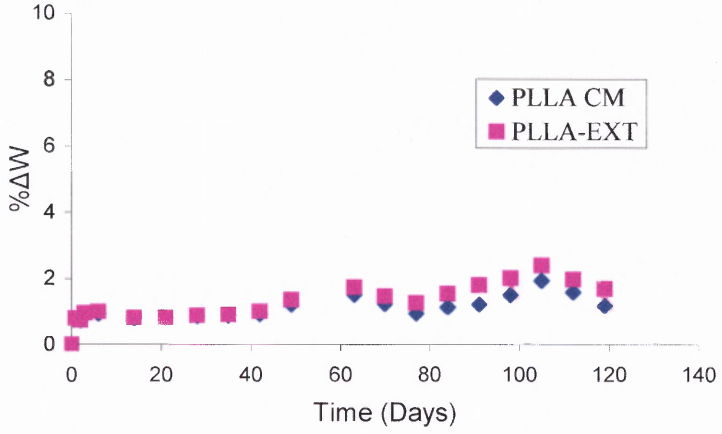

Figure 6.33 %Weight change versus time for PLLA CM and PLLA EXT. The designation CM and EXT denote compression molded and extruded samples, respectively. Two samples were tested per point. The points are the average of two determinations with an excellent reproducibility.

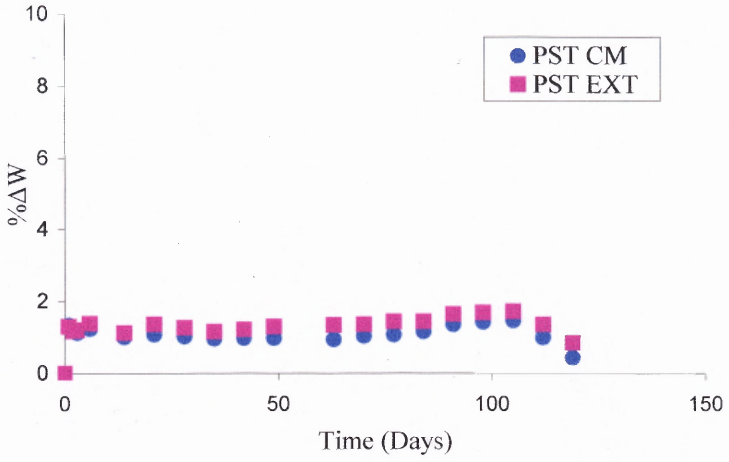

Figure 6.34 %Weight change versus time for PST CM and PST EXT. The designation CM and EXT denote compression molded and extruded samples, respectively. Two samples were tested per point. The points are the average of two determinations with an excellent reproducibility.

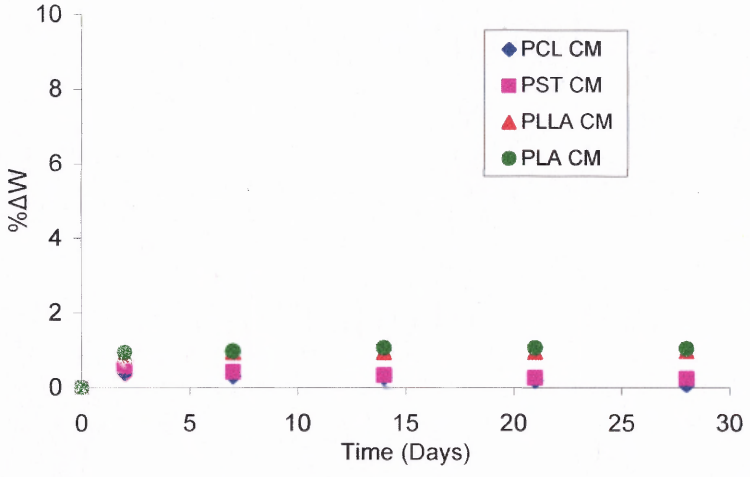

Figure 6.35 %Weight change versus time for PCL, PST, PLLA and PLA compression molded specimens. Two samples were tested per point. The points are the average of two determinations with an excellent reproducibility.

6.4.2 Intrinsic Viscosity Changes as a Function of Time

The intrinsic viscosity of the unfilled samples, before and after immersion, was calculated using the Solomon-Ciuta equation (5.2) for a single point measurement. Results are shown in Figure 6.36 and 6.37. Although no weight losses are shown above, there is

already an onset of degradation confirmed by the reduction in intrinsic viscosity (which corresponds, in turn, to reduction in MW) after immersion. Also, in Figure 6.36, the extruded PCL samples appear to have a lower IV than the compression molded samples, which confirms once more that thermal degradation of PCL occurred during extrusion. Figure 6.37 shows the reduction in intrinsic viscosity of the PLA samples that have been prepared by mixing in a batch mixer and by compression molding. No significant differences can be noticed between the two methods and, as a result, IV measurements for batch mixed samples were discontinued after 28 days. Both samples follow similar IV changes with respect of time.

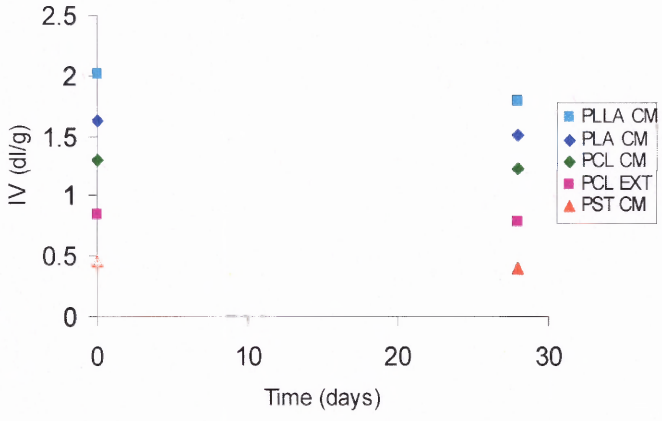

Figure 6.36 IV measurements for polyesters as a function of immersion time. The designation CM and EXT denote compression molded and extruded samples, respectively. The average of at least three measurements per sample is shown.

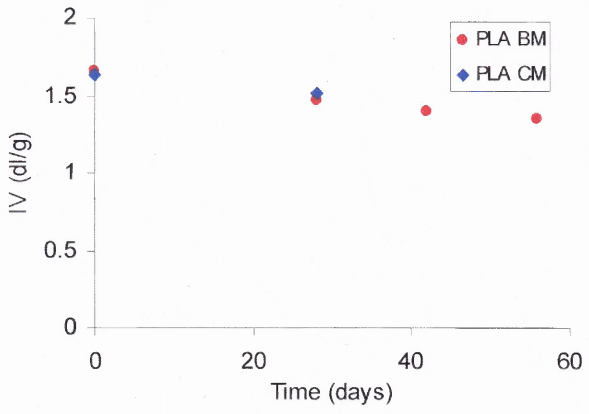

Figure 6.37 IV measurements for PLA under different processing methods as a function of immersion time. PLA BM and PLA CM correspond to batch mixer and compression molded samples, respectively. The average of at least three measurements per sample is shown.

6.4.3 Thermal Properties as a Function of Time

Tables 6.1 and 6.2 represent thermal data obtained by DSC for PCL and PST. % crystallinity was calculated from $(\Delta H_f - \Delta H_{cc})/\Delta H_{pf}$, where ΔH_f is the heat of fusion, ΔH_{cc} is the heat of cold crystallization, and ΔH_{pf} is the heat of fusion for a perfect crystal. For PCL and PST the values for ΔH_{pf} are 139.5J/g (Seretoudi et al. 2002) and 122.75 J/g (Tserki et al. 2006) (assuming a 50/50 comonomer content), respectively. In the case of unfilled PCL (Table 6.1), the method of processing appears to affect crystallinity, since the extruded samples show higher % crystallinity than the compression molded ones. For PST compression molded films, there are only slight differences, at the second heating, in the T_m and the % crystallinity before and after 28 days immersion.

Table 6.1 Thermal Data for PCL before and after Immersion in PBS

	2nd Heating		
Sample Description	**T_m (^{0}C)**	**ΔH_f (J/g)**	**% Crystallinity**
PCL CM	57.2	51.1	36.6
PCL CM 28 DAYS PBS	59.0	50.3	36.0
PCL EXTRUSION	60.1	47.3	33.9
PCL EXTRUSION 28 DAYS PBS	59.0	59.2	42.4
PCL EXTRUSION 378 DAYS PBS	60.5	65.7	47.1

Table 6.2 Thermal Data for PST before and after 28 days Immersion in PBS

	1st Heating					2nd Heating				
Sample Description	**T_m (^{0}C)**	**ΔH_f (J/g)**	**T_{cc} (^{0}C)**	**ΔH_{cc} (J/g)**	**% Crystal linity**	**T_m (^{0}C)**	**ΔH_f (J/g)**	**T_{cc} (^{0}C)**	**ΔH_{cc} (J/g)**	**% Crystal linity**
PST CM	99.8	58.5	73.6	4.2	44.5	98.4	48.6	76.7	5.8	34.8
PST 28 DAYS PBS	100.2	45.4	77.5	3.9	33.9	99.8	45.7	76.8	4.7	33.4

6.5 Degradation of PCL and its Composites

6.5.1 Weight and pH Changes as a Function of Time

Semicrystalline polyesters, such as PCL, degrade in two stages (Mano et al. 2004, Proikakis et al. 2006); initially water diffuses into the amorphous regions resulting in random hydrolytic scission of the ester groups and this may result in additional crystallization and overall increase of crystallinity. After degradation of the major

amorphous regions is initiated, hydrolytic attack shifts towards the center of the crystalline domains. Molecular weight reduction occurs during the water uptake step, although mass loss has not begun as yet.

Figures 6.38(a-c) represent the effect of the presence of the filler on the degradation of PCL. Weight change measurements were carried out on only two samples per time period and as a result data are presented in a form of a range. The hydrophilic fillers appeared to increase the water uptake of the otherwise hydrophobic PCL, up to about 5% after 119 days; this, in the long term, may be related to an enhanced rate of degradation of the composite vs. the unfilled polymer, which will eventually be accompanied by weight losses. The relatively short testing period (4 months) in the present work did not readily allow extrapolation to the complete degradation of PCL that is commonly believed to occur over a period of 24 months. It has been shown (Pena et al. 2006), however, that compression molded PCL samples with molecular weight of 65,000 (similar to the one used in this work), but much thinner (100μm), retain as much as 80% of their molecular weight after 18 months in PBS. The results are in reasonable agreement with data from Rich et al. (2002) who showed water absorption values of about 7% after 120 days for composites containing a slightly more hydrophilic PCL based matrix and a higher amount (40 wt%) of bioglass of similar particle size.

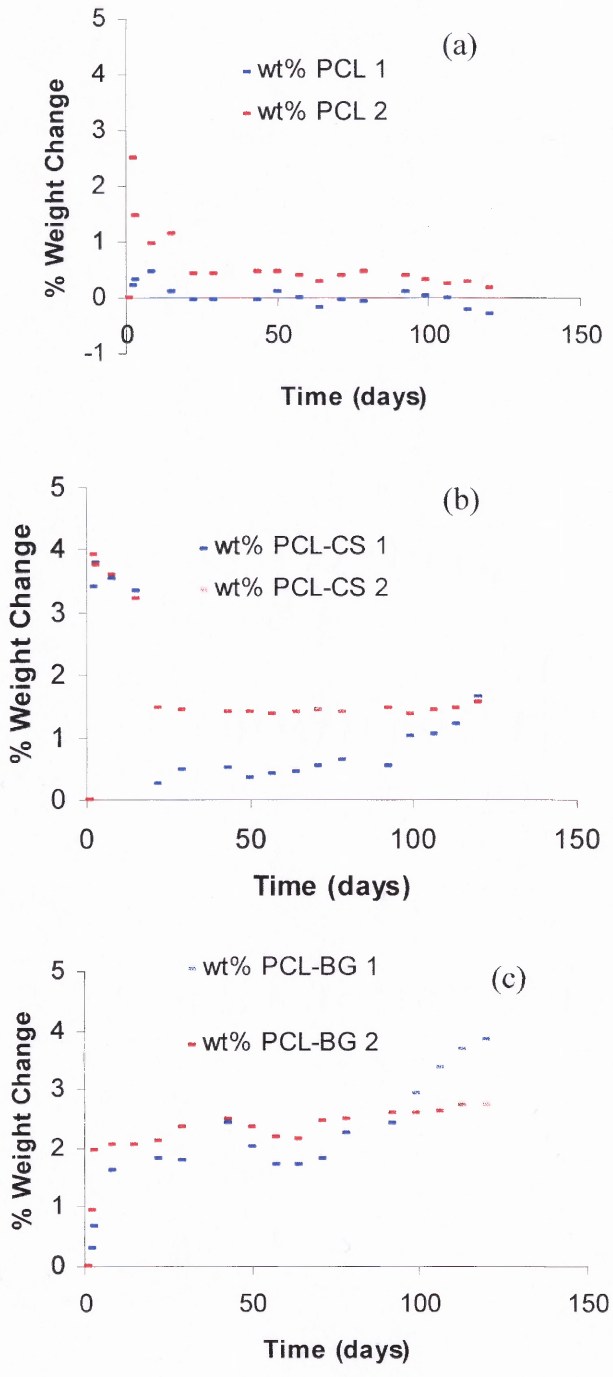

Figure 6.38 Percentage weight change vs. time for PCL and its composites. The fillers appear to have an effect on degradation by increasing water uptake. The polymer alone does not show any significant weight change. Two samples corresponding to 1 and 2 were tested for each system.

Figure 6.39 shows the pH change of the PBS solution as a function of immersion time. As shown earlier (Lu et al. 2005), the pH of solutions containing bioglass composites will be elevated due to the release of alkaline ions but will still remain within the physiological range, in agreement with our results. This behavior could compensate for the pH decrease due to the polymer degradation involving acidic byproducts. The Ca and Si ions released from the CS composite may act in a similar manner (De Aza et al. 2000, Sahai et al. 2005, Zhao et al. 2005). Degradation of PCL appears to occur very slowly, without appreciable weight changes, throughout the degradation period used in this study. Slow degradation is also supported by the small intrinsic viscosity changes as a function of immersion time for extruded PCL (see Section 6.4.2). Since no noteworthy degradation of PCL was observed, the release of a significant amount of acidic products that could produce considerable weight and pH changes would have not been expected. The data in Figure 6.39 show only small decreases from the original pH of 7.4 after 119 days.

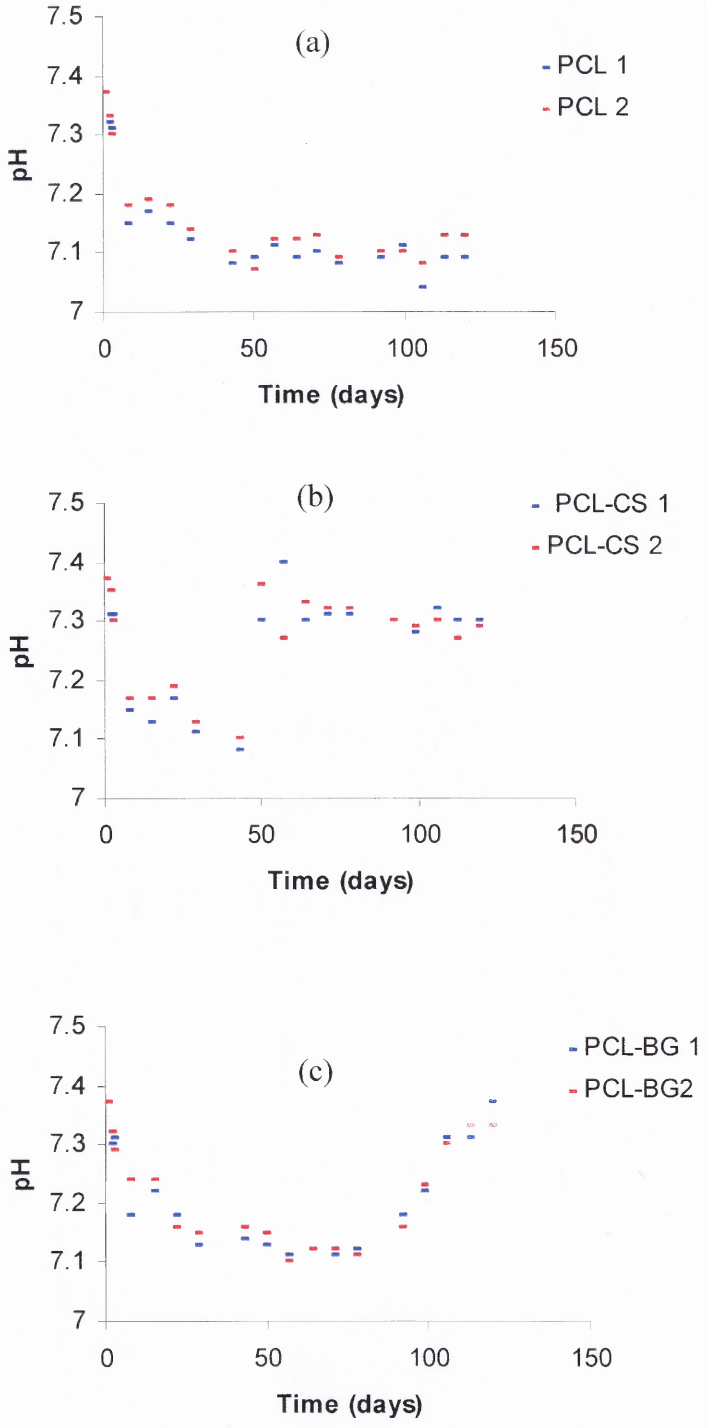

Figure 6.39 The pH of PBS solution as a function of immersion time for PCL and its composites. The fillers appear to neutralize the acidic degradation products and compensate for the pH decrease. Two samples corresponding to 1 and 2 were tested for each system.

6.5.2 Thermal Properties as a Function of Time

Table 6.3 represents thermal data for the PCL composites. It appears that % crystallinity increases in both PCL/bioglass and PCL/CS composites compared to the unfilled PCL with respect to immersion time (see Table 6.1). There are no significant differences in the peak melting temperature between the unfilled PCL and its composites.

Table 6.3 Thermal Data for PCL Composites before and after Immersion in PBS

	2nd Heating		
Sample Description	**T_m (^{0}C)**	**ΔH_f (J/g)**	**% Crystallinity**
PCL BIOGLASS	59.8	77.3	55.4
PCL BIOGLASS 28 DAYS PBS	60.9	79.1	56.7
PCL BIOGLASS EXTRUSION 378 DAYS PBS	59.6	92.3	66.2
PCL CS	58.7	60.1	43.1
PCL CS 28 DAYS PBS	58.3	62.1	44.5
PCL CS 378 DAYS PBS	59.8	67.7	48.5

6.6 Degradation of PLA and its Composites

A biomaterial for bone regeneration applications should firstly bond to the bone and then slowly degrade in such a way that mechanical properties of the implant will be adequate to support the regeneration process. Aliphatic polyesters that are tested in this study are known to degrade through hydrolysis. In the case of polylactic acid resins, degradation usually takes place in the bulk of the material and does not start from its surface. The cleavage of the ester bond that happens through hydrolysis, proceeds preferentially in the amorphous regions, and as a result, for semicrystalline materials crystallinity increases. Thus, the hydrolysis rate is expected to be higher in the amorphous PLA polymer, rather than in the semicrystalline PLLA. The chain cleavage leads to formation of lactic acid oligomers, which result in an increase of carboxylic groups that are known to catalyze the degradation reaction. Therefore, the hydrolytic degradation of PLA is considered as a self-catalyzed and self-maintaining process (Paul et al. 2005). The degradation mechanisms can be affected by several factors, such as chemical structure, molar mass and its distribution, purity, morphology, shape and history of the sample, as well as the conditions under which the degradation tests are conducted (Vert et al. 1995). In the case of composites, the processing parameters, as well as the hydrophilicity or the hydrophobicity of the filler along with the filler morphology and reactivity are expected to play important roles in the overall hydrolysis performance of the material.

6.6.1 Weight and pH changes as a Function of Time

Figure 6.40 shows the changes in water absorption for PLA and its composites during PBS immersion. It is obvious that the unfilled polymer shows no significant water

absorption, whereas each of the fillers appears to affect differently the water absorption/time curves, and consequently the degradation of the composite. For the PLA-CS composite the water absorption increases significantly during the first week (up to 50%), and reaches a plateau for the remaining 215 days. This is not the case for the PLA/bioglass composite whose water absorption continues to increase for the entire experimental period, up to a maximum value of 220% following an initial linear increase. Towards the end of the 215 day period, the process for the PLA/bioglass composite appears to have reached equilibrium. These results are in partial agreement with the study of Li and Chang (2005), who tested poly(lactic acid-co glycolic acid) (PLGA) composite scaffolds filled with 20 weight % wollastonite and bioglass. Both wollastonite and bioglass exhibited a similar water absorption profile that eventually showed a linear decrease from the fourth to eighth week. According to the authors, this decrease in water absorption could be correlated to a significant weight loss. Ara et al. (2002) suggested that the changes in water absorption could be the result of a balance between the dissolution of oligomers in the solution and the water uptake of the residual material.

The differences between the results of this study and the one of Li and Chang (2005) are due not only to the different polymer matrix, but also to the sample shape and history (melt processed solid compression molded samples vs. scaffolds prepared using a solvent casting-particulate leaching method), and differences in the filler content. A possible reason that in the present work no decrease in water absorption and consequently weight loss are observed, could be that the species formed by hydrolysis (shorter PLA chains and cyclic oligomers) are not soluble in the buffer solution (Paul et al. 2005).

Only dimers and trimers of lactic acid as well as lactic acid itself are soluble in the phosphate buffer solution.

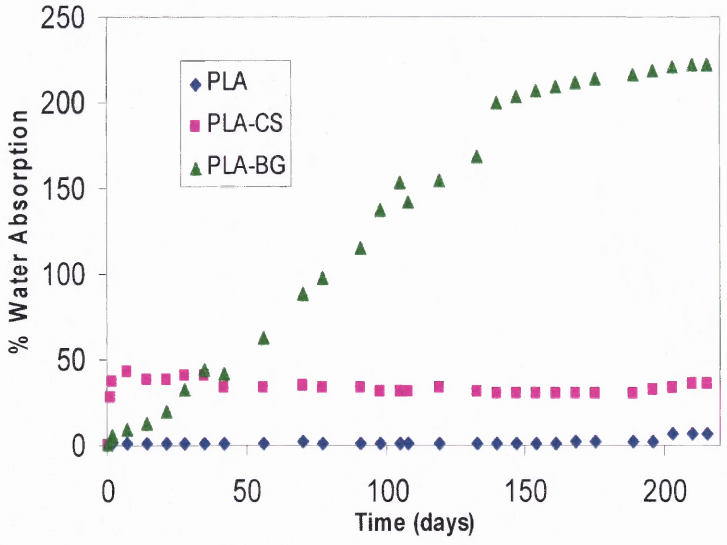

Figure 6.40 Water Absorption for PLA and its composites as a function of immersion time. Average values are shown. Initial number of samples was six and was reduced to two by the end of the degradation period.

In conclusion, although water absorption is evident for the PLA composites, PLA itself does not seem to absorb any significant amount of water. Each of the composites follows a different trend in their water absorption curves, possibly due to different degradation mechanisms that are controlled by particle size, as well as hydrophilicity and filler reactivity. Regarding hydrophilicity, Paul et al. (2005) suggest that degradation is directly related to the relative hydrophilicity of the filler, since water molecules penetrate more easily within the material to trigger the degradation process. In the present work, both CS and bioglass fillers are hydrophilic, but with different particle sizes and dissolution characteristics. The dissolution rate, according to Prabhakar et al. (2005) produces greater percentages of weight loss. Specifically, it is suggested that in the case of bioactive glasses, the glass components diffuse at various rates from the samples into

the solution, thus creating voids and microcracks within the sample. This will result to easier diffusion of water in the sample and, consequently, weight losses due to hydrolytic degradation. However, it is important to note that bioglass is highly reactive with a decay rate of 150μg/cm^2/day. This could also contribute to weight loss of the composite. A similar behavior is expected in the case of CS where Ca and Si ions will diffuse out of the composite.

Figure 6.41 shows pH changes vs. time of the PBS solution. Although it would be expected for PLA to exhibit a lower pH after a period of 215 days due to acidic by-products, it still holds a value of about 6.8. This is lower than the initial pH value of the solution, but still not acidic. PLA shows an initial pH decrease after a period of 70 days. Based on the low water uptake, no significant degradation of PLA would be observed and as a result no significant amount of low molecular weight, water soluble acidic by-products that could produce considerable pH change.

Although degradation has been initiated even for the unfilled PLA, it is probably not at the same stage as for the filled systems. For the PLA/bioglass composite, there is an initial pH increase that is probably related to the dissolution of the bioglass and the diffusion of its alkaline ions to the solution. This is in agreement with Boccaccini and Maquet (2003) who suggested that the elevated pH of their bioactive glass composite could be correlated with the dissolution of alkaline ions from the bioactive glass particles that locally compensate for the acidification of the solution due to acidic by-products of the polymer degradation. pH values for the PLA/bioglass composite are as high as 9.6 after 42 days and then gradually decrease to the original pH of 7.4 at 133 days and a value of 6.6 at the end of the immersion period of the study. These considerable changes

over the experimental period can be attributed to the combined effect of the filler alkaline ions and to the continuing hydrolytic degradation of the polymer, perhaps catalyzed by the filler. The pH values of this work are in general agreement with those of a PLGA/bioglass composite in the study of Li and Chang (2005) who observed a pH increase of 8.15 in the first seven days that eventually dropped to 7.1 after 56 days.

For the PLA-CS composite the pH values are stable for the first 133 days and drop to a value of pH 7.0 afterwards. At the end of the period of the study the pH drops to 6.02. This differs from the pH values reported by Li and Chang (2005) for the wollastonite composite that varied from 7.7 to 7.3. Possible reasons could be the differences not only between the polymer matrices, but also type and crystallinity of the CS filler.

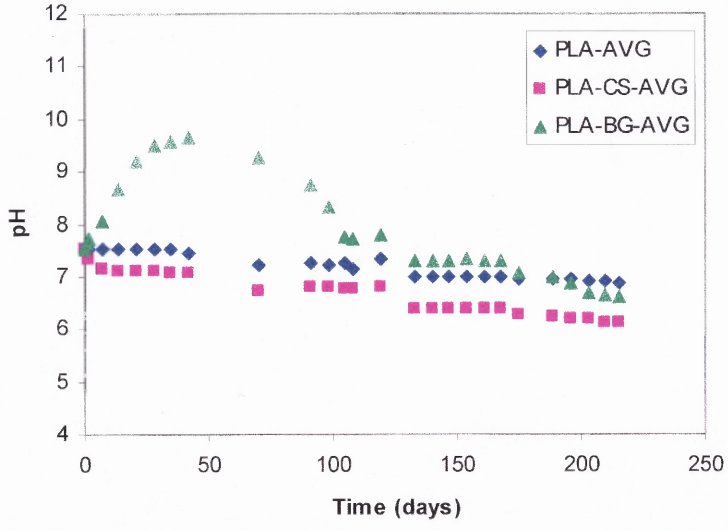

Figure 6.41 pH changes as a function of time for PBS solution containing for PLA and its composites. AVG corresponds to the average number of samples at existing time. Initial number of samples was six and was reduced to two by the end of the degradation period.

In summary, although pH measurements could give an indication of extent of degradation by observing the development of acidity due to degradation by-products, the results with the present filled systems are more complicated due to high water absorption values and alkaline ion diffusion to the solution.

6.6.2 Intrinsic Viscosity Changes as a Function of Time

Intrinsic viscosity (IV) changes provide an indication of molecular weight changes according to the Mark-Houwink equation:

$$[\eta] = KM_v^{\alpha} \tag{6.1}$$

where $[\eta]$ is the intrinsic viscosity, K and α are constants equal to 2.21 x 10^{-4} and 0.77 respectively (for chloroform as a solvent and 25^0C), and M_v is the viscosity average molecular weight (Proikakis et al. 2006).

Figure 6.42 shows IV changes for PLA in the absence and presence of bioglass filler during immersion in PBS solution. It is evident that there is a significant reduction in the MW of the PLA matrix after melt processing in the presence of BIOGLASS compared to the unfilled PLA. Calculated initial M_v values from Equation 6.1 are 108,000 and 33,000 in the absence and in the presence of bioglass filler, respectively. In both cases MW decreases exponentially with time, which for the PLA/bioglass system agrees with the observations from the weight and pH changes studies. For the unfilled PLA it seems that changes in weight and pH would take place after IV has been reduced below a certain critical value.

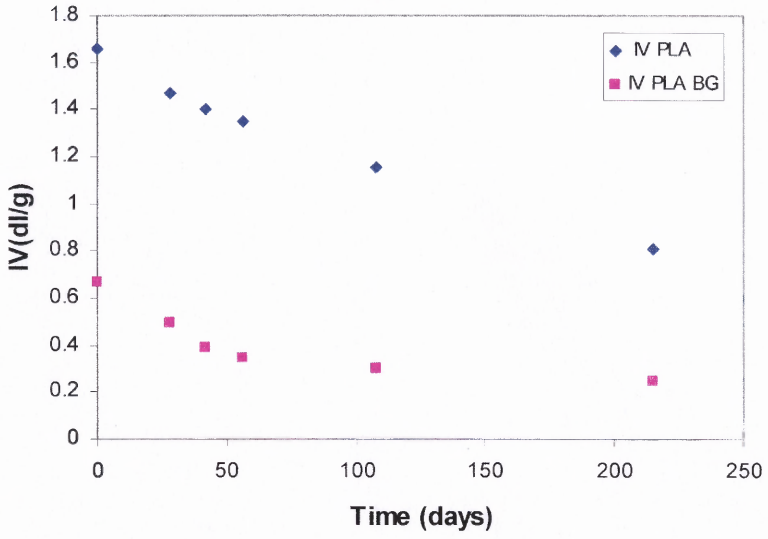

Figure 6.42 IV measurements as a function of immersion time in PBS for PLA in the presence and absence of bioglass filler. The average of at least three measurements per sample is shown.

6.6.3 Thermal Properties as a Function of Time

Table 6.4 represents thermal data for PLA and its composites. It is interesting to note that the presence of bioglass appears to decrease somewhat the T_g of the composite after immersion (both first and second heating), whereas CS decreases T_g to a much lesser extent. Results for PLA do not allow the establishment of a definite decreasing trend, although all T_g values are higher than those of the PLA/bioglass and PLA/CS composites. Navarro et al. (2005), when incorporating a soluble calcium phosphorus containing bioglass in a PLA matrix, reported similar decreases in T_g that were consistent with the decrease in MW during the immersion period.

Table 6.4 Thermal Data for PLA and its Composites

	1st Heating	2nd Heating
Sample Description	**T_g (^{0}C)**	**T_g (^{0}C)**
PLA before immersion	63.5	61.9
PLA 28 days PBS	66.6	62.0
PLA 42 days PBS	66.8	61.4
PLA 56 days PBS	67.3	62.3
PLA 108 days PBS	64.1	61.5
PLA 215 days PBS	63.4	60.3
PLA BIOGLASS before immersion	60.3	59.6
PLA -BIOGLASS 28 days PBS	54.9	57.1
PLA -BIOGLASS 42 days PBS	52.4	48.7
PLA -BIOGLASS 56 days PBS	52.7	57.4
PLA -BIOGLASS 108 days PBS	54.5	57.2
PLA -BIOGLASS 215 days PBS	55.3	58.1
PLA -CS before immersion	61.2	59.8
PLA -CS 28 days PBS	61.6	61.4
PLA -CS 42 days PBS	59.4	60.6
PLA CS 56 days PBS	62.7	61.9
PLA -CS 215 days PBS	55.9	60.4

6.6.4 Mechanical Properties as a Function of Time

6.6.4.1 Tensile Properties of Unfilled PLA. Figures 6.43-6.46 show tensile properties of PLA films as a function of immersion time in PBS. Elongation at break of PLA decreases as early as after two weeks of immersion (Figure 6.43), whereas the other properties are less sensitive to immersion in PBS for the same time period. Elongation at break is the only mechanical property that shows significant reduction even after two weeks- immersion, indicating significant embrittlement associated with a reduction in MW of about 13% as per Fig. 6.42. Other properties show little or no difference even after eight weeks immersion. For longer time periods though, stress at yield as well as stress at break appear to decrease with immersion time.

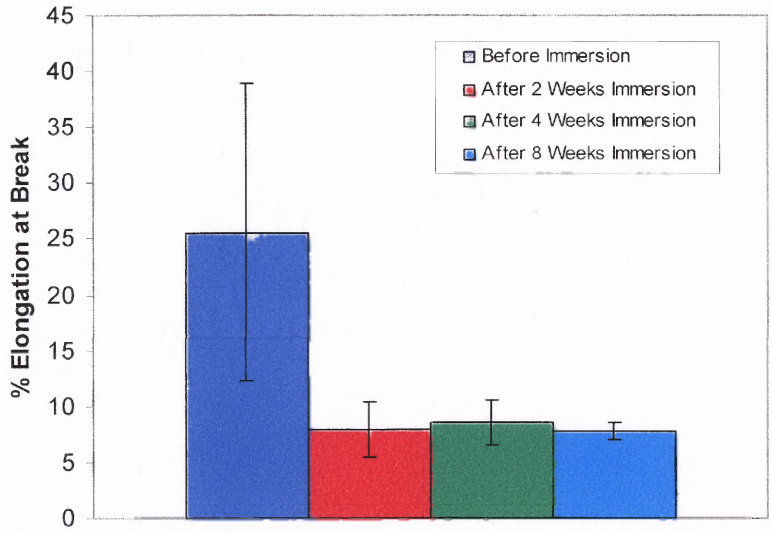

Figure 6.43 % Elongation at Break of PLA before and after immersion.

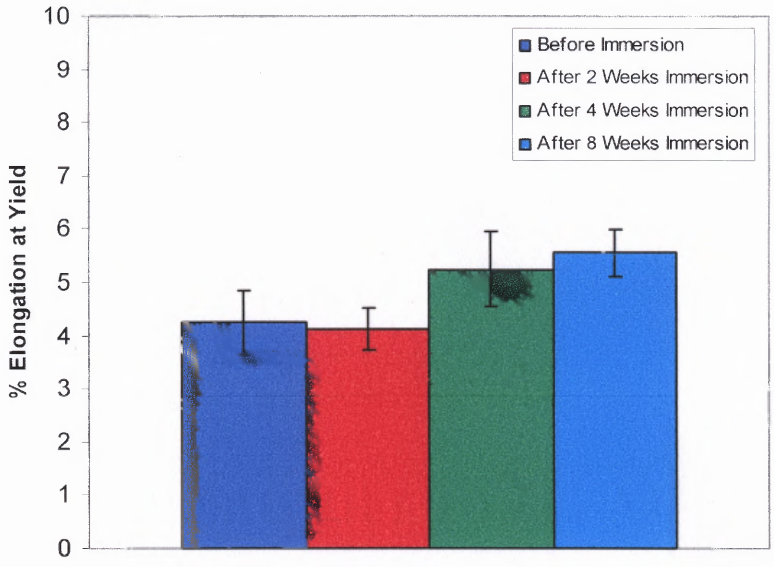

Figure 6.44 % Elongation at Yield of PLA before and after immersion.

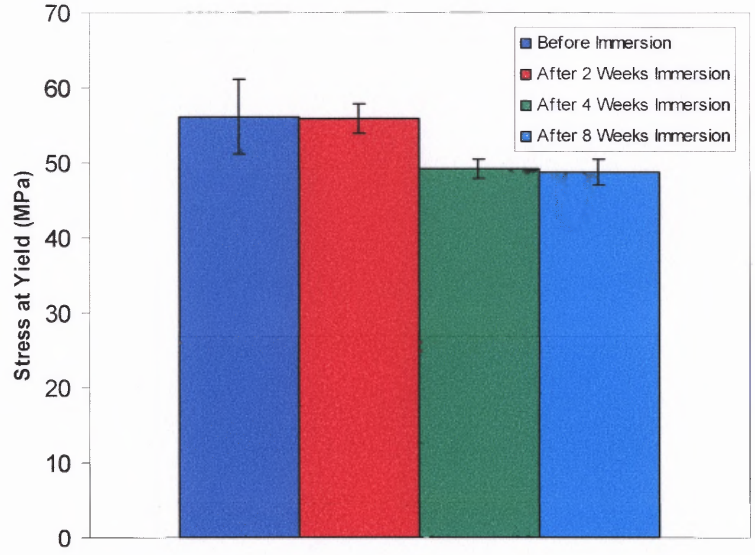

Figure 6.45 Stress at Yield of PLA before and after immersion.

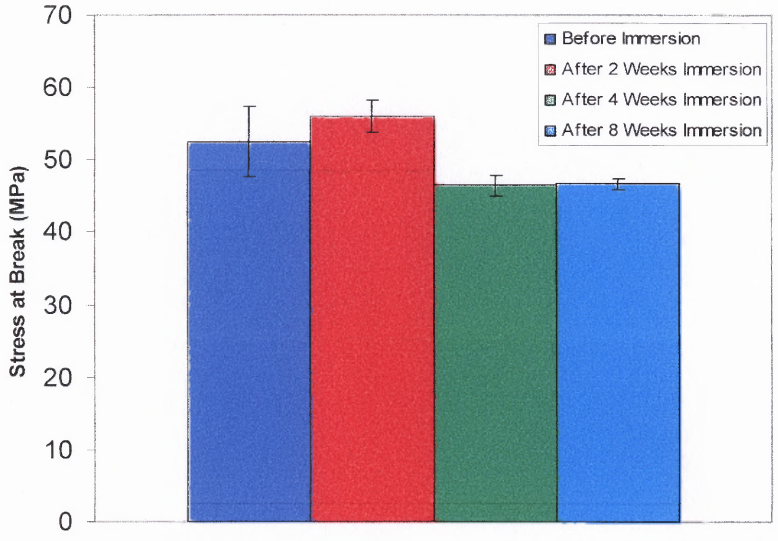

Figure 6.46 Stress at Break of PLA before and after immersion.

6.6.4.2 Compressive Properties of Filled PLA. Figures 6.47-6.51 show the compressive properties of PLA and PLA-CS composites as a function of immersion time in PBS. Relatively large changes can only be observed for compressive modulus and strain at break of the unfilled PLA (Figs. 6.47-6.48). Other compressive properties show little or no changes similarly to the tensile data reported in Section 6.4.4.1. Data for stress at yield, stress at break and % strain at yield are shown in Appendix E. In the case of the CS filled system, more significant changes can be observed in the mechanical properties even after two weeks immersion. Significant changes for the PLA-CS system can be observed in the compressive stress at yield (Figure 6.49), compressive stress at break (Figure 6.50) and the initial compressive modulus (Figure 6.51). Data for % strain at yield and % strain at break are shown in Appendix E. These changes in mechanical properties could be due, as per Prabhakar et al. (2005), to voids and microcracks formed

on the sample as the filler components diffuse into the solution. When water diffuses back into these cavities, the mechanical integrity of the samples is lost.

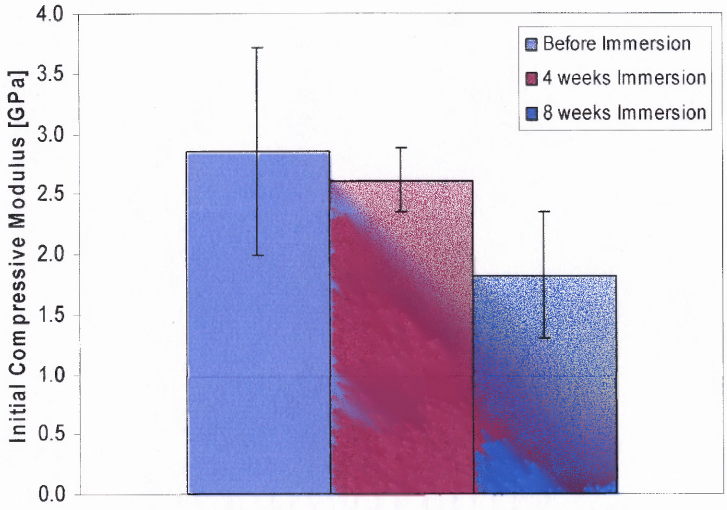

Figure 6.47 Initial Compressive Modulus of PLA before and after immersion.

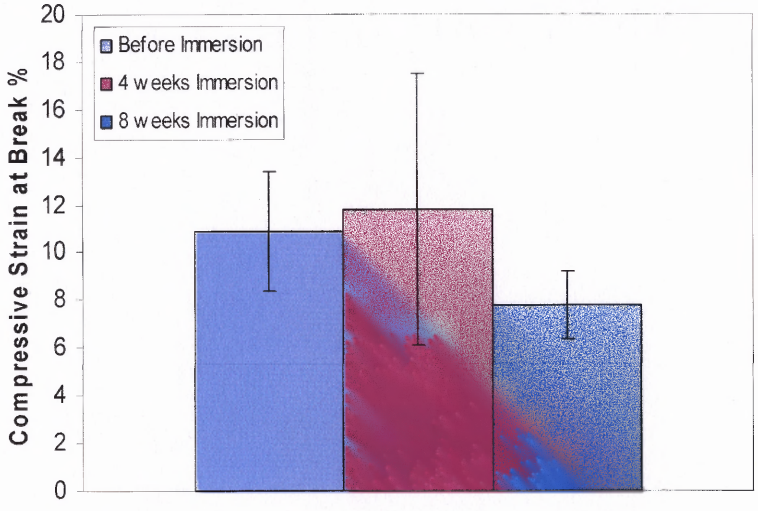

Figure 6.48 Compressive Strain at Break % of PLA before and after immersion.

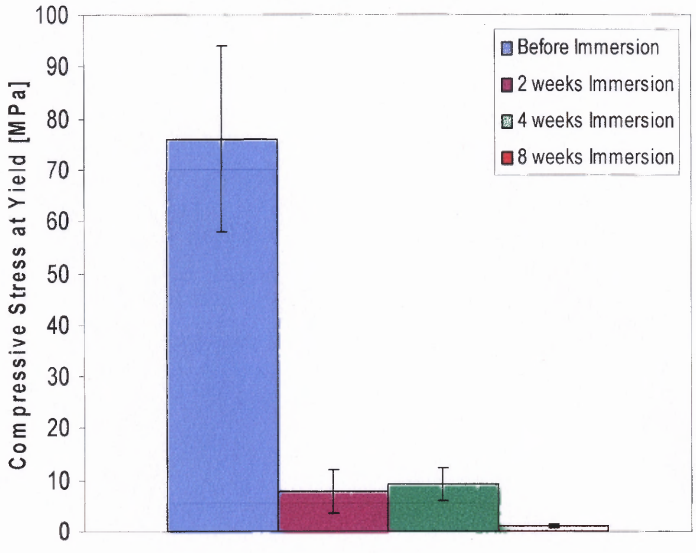

Figure 6.49 Compressive Stress at Yield of PLA/CS before and after immersion.

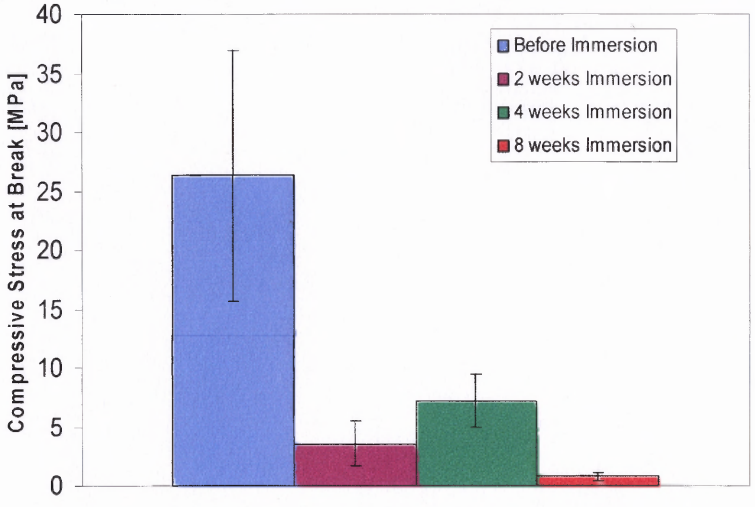

Figure 6.50 Compressive Stress at Break of PLA/CS before and after immersion.

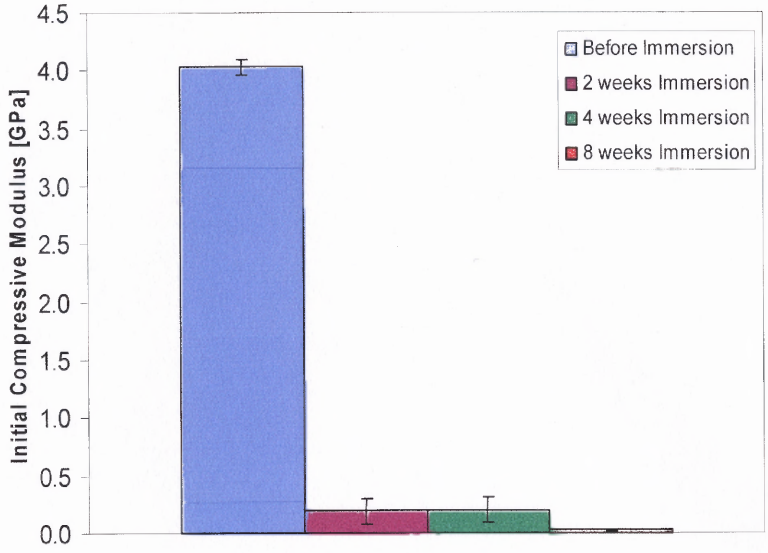

Figure 6.51 Initial Compressive Modulus of PLA/CS before and after immersion.

Figure 6.52 includes photographs of unfilled PLA as a function of immersion time in PBS. Samples appear to maintain their integrity even after a four week period. By contrast, hydrolytic degradation and loss of integrity has been initiated for the PLA-CS composites even after a short period of one week as can be seen in the photographs of Figure 6.53. Significant dimensional changes on wet samples are as high as 19.6% increase in length, 38.4% increase in diameter after four weeks; weight increase (88.1%) are also observed. Composite degradation is accompanied by debonding of the hydrophilic filler since no additional coupling agent is present in the composite. The alkaline CS could also affect catalytically the hydrolytic degradation of PLA although IV data are not available. It is important to note that the sample dimensions in compressive testing are different than those of samples used for viscosity measurements (cylinders vs. discs).

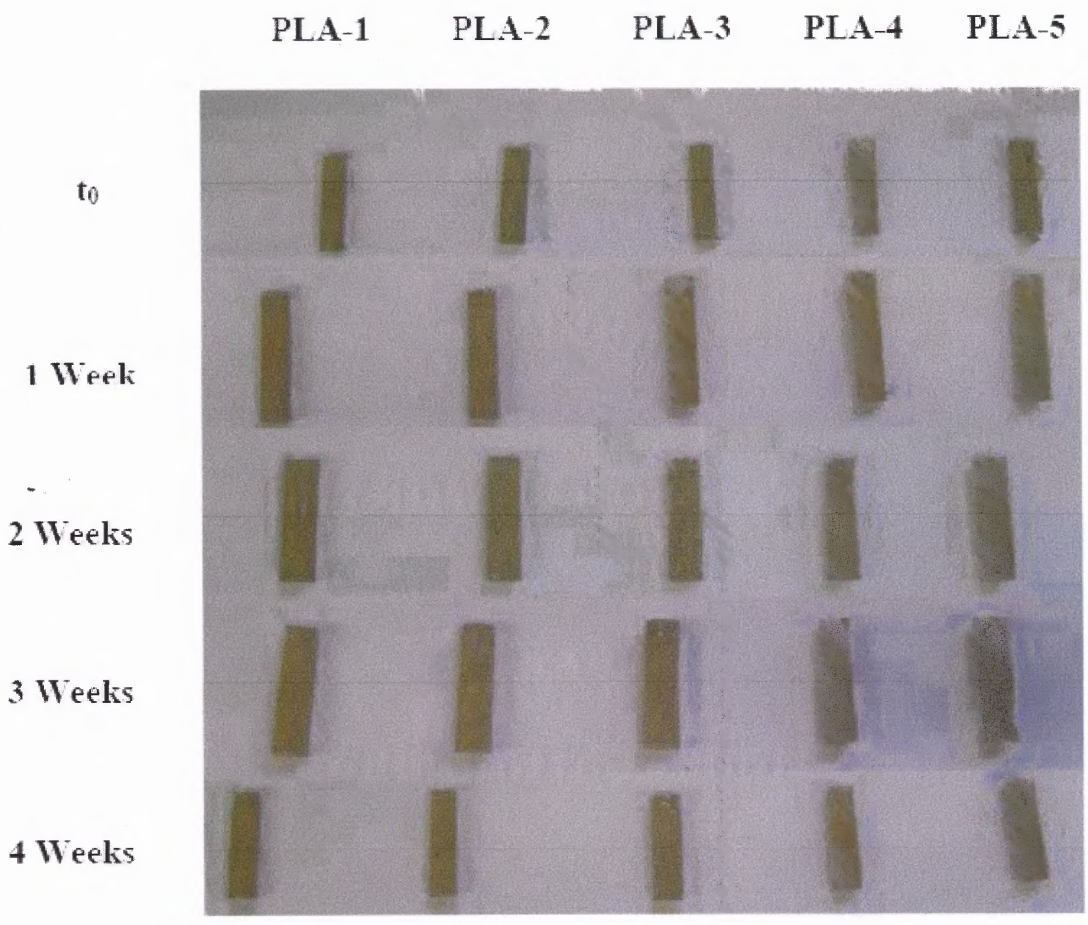

Figure 6.52 PLA specimens for compression testing after 0, 1, 2, 3, and 4 weeks in PBS.

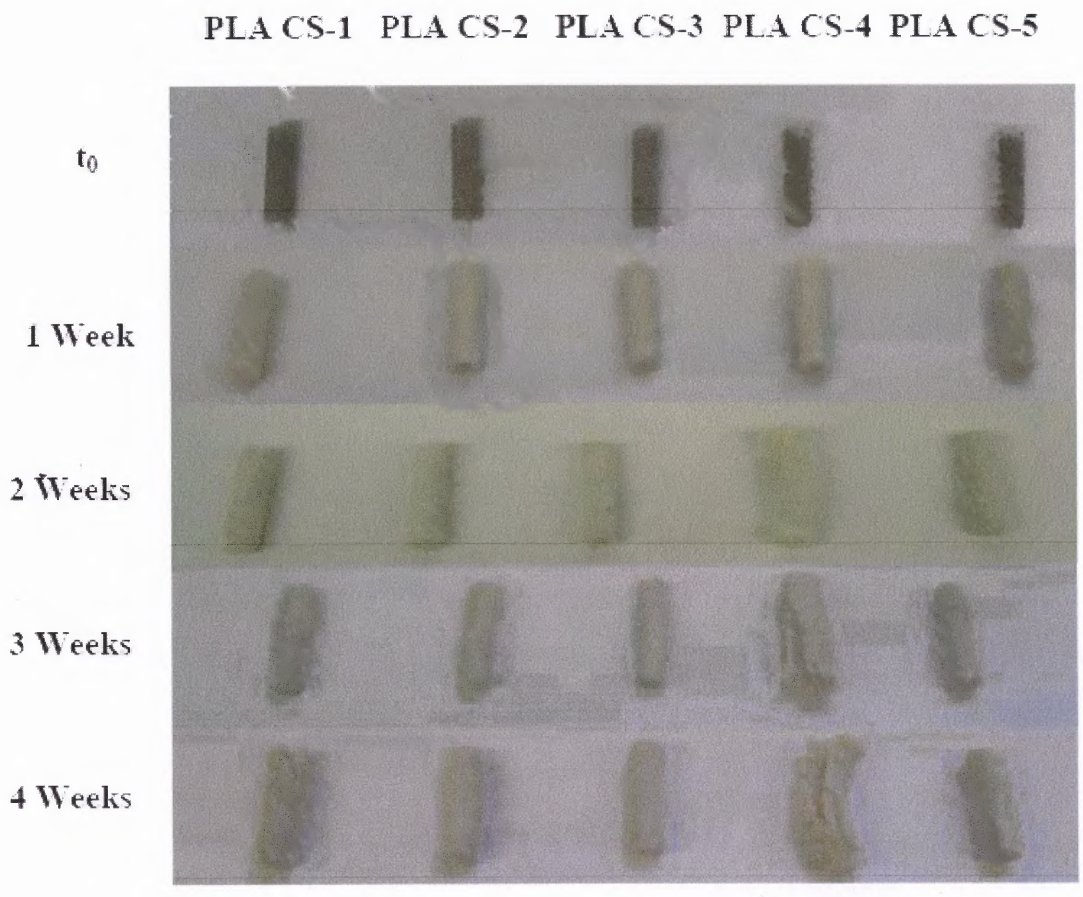

Figure 6.53 PLA-CS specimens for compression testing after 0, 1, 2, 3, and 4 weeks in PBS.

6.6.5 Degradation and Modeling

Many researchers have studied the degradation mechanisms of aliphatic polyesters and derived mathematical models to fit experimental data.

According to Burkersroda et al (2002), all the water insoluble degradable polymers could undergo surface erosion or bulk erosion depending on process conditions. Equation 6.2 was based on a theoretical model, proposed to predict the hydrolytic degradation mechanism of polymers. A polymer matrix erodes depending on the diffusivity of water inside the matrix, the degradation rate of the polymer functional

groups and the matrix dimensions. Taking into account these parameters, the model allows to calculate for an individual polymer matrix a dimensionless "erosion number" ε (Qian et al. 2004). This number can be considered as a Deborah number (the ratio of a characteristic material time to a characteristic process time) and its values fall into three categories: a) for polymer matrices with ε » 1 the reaction between water and polymer is faster than water diffusion and as a result the systems undergo surface erosion; b) for polymer matrices with ε « 1, the diffusion of water is faster than the erosion resulting to systems that undergo bulk erosion; c) for polymer matrices with ε = 1 the erosion mechanism cannot be predicted unequivocally.

$$\varepsilon = \frac{< x >^2 k\pi}{4D_o\left(\ln[< x >] - \ln[\sqrt[3]{\overline{M_n} / N_A(N-1)\rho}]\right)} \tag{6.2}$$

where $< x >$ is the half thickness of polymer matrix, k is the rate constant that accounts for the differences in the reactivity of polymer functional groups (k is equivalent to a first order rate constant such as used in reaction kinetics), D_o is the effective diffusion coefficient of water inside the polymer, $\overline{M_n}$ is the number average molecular weight, N is the average degree of polymerization, N_A is Avogadro's number, and ρ is the density of the polymer.

The half thickness of the polymer matrix, $< x >$, is in our case equal to 0.0375 cm for PLA samples. The rate constant, k, can be calculated through numerous relationships that have been derived relating the changes in $\overline{M_n}$ with time to the hydrolysis rate of the unstable ester linkages (Weir et al. 2004). Anderson (1995), assuming that the extent of degradation was not large, reported a statistical method to relate number average molecular weight to the hydrolysis rate, resulting in Equation 6.3:

$$1/\overline{M_n} = 1/\overline{M_{no}} + kt \tag{6.3}$$

where $\overline{M_{no}}$ is $\overline{M_n}$ at time t=0 and k is the rate constant.

In this study, intrinsic viscosities were measured for PLA in the absence and presence of the bioglass filler and from their values viscosity average molecular weights ($\overline{M_v}$) were calculated from Equation 6.1. $\overline{M_v}$ was considered to be directly proportional to $\overline{M_n}$, and $1/\overline{M_v}$ values were plotted according to Equation 6.3 (Figures 6.54-6.55) with respect to time. The derived regression k values were 8×10^{-13} s^{-1} and 4×10^{-12} s^{-1} for the PLA and the PLA/bioglass composite, respectively. Correlation was excellent in the case of PLA and poor in the case of the PLA/bioglass as shown by the R^2 values. Please note that the k value for the PLA/bioglass system is higher by an order of magnitude than that of the unfilled PLA.

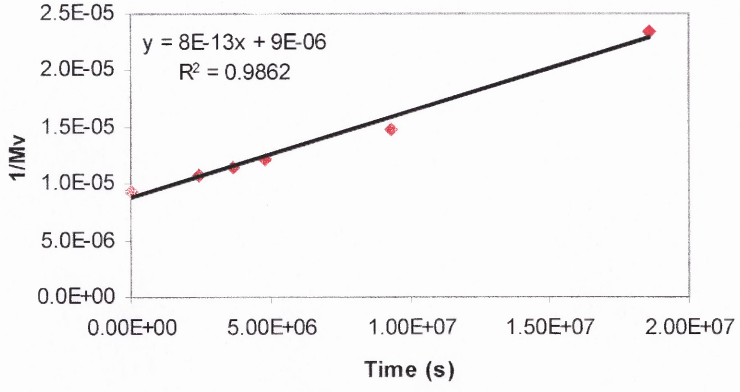

Figure 6.54 Hydrolytic degradation data for PLA based on $1/\overline{M_v}$ and Equation 6.3.

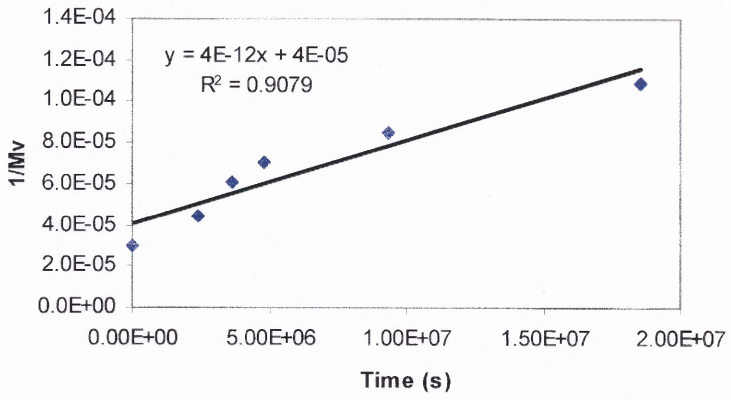

Figure 6.55 Hydrolytic degradation data for PLA/bioglass based on $1/\overline{M_v}$ and Equation 6.3.

However, Equation 6.3 has the disadvantage that does not account for the possibility of autoacceleration due to the generated carboxylic acid end groups during hydrolysis.

Pitt and Gu (1987) used the following relationship that accounts for autocatalysis by the carboxyl end groups.

$$\ln \overline{M_n} = -kt + \ln \overline{M_{no}} \tag{6.4}$$

$\overline{M_v}$ values measured in this work were considered again to be directly proportional to $\overline{M_n}$. $\ln(\overline{M_v}/\overline{M_{vo}})$ was plotted vs. time according to Equation 6.4 (Figures 6.56-6.57) and the derived new k values were $5\text{x}10^{-8}$ $s^{-1}$and $9\text{x}10^{-8}$ s^{-1} for PLA and the PLA/bioglass composite, respectively. As before, correlation is excellent in the case of PLA and very poor for PLA/bioglass. Note that the value for PLA is fairly close to the one estimated by Burkersroda et al. (2002) ($6.6\text{x}10^{-9}$ s^{-1}) for poly(α-hydroxy esters), and higher than that calculated from Equation 6.3.

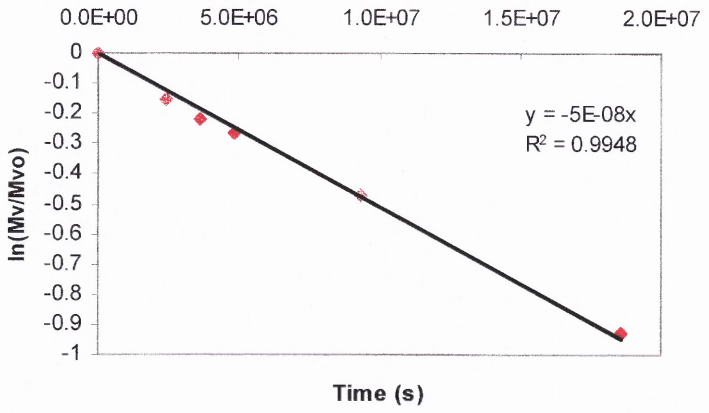

Figure 6.56 Hydrolytic degradation data for PLA based on $\ln M_v$ and Equation 6.4.

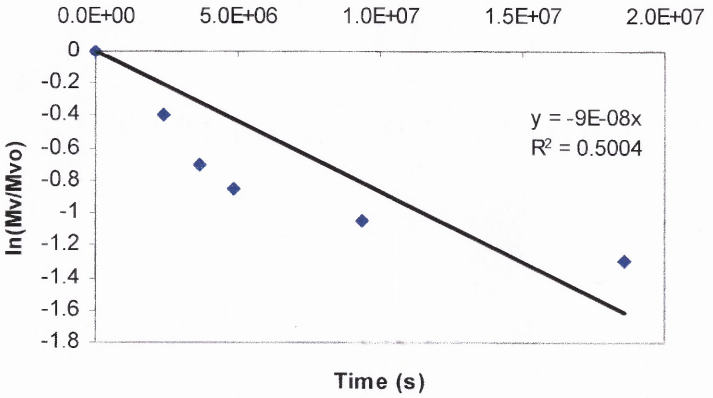

Figure 6.57 Hydrolytic degradation data for PLA/bioglass based on $\ln M_v$ and Equation 6.4.

The poor fit of the PLA/bioglass data to the first order kinetic Equations 6.3 and 6.4 suggest a complex degradation mechanism controlled by the presence and reactivity (decay) of the fillers. In the case of filled systems, only the initial points up to 56 days obey linearity. This allows the calculation and comparison of the initial rate constants. The graphs up to 56 days for both uncatalyzed and autocatalyzed PLA/bioglass systems are shown in Figures 6.58 and 6.59. The calculated rate constant values by both equations (although different in absolute terms) are still higher for the composite by an

order of magnitude. This further confirms the catalytic effect of the bioglass filler on the hydrolytic degradation of PLA.

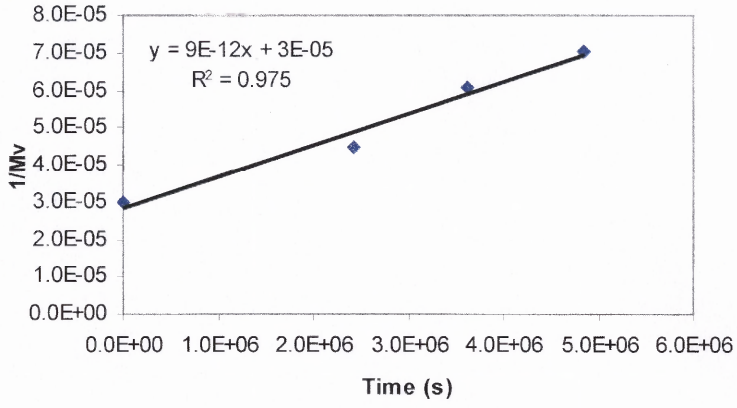

Figure 6.58 Hydrolytic degradation data up to 56 days for PLA/bioglass based on $1/\overline{M_v}$ and Equation 6.3.

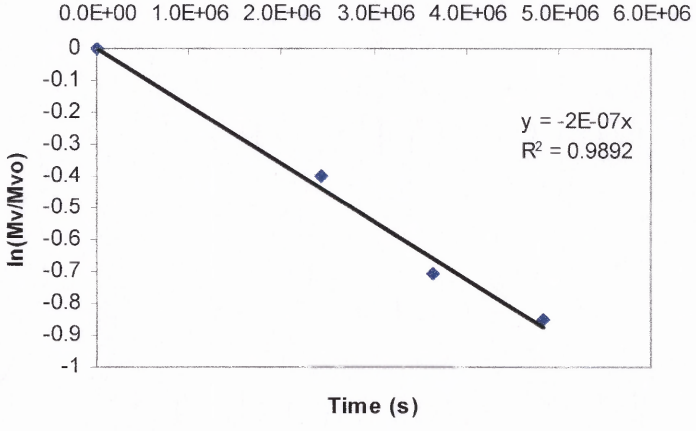

Figure 6.59 Hydrolytic degradation data up to 56 days for PLA/bioglass based on $\ln M_v$ and Equation 6.4.

The weight gain (M_t) resulting from moisture absorption can be expressed in terms of the diffusion coefficient or diffusivity, D_o, and the effective moisture equilibrium content %, M_m, as shown in Equation 6.5.

$$\frac{M_t}{M_m} = 1 - \frac{8}{\pi^2}\exp\left[-\left[\frac{D_o t}{h^2}\right]\pi^2\right] \tag{6.5}$$

where h is the thickness of the sample (Yew et al. 2005).

According to ASTM Standard D5229 (ASTM Book of Standards, 1992), the diffusivity can be calculated from the following equation:

$$D_o = \pi\left(\frac{h}{4M_m}\right)^2 \times \left(\frac{M_2 - M_1}{\sqrt{t_2} - \sqrt{t_1}}\right)^2 \tag{6.6}$$

where h is the average specimen thickness (cm), and $\frac{M_2 - M_1}{\sqrt{t_2} - \sqrt{t_1}}$ is the slope of moisture absorption plot in the initial linear portion of the curve.

D_o can be calculated from the initial linear slope of the absorption curve (slope of M_t vs. $t^{1/2}$). The percentage gain at any time t, M_t, can be determined by Equation 6.7.

$$M_t(\%) = (W_w - W_d)/W_d \times 100 \tag{6.7}$$

where W_w and W_d refer to the weight of the material after exposure to water and the initial weight of the material before exposure.

In order to calculate D_o, plots of M_t versus $t^{1/2}$ were generated (Figure 6.60) and the initial linear slopes of these plots were used for further calculations.

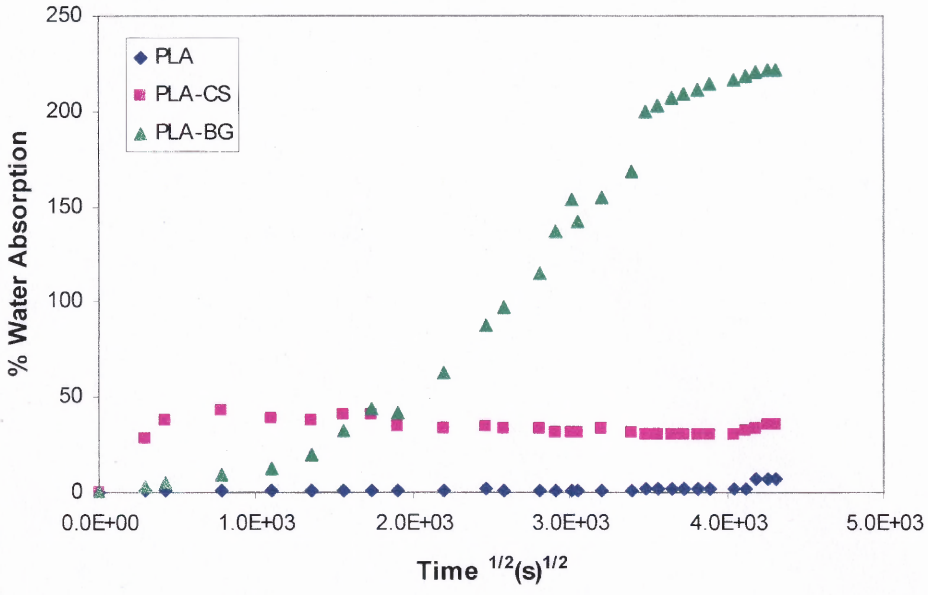

Figure 6.60 % Water absorption versus $t^{1/2}$ for PLA and its composites. Average values are shown. See comments on method of testing in Figure 6.40.

From the initial portions of the curves, the derived slope values for PLA (after magnification of the y axis) was 0.0031 (R^2=0.9608) and for PLA-CS was 0.0919 (R^2=0.9966). The % M_m, as shown in the curves, is 1.2 and 43.1 for PLA and PLA-CS, respectively, and the calculated D_o value from Equation 6.6 is 7.66×10^{-9} $cm^2 s^{-1}$. It is evident that PLA/bioglass does not follow Fickian behavior since no equilibrium is observed for M_m. As mentioned earlier, bioglass is a highly reactive material with a decay rate of 150μg/cm^2/day. For such materials, the mechanism of the composite degradation could be very complex and not easily predictable by mathematical models.

In order to ascertain the type of erosion mechanism for PLA in the present work the following values were substituted into equation 6.2: N=1180, ρ=1.25 g/cm^3 and N_A = 6.023×10^{23}. D_o=$7.66*10^{-9}$ cm^2 s^{-1}, and k from Equation 6.4 is equal to 5×10^{-8} s^{-1}. $\overline{M_n}$ =85,000 and this value falls within the expected range from our calculated $\overline{M_v}$ value

(see section 6.6.2). It is also in agreement with a value reported by Paul at al. (2005) on an amorphous PLA by the same manufacturer. Again, by substituting the values into Equation 6.2, the erosion number $\varepsilon = 5.29 \times 10^{-4} \ll 1$, which confirms that PLA undergoes bulk erosion as expected.

Diffusion behavior of composite systems containing fillers has been modeled by several authors (Lape et al. 2002, Moggridge et al. 2003, Nuxoll and Cussler, 2005). The flakes are usually considered impermeable to the permeant and mostly perfectly aligned. In this study, for PLA/bioglass composites, the processing method used does not promote flow induced orientation, and aspect ratios do not remain the same as in the original after mixing and processing. It would be safe to assume that flakes are equally aligned and misaligned after processing. According to Moggridge et al. (2003), in the case of a flake-filled film, where flakes have alignment and misalignment with equal probability, the following equation describes a transport for a particular arrangement of long ribbon-like flakes in layers model:

$$\frac{D_0}{D_{comp}} = 1 + \frac{1}{2}\frac{\alpha^2 \phi^2}{1-\phi} \tag{6.8}$$

where D_0 is the diffusion coefficient in the absence of flakes, α is the flake aspect ratio, and ϕ is the flake volume fraction. D_0 for PLA from the above data is equal to $7.66*10^{-9}$ cm^2 s^{-1}, α taken as 8.7 (from SEM images for bioglass after taking the average of 6 measurements, see Appendix A1), and ϕ is equal to 0.1765. Substituting into Equation 6.8, D_{comp} is equal to $3.149*10^{-9}$ cm^2 s^{-1}. This would indicate reduction of permeability due to the presence of flakes. However, due to the hydrophilicity and reactivity of

polymer and bioglass filler, flakes may not reduce permeability or increase the lag before permeation as predicted by reactive membrane models described by Moggridge et al. (2003).

The issue of the presence of additives reactive towards the permeant in thin films have been considered in the above reference. It has been shown that immobilized reactive groups do not alter steady state permeability, but increase lag before penetration. The time decaying bioglass maybe considered as a mobile reactive species which can actually enhance transport by facilitating diffusion. Modeling in the present case becomes extremely difficult due to occurrence of simultaneous time dependent diffusion phenomena that alter the integrity of the samples. For example, microcracks and voids accompanying the degradation of the glass result in acceleration of the polymer degradation process (Prabhakar et al. 2005). At the same time, degraded PLA becomes negatively charged and attracts positively charged calcium ions resulting in apatite formation through the attraction of phosphate groups from the solution. Uniform coverage by the formed HA will further affect permeation of the solution contributing to the complexity of the process.

CHAPTER 7

CONCLUSIONS AND RECOMMENDATIONS

General: Although, there is a significant amount of research conducted in the tissue engineering field to produce composite materials capable of bone regeneration, a thorough understanding of all the mechanisms involving degradation and bioactivity has yet to be accomplished. The experimental data of this study along with their engineering interpretation could provide an initial step in understanding the fundamentals in designing materials for bone regeneration. Previous investigations in this field have focused on the *in vitro* bioactivity mechanisms of neat ceramic fillers, in terms of apatite growth, without taking into account the interactions between polymer and filler, which in the case of the composites, could also affect the kinetics of apatite formation. Diffusion mechanisms along with nucleation and growth kinetics are of great importance and should be considered simultaneously. In addition, degradation studies and hydrophilicity enhancement resulting from both the filler and the polymer, filler surface area, as well as processing characteristics are parameters that should be taken into account.

Experimental: Regarding bioactivity mechanisms, several experimental methods to test bioactivity as SEM, EDX, XRD and changes in ion concentration were used in this work. There were experimental limitations due to the adopted testing procedures that created challenges in the interpretation of the experimental results. Examples are: a) non replenishment of the SBF, b) SEM and EDX analysis results specific to localized small areas, whereas XRD results reflected the entire macroscopic sample area and c) P and Ca ion concentrations inferred from wet chemistry experiments that would not necessarily correspond to surface changes due to mineral deposition.

Neat fillers: In the case of the neat fillers, the form at which the fillers were tested for apatite growth (powders, tablets, rods that were cut in polished and non polished discs) was of great importance and showed significant differences as a result of the different manufacturing conditions. From the six fillers tested, bioglass and CS powders were the ones that showed faster nucleation and growth rates in the screening experiments. Other experiments showed that polished vs. non polished bioglass rods exhibited differences in bioactivity. For the non polished rods, mineral precipitation did not occur, whereas the non polished ones showed a fast apatite layer formation. This is due to irregularities of the non polished rods that act as nucleation sites for further nucleation and growth of the apatite layer.

PCL composites: PCL composites containing five different fillers were evaluated. Different processing methods (solution vs. melt processed samples) showed differences in apatite growth. For the PCL/HA and PCL/β-TCP composites, differences in apatite formation behavior may be related to differences of extrusion vs. solution mixed samples in terms of: a) thermal history and its effects on the stability of the calcium phosphate fillers, b) crystallinity and thickness of the outer surface polymer layer and their effects on permeation rate and degradation, and c) distribution of filler particles at/or near this outer layer and its effect on uniformity of mineral coverage.

For melt mixed PCL/$CaCO_3$ composites, a fast precipitation of mineral globules can be seen after one week immersion and is limited after four weeks possibly due to the lack of SBF replenishment. This is in agreement with XRD data that apatite peaks are evident after one week and weaker after four weeks.

SEM images for the melt processed PCL/bioglass composites showed mineral precipitation after the first week of immersion and lack of additional bioactivity for the remaining testing period. This was not in agreement with the XRD data. A possible explanation could be that the coverage area examined in SEM and EDX is much more localized compared to the larger testing area of the XRD samples. The limited apatite growth in the bioglass composites could be also due to the PCL hydrophobicity and the resulting slow polymer degradation rate, as well as the relatively low concentration of the bioactive filler. Results from AA and UV-Vis spectroscopy on bioglass composites, showed no change in Ca concentration during the first four weeks, possibly due to the establishment of equilibrium as Ca diffuses in and out of the composite and a continuous consumption of P from the SBF up to four weeks.

In the case of melt processed PCL/CS composites SEM data showed mineral surface coverage after the first four week period. AA and UV-Vis spectroscopy experiments were in agreement with SEM data since there was a continuous Ca release and P consumption, denoting that reactions could still take place after four weeks. In the case of solution mixed CS composites there was a faster nucleation and growth that could be due to different processing history, but also due to differences in surface morphology.

PLA composites: PLA composites containing two different fillers, both melt mixed, were evaluated for bioactivity, in terms of apatite growth. PLA/bioglass composites showed mineral precipitation after one week immersion. XRD data were in agreement with SEM and EDX data, since the peak at 32^{o} was evident after one and four weeks, but no longer visible after eight weeks immersion. AA and UV-Vis results

suggest that, in the case of PLA composites, faster degradations rates apply, possibly due to the higher polymer hydrophilicity enhanced by the hydrophilic nature of the filler.

In the case of PLA/CS composites the SEM images showed globules of mineral precipitates that fully covered the exposed area after one and four weeks immersion. Similarly to bioglass composites, Ca diffuses out of the CS composites, but reaches equilibrium after eight weeks immersion. In the case of P consumption, a similar trend as for the bioglass composite is observed, but at higher consumption rates implying higher hydrophilicity for the CS composites. It appears that after the eight week period, ionic activity is limited; thus, bioactivity of the composites (as shown by SEM, EDX and XRD data) is also limited.

Degradation: Regarding degradation results, there were indications that the hydrolysis rate was higher in an amorphous polymer such as PLA, than in the semicrystalline PCL from weight changes and IV measurements. The presence of CS and bioglass fillers appeared to enhance the degradation behavior of both PCL and PLA. pH changes, during hydrolytic degradation, depend not only on the polymer used, but also on the filler; bioglass due to its reactivity and decay results in significant pH increase in the case of PLA, but not in the case of PCL. In the case of PLA composites, there is a significant reduction in MW of the matrix after melt processing in the presence of bioglass as compared to the unfilled PLA. The presence of CaO in bioglass that is known to catalyze thermal degradation of PLA would be responsible for this phenomenon. MW decreases exponentially with time for both unfilled and filled PLA; for the filled system this agrees with observations from weight and pH change studies.

Thermal data showed crystallinity increase with immersion time in all samples, although crystallinity appears to increase more in extruded vs. compression molded samples. Bioglass appears to affect more the crystallinity of PCL than the CS. In the case of PLA, bioglass appears to decrease somewhat the T_g of the matrix as immersion time increases, whereas CS decreases T_g to a much lesser extent. Mechanical testing showed a significant decrease of elongation at break for unfilled PLA even after a two week immersion period, indicating significant embrittlement associated with a reduction in MW of about 13% as suggested by IV measurements. For the compressive properties of unfilled PLA, relatively large changes can only be observed for compressive modulus and strain at break. In the case of the CS filled system, more significant changes can be observed in the compressive stress at yield, compressive stress at break and in the initial compressive modulus even after two weeks immersion.

Modeling: IV data for PLA and PLA/bioglass composites were fitted in two models after hydrolytic degradation. IV data for unfilled PLA in the absence of bioglass were well represented by both predictive models up to 215 days. However, for PLA/bioglass systems significant deviations from linearity were observed after 56 days. Based on these models, initial degradation rates were calculated and were found to be affected by the presence of the bioglass filler which presumably acted catalytically. Experimental data were also fitted into an equation proposed to calculate erosion number, and in the case of unfilled PLA were found to agree with literature findings suggesting bulk erosion. Available models for systems recognizing the presence of non reactive misaligned flakes, confirmed the reduction in the diffusion coefficient vs. the unfilled polymer. Modeling of transport in the case of a composite consisting of a degrading

polymer and a reactive decaying filler, becomes extremely difficult due to the occurrence of simultaneous time dependent diffusion phenomena that alter the integrity of the sample.

Recommendations: The following are recommendations for future work.

- Future work should include experiments on composites containing degradable polyesters with different crystallinity and molecular weight and the most promising bioactive silicate fillers studied in the present work. In particular, polyester blends or copolymers could be used to tailor the mechanical properties of the composite and promote the desirable physiochemical interactions with the surface of the bioactive filler.
- A more detailed investigation is required to explore the reasons for the diminishing bioactivity, in terms of apatite growth, of certain aliphatic polyester/filler systems at longer immersion time periods.
- Further efforts should be made to model water transport in the case of composites containing degrading polymers and reactive decaying fillers, and to determine the required assumptions for the case of anisodimensional bioactive reinforcements.
- Selected systems of this work should be evaluated on bioactivity and degradation in the presence of biological growth factors that will participate in a series of cellular events.

APPENDIX A

SEM OF CALCIUM SILICATE AND BIOGLASS POWDERS

A.1 Calcium Silicate Powder

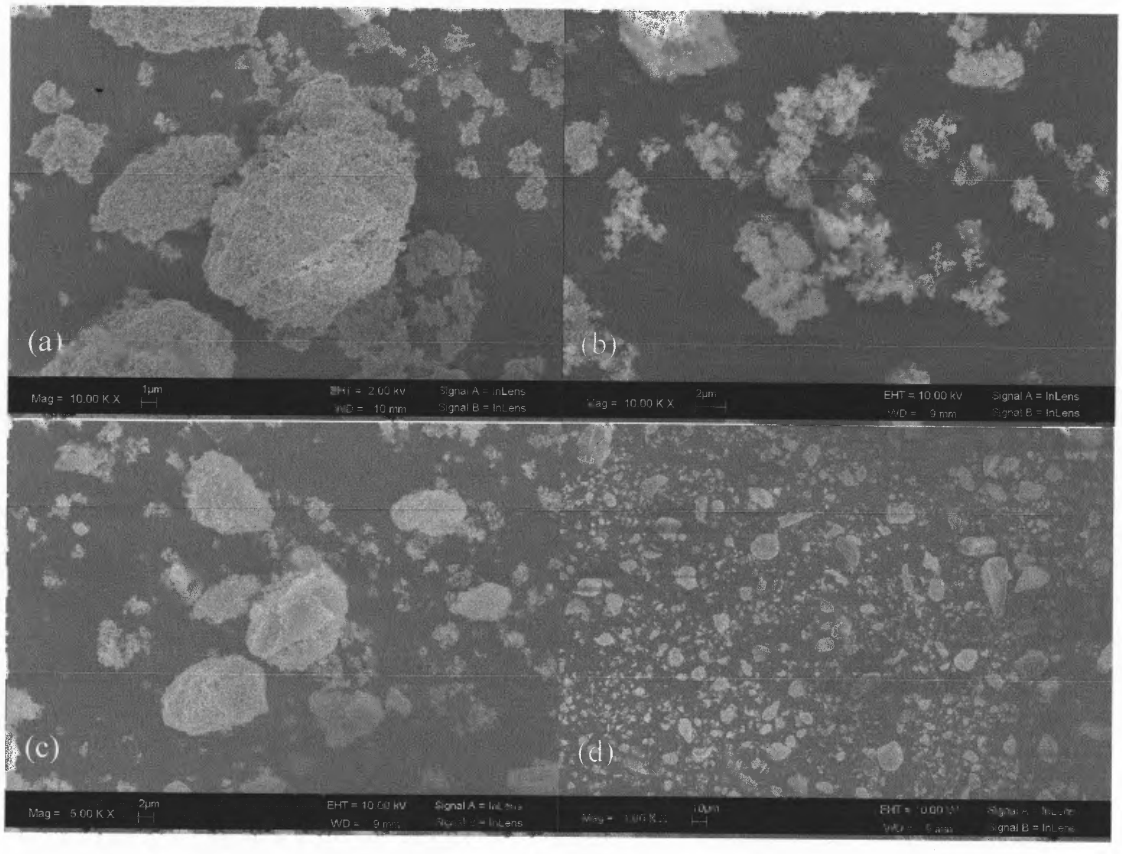

Figure A.1 SEM micrographs of CS powder. (a), (b) 10,000 magnification. (c) 5,000 magnification. (d) 1,000 magnification.

A.2 Bioglass 45S5 Powder

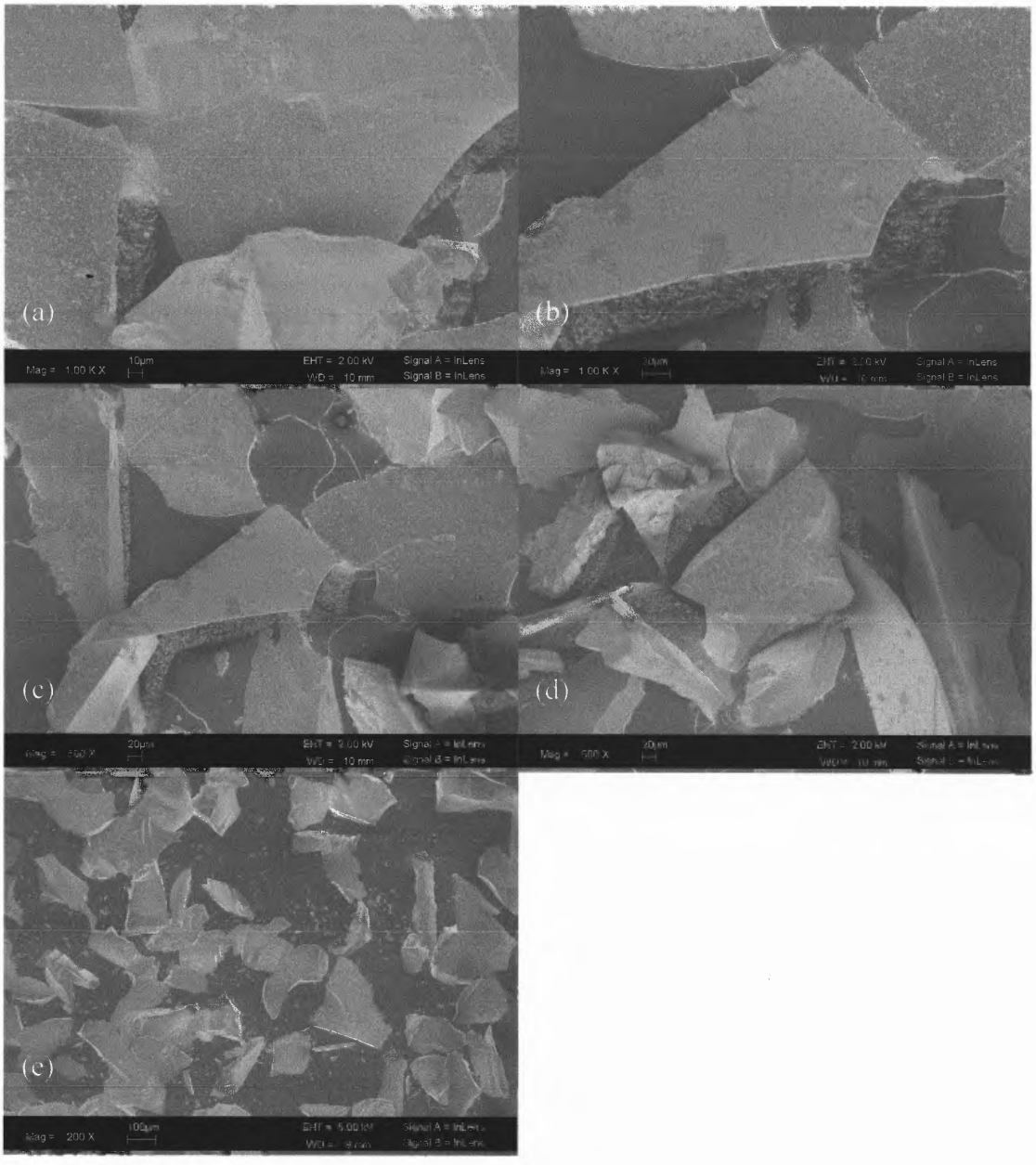

Figure A.2 SEM micrographs of bioglass powder. (a), (b) 1,000 magnification. (c), (d) 500 magnification. (e) 200 magnification.

APPENDIX B

PREPARATION OF SBF SOLUTION

The procedure followed for SBF preparation is described below (Ohtsuki website).

Cleaning

Firstly, all the bottles including flasks, beakers etc. should be cleaned with dilute hydrochloric acid solution and distilled water.

Dissolution of chemicals

Put 750 ml of DW into a 1 liter beaker. Stir the water and keep its temperature at 36.5°C with magnetic stir with heater.

Add each chemical given in Table B1 into the water until #8, one by one in the order given in Table B1, after each reagent was completely dissolved. Weigh each chemical with weighing bottle. Add it in the water. Wash the remaining chemical on the weighing bottle with DW water and add the solution in the water.

Addition of reagent #9 should be little by little with less than about 1g, in order to avoid local increase in pH of the solution.

Table B.1 Reagents for Preparation of SBF

Order	Reagent	Amount
#1	NaCl	7.996 g
#2	$NaHCO_3$	0.350 g
#3	KCl	0.224 g
#4	$K_2HPO_4 \cdot 3H_2O$	0.228 g
#5	$MgCl_2 \cdot 6H_2O$	0.305 g
#6	1 kmol/m^3 HCl	40 cm^3
#7	$CaCl_2$	0.278 g
#8	Na_2SO_4	0.071 g
#9	$(CH_2OH)_3CNH_2$	6.057 g
#10	1 kmol/m^3 HCl	Appropriate amount for adjusting pH

Adjustment of pH

Calibrate the pH meter with fresh standard buffer solution.

After #9 on the order in Table B1, check the temperature of the solution in the beaker, and place the electrode of pH meter in the solution. Measure its pH while the temperature is at 36.5 °C. At this point, pH of the solution is approximately 7.5. Titrate 1kmol/dm^3-HCl solution with pipette to adjust the pH at 7.25 (or 7.40).

After the adjustment of pH, transfer the solution from the beaker to a glass volumetric flask of 1000 ml. Wash the inside of the beaker with DW several times and add the solution to the flask. Add DW water to the solution, adjusting the total volume of the solution to 1 liter, and then shake the flask well.

Storage

Store the flask in a refrigerator at 5-10 °C.

Stability of the solution must be examined. Put 50 ml of the solution in a polystyrene bottle and place it in incubator at 36.5 °C. After 2-3 days, check whether the solution has any precipitation or not. If any precipitation would be found, do not use the solution.

APPENDIX C

STANDARDS AND SAMPLES PREPARATION FOR SOLUTION ANALYSIS

C.1 Ascorbic Acid Method

The standards and the samples for the Ascorbic Acid Method were prepared according to Stannous Chloride method 4500-P E (Standard Methods for the Examination of Water and Wastewater).

Reagents

1) Sulfuric Acid H_2SO_4, 5N: Slowly dilute 70 ml concentrated H_2SO_4 to 500 ml with deionized water.

2) Potassium Antimonyl Tartrate solution: Dissolve 1.3715 g $K(Sbo)C_4H_4O_6 \cdot 1/2H_2O$ in 500 ml deionized water.

3) Ammonium Molybdate solution: Dissolve 20 g $(NH_4)_6Mo_7O_{24} \cdot 4H_2O$ in 500 ml deionized water.

4) Ascorbic Acid 0.01 M: Dissolve 1.76 g ascorbic acid in 100 ml deionized water. Keep solution refrigerated. It is stable for one week if it is kept refrigerated at 4 ^{0}C.

5) Combined Reagent: Mix above reagents in the following proportions.

50 ml 5N H_2SO_4, 5 ml $K(Sbo)C_4H_4O_6 \cdot 1/2H_2O$, 15 ml $(NH_4)_6Mo_7O_{24} \cdot 4H_2O$ and 30 ml ascorbic acid solution. Mix it well until all combined reagent solution reaches room temperature. The solution is stable for four hours.

Preparation of standards

Standard 50 ppm phosphate solution: Dilute 219.5 mg anhydrous KH_2PO_4 to 1 liter deionized water.

1) Blank.

2) 0.15 ppm phosphate solution: Dilute 6 ml of 50 ppm phosphate solution to 100 ml.

3) 0.50 ppm phosphate solution: Dilute 1 ml of 50 ppm phosphate solution to 100 ml.

4) 1 ppm phosphate solution: Dilute 2 ml of 50 ppm phosphate solution to 100 ml.

5) 1.3 ppm phosphate solution: Dilute 2.6 ml of 50 ppm phosphate solution to 100 ml.

Procedure

Put 50 ml sample into 250 ml flask. Add 0.05 ml (one drop) phenolphthalein. If a red color develops, add 5N H_2SO_4 drop wise to discharge the color. Then add 8 ml combined reagent and mix well. Wait at least 10 minutes but no more than 30 minutes to test the samples. Absorbance of each sample/standard should be measured at 880 nm. Prepare the calibration curve and test the samples.

C.2 Direct Air-Acetylene Flame Method

The preparation of the standards and the samples for the Direct Air-Acetylene Flame method is described bellow.

Reagents

Calcium chloride: Suspend 0.2497 g of calcium carbonate, $CaCO_3$, dried for 1 hour at 180 ^0C, in deionized water and dissolve cautiously by adding a minimum amount of dilute HCl. Dilute to 1 liter with deionized water.

Lanthanum chloride solution: Dissolve 58.65 g of La_20_3, slowly and in small portions, in 250 ml conc. HCl and dilute to 1 liter with deionized water.

Prepare 1, 2, 3, 4, 5 ppm calcium standards and plot calibration curve. For samples, put 5 ml sample, add 2 ml La_20_3 and dilute to 100 ml.

APPENDIX D

BIOACTIVITY OF NEAT FILLERS

D.1 Hydroxyapatite

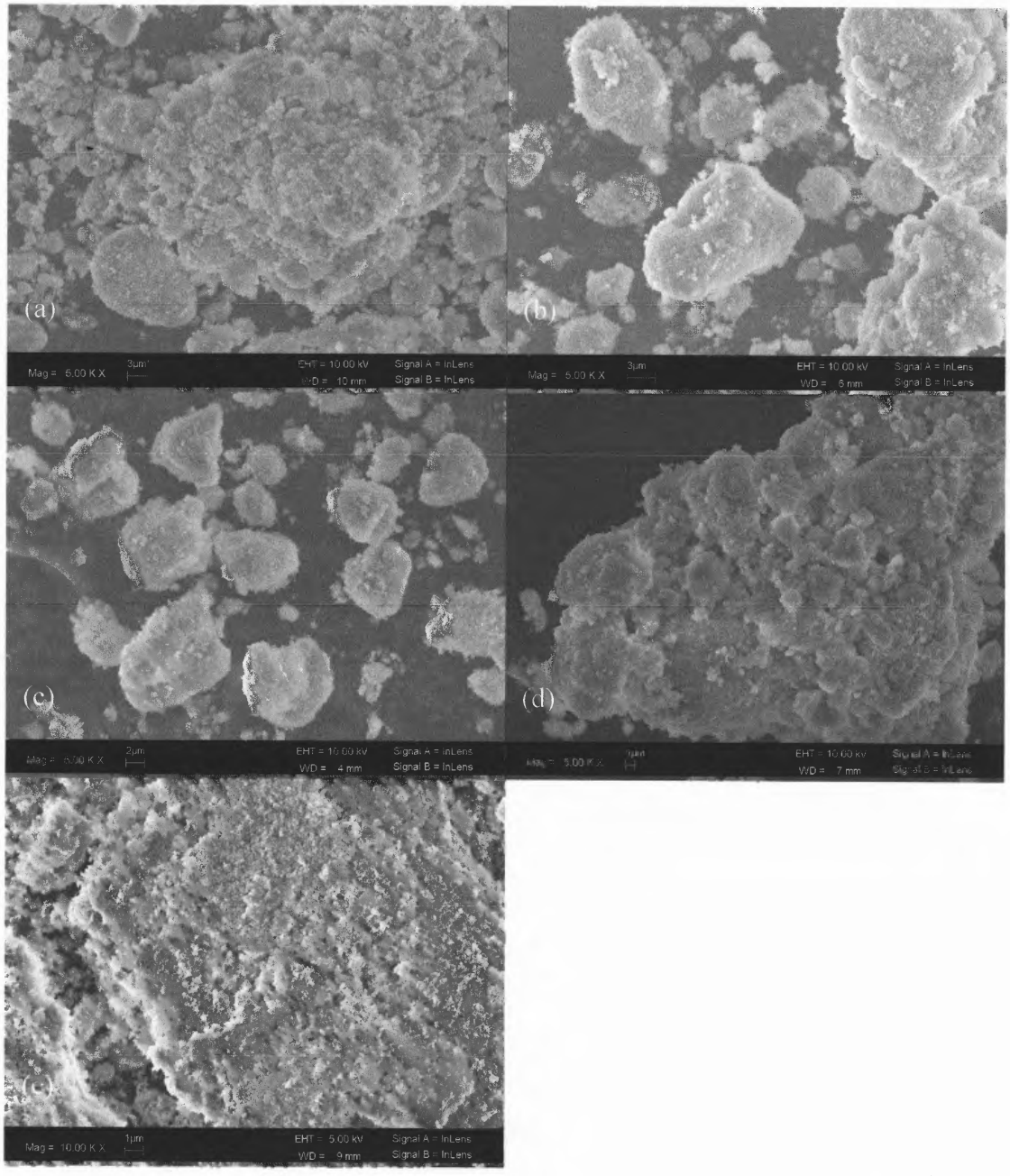

Figure D.1 HA powder before and after immersion in DW and SBF. (a) Before immersion (x5000). (b) After 6 hrs immersion in DW (x5,000). (c) After 6 hrs immersion

in SBF (x5,000). (d) After 24 hours immersion in SBF (x5,000). (e) After 168 hrs (1 week) immersion in SBF (x10,000).

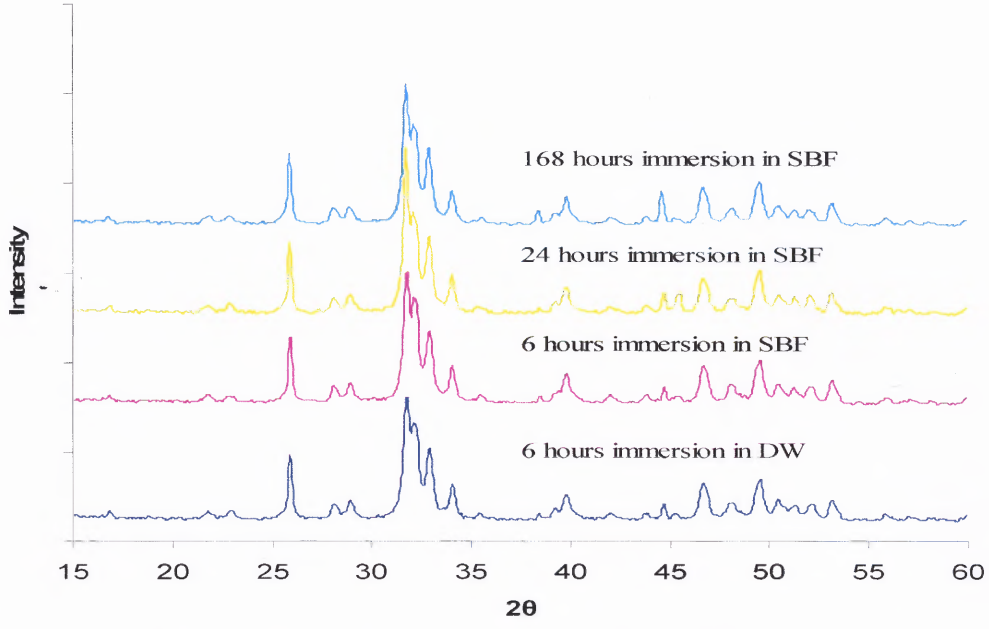

Figure D.2 XRD spectra of HA after exposure to DW and SBF.

D.2 Tricalcium Phosphate

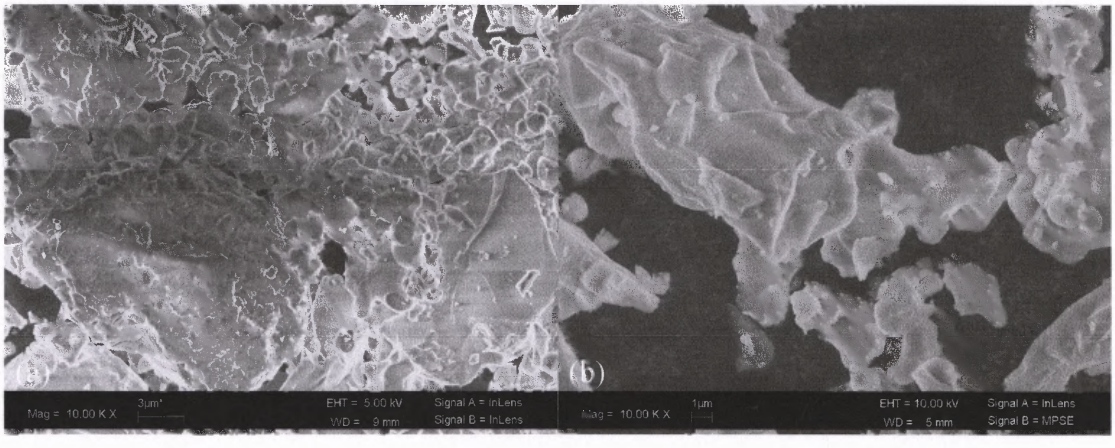

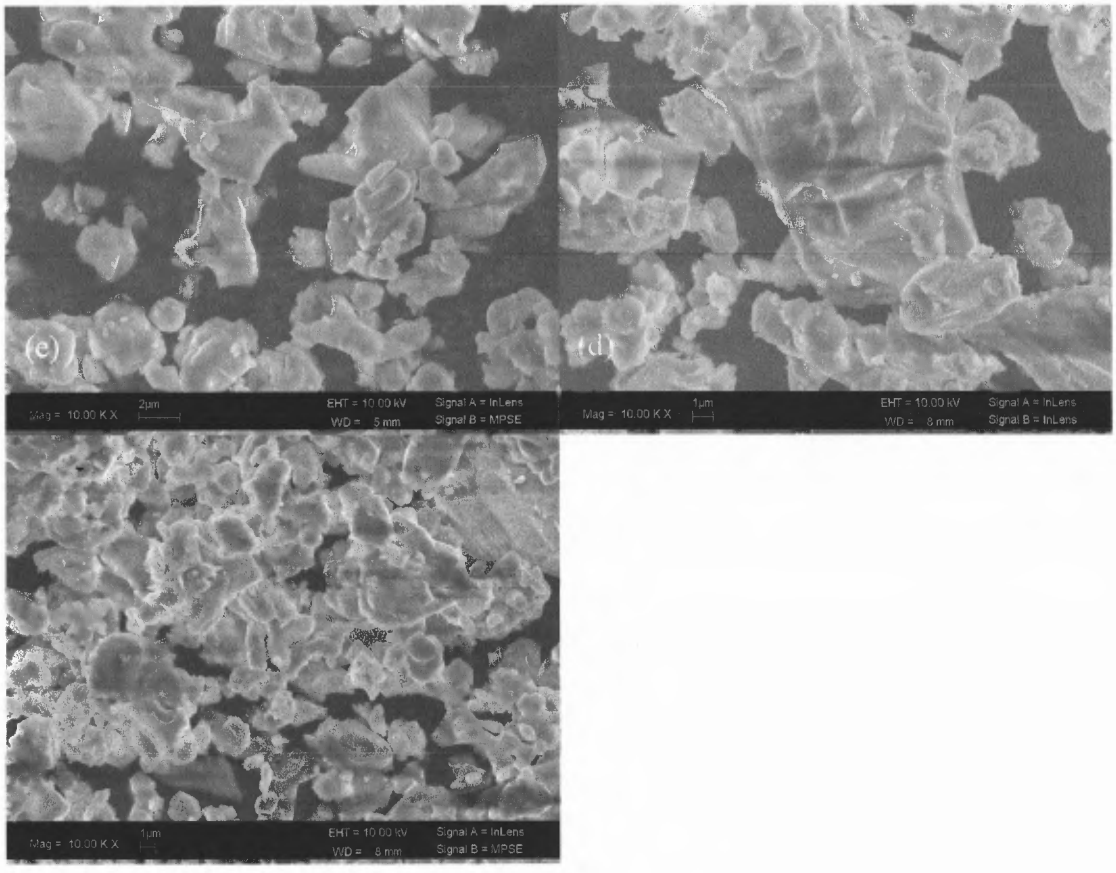

Figure D.3 TCP powder before and after immersion in DW and SBF. (a) Before immersion (x10,000). (b) After 6hrs immersion in DW (x10,000).(c) After 6hrs immersion in SBF (x10,000). (d) After 24 hrs immersion in SBF (x10,000). (e) After 168hrs (1week) immersion in SBF (x10,000).

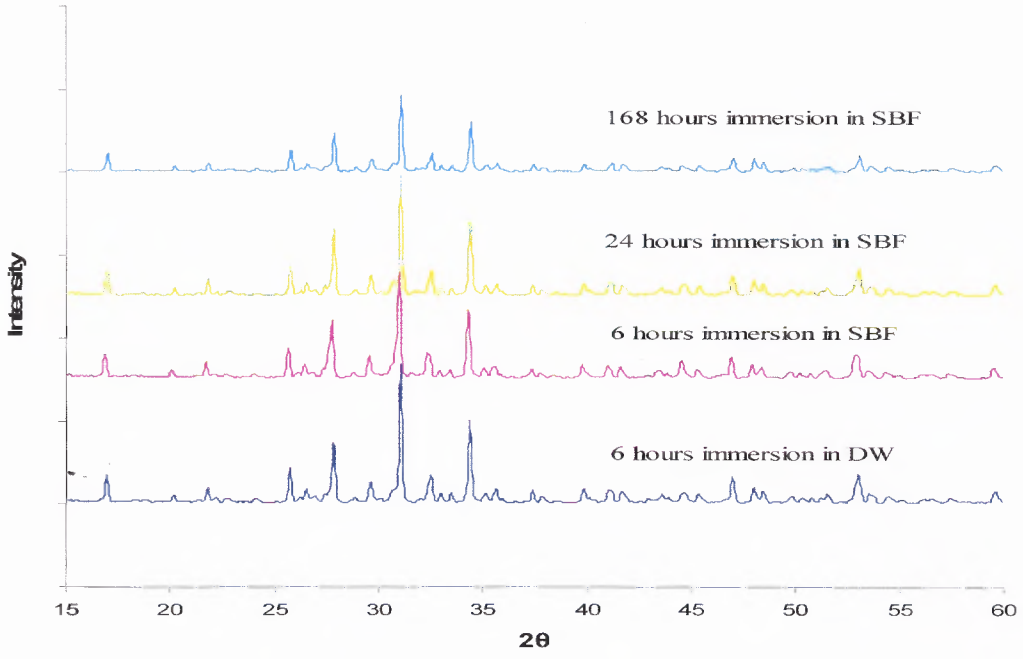

Figure D.4 XRD spectra of TCP after exposure to DW and SBF.

D.3 Calcium Carbonate

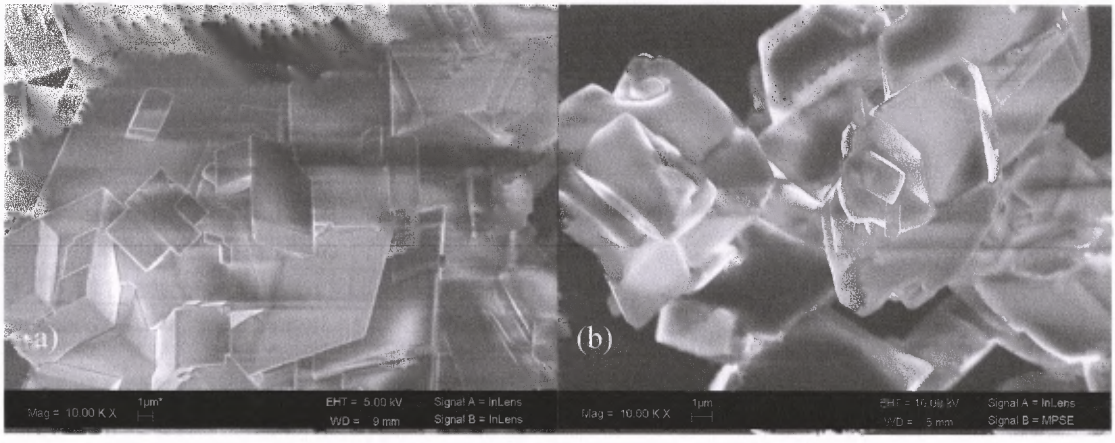

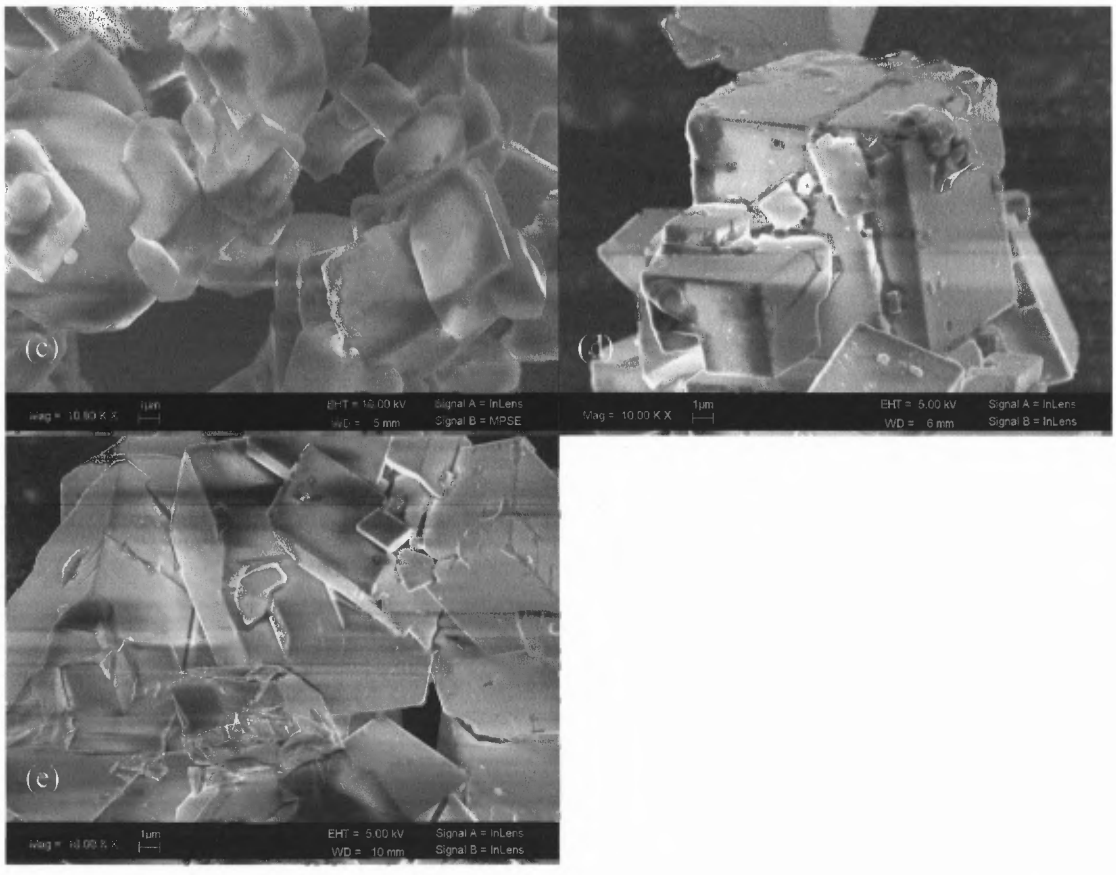

Figure D.5 Calcium carbonate (CC) powder before and after immersion in DW and SBF. (a) Before immersion (x10,000). (b) After 6hrs immersion in DW (x10,000).(c) After 6hrs immersion in SBF (10,000). (d) After 24 hrs immersion in SBF (x10,000). (e) After 168hrs (1week) immersion in SBF (10,000).

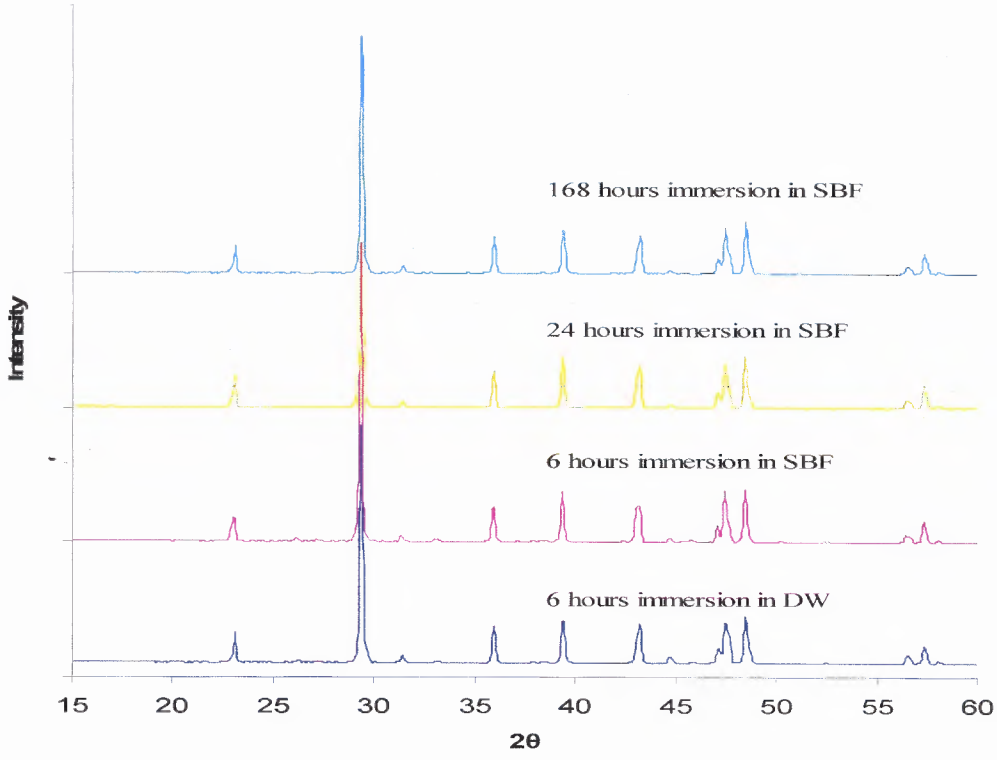

Figure D.6 XRD spectra of CC after immersion in DW and SBF.

D.4 Bioactive Glass 1393

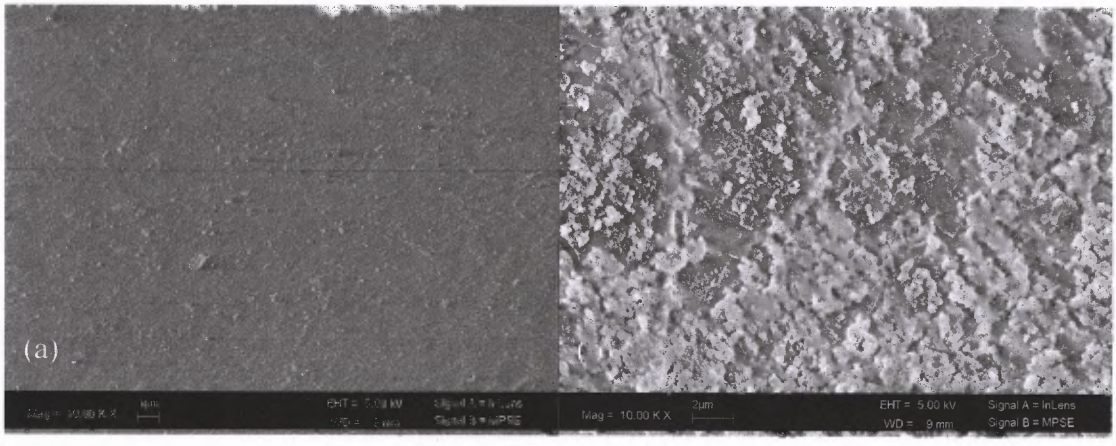

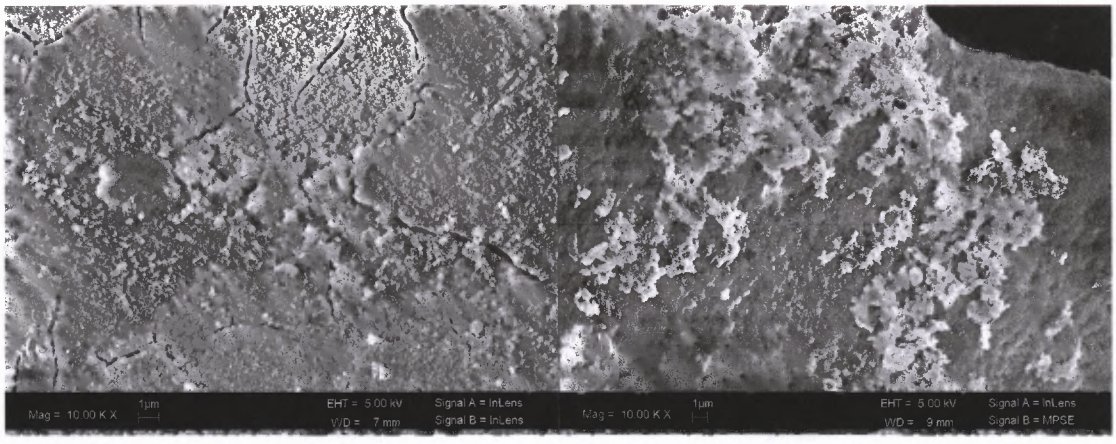

Figure D.7 BG1393 powder after immersion in DW and SBF. (a) After 6hrs immersion in DW (x10,000).(b) After 6hrs immersion in SBF (10,000). (c) After 24 hrs immersion in SBF (x10,000). (d) After 168hrs (1week) immersion in SBF (10,000).

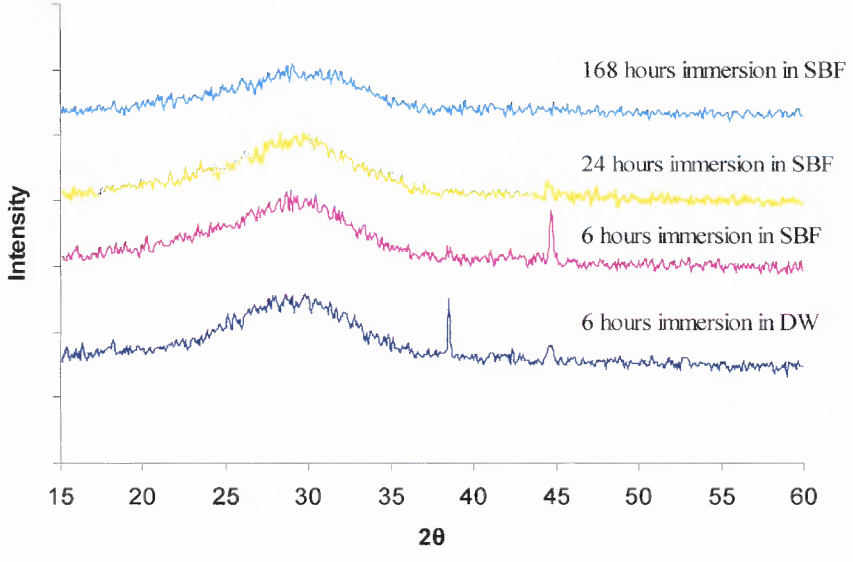

Figure D.8 XRD spectra for BG1393 after immersion in DW and SBF.

APPENDIX E

COMPRESSIVE PROPERTIES OF PLA COMPOSITES

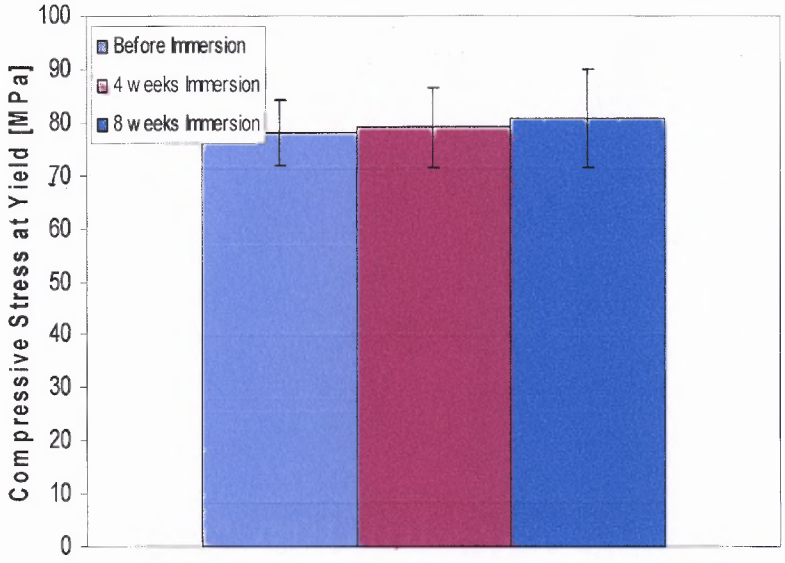

Figure E.1 Compressive Stress at Yield of PLA before and after immersion.

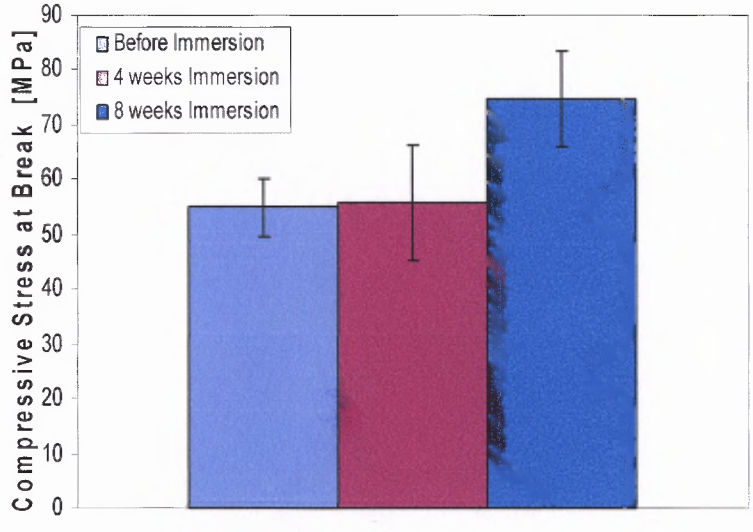

Figure E.2 Compressive Stress at Break of PLA before and after immersion.

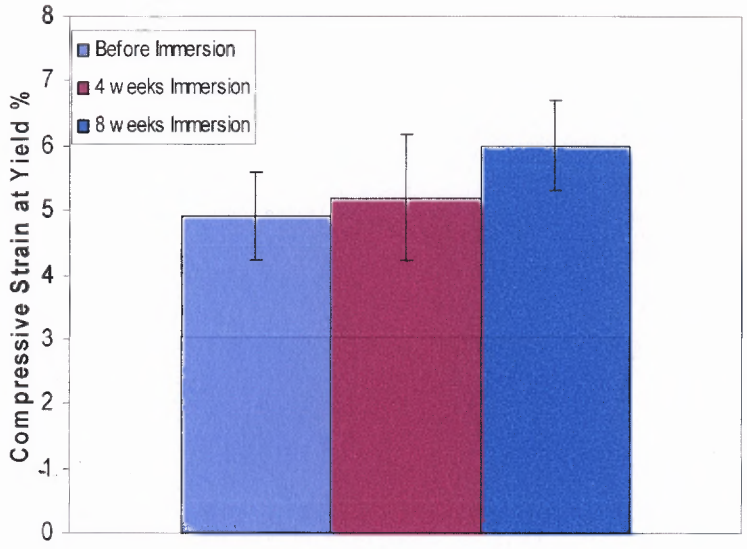

Figure E.3 Compressive Strain at Yield % of PLA before and after immersion.

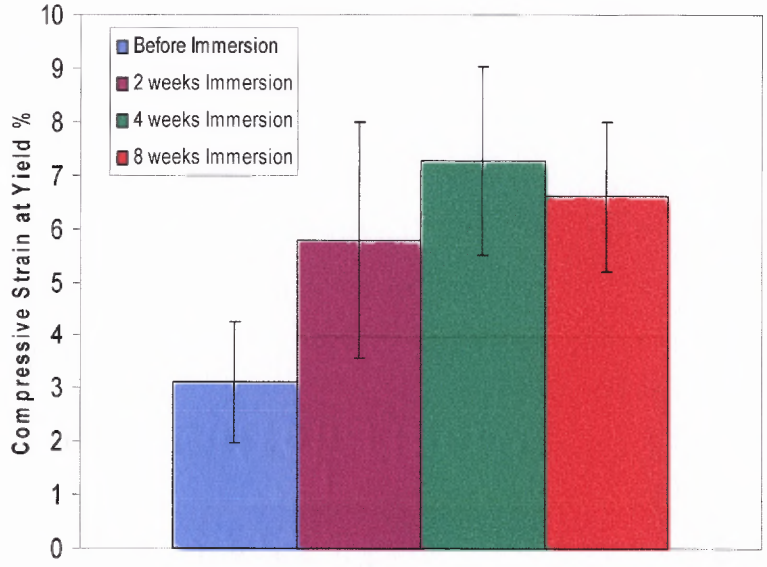

Figure E.4 Compressive Strain at Yield % of PLA-CS before and after immersion.

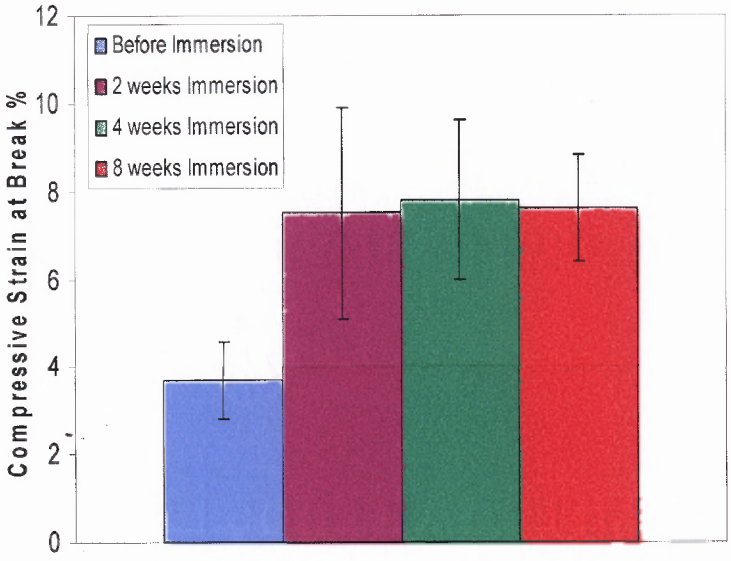

Figure E.5 Compressive Strain at Break % of PLA-CS before and after immersion.

REFERENCES

American Academy of Orthopedic Surgeons website, www.aaos.org, (03/06).

Anderson JM. Perspectives of the in vivo responses of biodegradable polymers. In: Hollinger JO, editor. Biomedical applications of synthetic biodegradable polymers. Boca Raton: CRC Press, 1995. p. 223-233.

Ara M, Watanabe M, Imai Y. Effect of blending calcium compounds on hydrolytic degradation of poly(DL-lactic-co-glycolic acid). Biomaterials 2002; 23: 2479-2483.

Ashman A, Gross JD. Synthetic osseous-grafting. In: Wise DL, Trantolo DB, Lewandrowski KU, Gresser JD, Cattaneo MV, Yaszemski MJ, editors. Biomaterials engineering and devices: Human applications. New Jersey: Humana Press, 2000. p. 133-154.

ASTM Book of Standards, ASTM D5229/D5229M-92, ASTM International. West Conshohocken, PA 1992.

Azevedo MC, Reis RL, Claase MB, Grijpma DW, Feijen J. Development and properties of polycaprolactone/hydroxyapatite composite biomaterials. J Mater Sci: Mater Med 2003; 14: 103-107.

Bagot D'Arc M and Daculsi G. Micro macroporous biphasic ceramics and fibrin sealent as a moldable material for bone reconstruction in chronic otitis media surgery. A 15 years experience. J Mater Sci: Mater Med 2003; 14: 229-233.

Boccaccini A.R. and Maquet V. Bioresorbable and bioactive polymer/Bioglass® composites with tailored pore structure for tissue engineering applications. Comp Sci Tech 2003; 63: 2417-2429.

Boskey AL. The organic and inorganic matrices. In: Hollinger JO, Einhorn TA, Doll BA, Sfeir C, editors. Bone tissue engineering. Boca Raton: CRC Press, 2005. p. 91-124.

Braun PV. Natural nanocomposites, biomimetic nanocomposites, and biologically inspired nanocomposites. In: Ajayan PM, Schadler LS, Braun PV, editors. Nanocomposite science and technology. Weinheim, Germany: Wiley VCH, 2003. p. 160-165.

Brink M, Turunen T, Happonen RP, Yli-Urpo A. Compositional dependence of bioactivity of glasses in the system Na_2O-K_2O-MgO-CaO-B_2O_3-P_2O_5-SiO_2. J Biomed Mater Res 1997; 37: 114-121.

Burkersroda F, Schedl L, Gopferich A. Why degradable polymers undergo surface erosion or bulk erosion. Biomaterials 2002; 23: 4221-4231.

Callister WD. Materials science and engineering, An introduction. Hoboken: John Wiley & Sons, 2003. p. 598.

Causa F, Netti PA, Ambrosio L, Ciapetti G, Baldini N, Pagani S, Martini D, Giunti A. Poly-ε-caprolactone / hydroxyapatite composites for bone regeneration: in vitro characterization and human osteoblast response. J Biomed Mater Res Part A 2006; 76A:151-162.

Chen LJ and Wang M. Production and evaluation of biodegradable composites based on PHB-PHV copolymer. Biomaterials 2002; 23: 2631-2639.

Cheng W. Fabrication and characterization of polysulfone-dicalcium silicate composite films. J Biomaterials Applications 2006; 20: 361-376.

Chouzouri G, Xanthos M. Bioactive fillers. In: Xanthos M, editor. Functional fillers for plastics. Weinheim, Germany: Wiley VCH, 2005. p. 387-399.

Chu CC. Degradation and biocompatibility of synthetic absorbable suture materials: general biodegradation phenomena and some factors affecting biodegradation. In: Hollinger JO, editor. Biomedical applications of synthetic biodegradable polymers. Boca Raton: CRC Press, 1995. p. 103-128.

Daculsi G. Biphasic calcium phosphate concept applied to artificial bone, implant coating and injectable bone substitute. Biomaterials 1999; 19: 1473-1478.

Daculsi G, Laboux O, Malard O, Weiss P. Current state of the art of biphasic calcium phosphate bioceramics. J Mater Sci: Mater Med 2003; 14: 195-200.

Davis JR. Handbook of materials for medical devices. Ohio: ASM International, 2003. p. 137-170.

De Aza PN, Luklinska ZB, Martinez A, Anseau MR, Guitian F, De Aza S. Morphological and structural study of pseudowollastonite implants in bone. J Microscopy 2000; 197: 60-67.

Doll B. Developmental biology of the skeletal system. In: Hollinger JO, Einhorn TA, Doll BA, Sfeir C, editors. Bone tissue engineering. Boca Raton: CRC Press, 2005. p. 3-26.

Ducheyne P, Qiu Q. Bioactive ceramics: the effect of surface reactivity on bone formation and bone cell function. Biomaterials 1999; 20: 2287-2303.

Fernandez E, Gil F, Ginebra M, Driessens F, Planell J, Best S. Calcium phosphate bone cements for clinical applications. Part I: Solution chemistry. J Mater Sci: Mater Med 1999; 10: 169-176.

Fujibayashi S, Neo M, Kim HM, Kokubo T, Nakamura T. A comparative study between in vivo bone ingrowth and in vitro apatite formation on Na_2O-CaO-SiO_2 glasses. Biomaterials 2003; 24:1349-1356.

Fujihara K, Kotaki M, Ramakrishna S. Guided bone regeneration membrane made of polycaprolactone / calcium carbonate composite nano-fibers. Biomaterials 2005; 26:4139-4147.

Fulgueiras MR, La Torre GP, Hench LL. Solution effects on the surface reactions of a bioactive glass. J Biom Mater Res 1993; 27: 445-453.

Gopferich A and Lang R. Modeling of polymer erosion. Macromolecules 1993; 26: 4105-4112.

Hao J, Yuan M, Deng X. Biodegradable and biocompatible nanocomposites of poly(ε-caprolactone) with hydroxyapatite nanocrystals: thermal and mechanical properties. J Appl Polym Sci 2002; 86:676-683.

Hasegawa S, Tamura J, Neo M, Goto K, Shikinami Y, Saito M, Kita M, Nakamura T. In vivo evaluation of a porous hydroxyapatite/poly-DL-lactide composite for use as a bone substitute. J Biom Mater Res 2005; 75A: 567-579.

Hasegawa S, Ishii S, Tamura J, Furukawa T, Neo M, Matsusue Y, Shikinami, Okuno M, Nakamura T. A 5–7 year in vivo study of high-strength hydroxyapatite/poly(l-lactide) composite rods for the internal fixation of bone fractures. Biomaterials 2006; 27: 1327-1332.

Hench LL. Bioactive ceramics. In: Ducheyene P, Lemons JE, editors. Part II of Bioceramics: Material characteristics versus in vivo behavior. New York: The New York Academy of Sciences, 1988. p. 54-71.

Hench LL. Ceramics, glasses and glass-ceramics. In: Ratner BD, Hoffman AS, Schoen FJ, Lemons JE, editors. Biomaterials science: An introduction to materials in medicine. San Diego: Academic Press, 1996. p. 84.

Hench LL. Biomaterials: a forecast for the future. Biomaterials 1998; 19: 1419-1423.

Hench LL. Website http://www.in-cites.com/papers/ProfLarryHench.html, (02/04).

Hench LL. Website http://www.bg.ic.ac.uk/Lectures/Hench/BioComp/Chap3.html, (04/04)

Higashi S, Yamamuro T, Nakamura T, Ikada Y, Hyon SH, Jamshidi K. Polymer-hydroxyapatite composites for biodegradable bone fillers. Biomaterials 1986; 7: 183-187.

Jaakola T, Rich J, Tirri T, Narhi T, Jokinen M, Seppala J, Yli-Urpo A. In vitro Ca-P precipitation on biodegradable thermoplastic composite of poly(ε-caprolactone-co-DL-lactide) and bioactive glass (S53P4). Biomaterials 2004; 25: 575-581.

Jallot E. Nanoscale physicochemical reactions at bioceramics-bone tissue interfaces. In: Nalwa HS. Handbook of nanostructure biomaterials and their applications in nanobiotechnology. California: American Scientific Publishers, 2005. p. 495-509.

Jiang G, Evans ME, Jones IA, Rudd CD, Scotchford CA, Walker GS. Preparation of poly(ε-caprolactone)/continuous bioglass fibre composite using monomer transfer moulding for bone implant. Biomaterials 2005; 26: 2281-2288.

Juhasz JA, Best SM, Brooks R, Kawashita M, Miyata N, Kokubo T, Nakamura T, Bonfield W. Mechanical properties of glass-ceramic A–W-polyethylene composites: effect of filler content and particle size. Biomaterials 2004; 25: 949-955.

Kasuga T, Maeda H, Kato K, Nogami M, Hata KI, Ueda M. Preparation of poly(lactic acid) composites containing calcium carbonate (vaterite). Biomaterials 2003; 24: 3247-3253.

Kazarian SG, Chan KLA, Maquet V, Boccaccini AR. Characterization of bioactive and resorbable polylactide/ Bioglass® composites by FTIR spectroscopic imaging. Biomaterials 2004; 25: 3931-3938.

Kim HM, Himeno T, Kokubo T, Nakamura T. Process and kinetics of bonelike apatite formation on sintered hydroxyapatite in a simulated body fluid. Biomaterials 2005; 26: 4366-4373.

Kokubo T, Kushitani H, Sakka S, Kitsugi T, Yamamuro T. Solutions able to reproduce in vivo surface structure changes in bioactive glass-ceramic A-W. J Biom Mater Res 1990; 24: 721-734.

Kokubo T. Apatite formation on surface of ceramics, metals and polymers in body environment. Acta Mater 1998; 46: 2519-2527.

Kontonasaki E, Zorba T, Papadopoulou L, Pavlidou E, Chatzistavrou X, Paraskevopoulos K, Koidis P. Hydroxy carbonate apatite formation on particulate bioglass in vitro as a function of time. Cryst Res Tech 2002; 37: 1165-1171.

Krajewski A and Ravaglioli A. Bioceramics and biological glasses. In: Barbucci R, editor. Integrated Biomaterials Science. New York: Kluwer Academic / Plenum Publishers, 2002. p. 208-254.

Kumta PN, Sfeir C, Lee DH, Olton D, Choi D. Nanostructured calcium phosphates for biomedical applications: novel synthesis and characterization. Acta Biomat 2005; 1: 65-83.

Lape NK, Yang C, Cussler EL. Flake filled reactive membranes. J Membr Sci 2002; 209: 271-282.

Laurencin CT and Khan Y. Polymer/Calcium phosphate scaffolds for bone tissue engineering. In: Ma PX and Elisseeff J, editors. Scaffolding in tissue engineering. Boca Raton: CRC Taylor & Francis, 2006. p. 253-263.

Lei Y, Rai B, Ho KH, Teoh SH. In vitro degradation of novel bioactive polycaprolactone-20% tricalcium phosphate composite scaffolds for bone engineering. Mat Sci Eng C 2007; 27: 293-298.

Leonor IB, Ito A, Onuma K, Kanzaki N, Reis RL. In vitro bioactivity of starch thermoplastic/hydroxyapatite composite materials: an in situ study using atomic force microscopy. Biomaterials 2003; 24: 579-585.

Leonor IB, Sousa RA, Reis RL. Development of bioactive composites based on biodegradable systems for bone replacement applications. In: Reis RL and San Roman J, editors. Biodegradable systems in tissue engineering and regenerative medicine. Boca Raton: CRC Press; 2005. p. 115-126.

Li H and Chang J. pH-compensation effect of bioactive inorganic fillers on the degradation of PLGA. Comp Sci Tech 2005; 65: 2226-2232.

Li S. Degradation of biodegradable aliphatic polyesters. In: Ma PX and Elisseeff J, editors. Scaffolding in tissue engineering. Boca Raton: CRC Taylor & Francis, 2006. p. 335-352.

Li X, Chang J. Preparation and characterization of bioactive collagen / wollastonite composite scaffolds. J Mater Sci: Mater M 2005; 16: 361-365.

Liu X, Ding C, Chu PK. Mechanism of apatite formation on wollastonite coatings in simulated body fluids. Biomaterials 2004; 25: 1755-1761.

Livingston T, Gordon S, Archmbault M, Kadiyala S, Mcintosh K, Smith A, Peter J. Mesenchymal stem cells combined with biphasic calcium phosphate ceramics promote bone regeneration. J Mater Sci: Mater Med 2003; 14: 211-218.

Lowry KJ, Hamson KR, Bear L, Peng YB, Calaluce R, Evans ML, Anglen JO, Allen WC. Polycaprolactone/glass bioabsorbable implant in a rabit humerus fracture model. J Biomed Mat Res 1997; 36: 536-541.

Lu HH, Tang A, Oh SC, Spalazzi JP, Dionisio K. Compositional effects on the formation of a calcium phosphate layer and the response of osteoblast-like cells on polymer-bioactive glass composites. Biomaterials 2005; 26: 6323-6334.

Lutton C, Read J, Trau M. Current chemistry: nanostructured biomaterials: a novel approach to artificial bone implants. Austr J Chem 2001; 54:621-623.

Maeda H, Kasuga T, Hench LL. Preparation of poly(L-lactic acid)- polysiloxane-calcium carbonate hybrid membranes for guided bone regeneration. Biomaterials 2006; 27: 1216- 1222.

Manjubala I, Kumar S, Sastry T. Biocompatibility evaluation of biphasic calcium phosphate ceramics: An in vivo study. Trends in Biomaterials & Artificial Organs 2001; 14: 27-29.

Mano J, Sousa RA, Boesel LF, Neves NM, Reis RL. Bioinert, biodegradable and injectable matrix composites for hard tissue replacement: state of the art and recent developments. Comp Sci Tech 2004; 64: 789-817.

Moggridge GD, Lape NK, Yang C, Cussler EL. Barrier films using flakes and reactive additives. Prog Org Coat 2003; 46: 231-240.

Mo-Sci Technical Information. http://www.mosci.com, (01/07).

Murugan R, Ramakrishna S. Development of nanocomposites for bone grafting. Comp Sci Technol 2005; 65: 2385-2406.

Narhi TO, Jansen JA, Jaakkola T, Ruijter A, Rich J, Seppala J, Urpo AY. Bone response to degradable thermoplastic composite in rabbits. Biomaterials 2003; 24: 1697-1704.

Navarro M, Ginebra MP, Planell JA, Barrias CC, Barbosa MA. In vitro degradation behavior of a novel bioresorbable composite material based on PLA and a soluble CaP glass. Acta Biomaterialia 2005; 1: 411-419.

Neves NM, Mano JF, Reis RL/ Biodegradable composites for biomedical applications. In: Reis RL and San Roman J, editors. Biodegradable systems in tissue engineering and regenerative medicine. Boca Raton: CRC Press; 2005. p. 91-113.

Ni J and Wang M. In vitro evaluation of hydroxyapatite reinforced polyhydroxybutyrate composite. Mat Sci Eng C 2002; 20: 101-109.

Nuxxol A and Cussler EL. The third parameter in reactive barrier films. AICHE J 2005; 51: 456-463.

Ohtsuki C. Website http://mswebs.naist.jp/LABs/tanihara/ohtsuki/SBF/index.html, (02/04).

Oliveira AL, Reis RL. Pre-mineralization of starch/polycaprolactone bone tissue engineering scaffolds by a calcium silicate process. J Mater Sci: Mater Med 2004; 15: 535-540.

Paul MA, Delcourt C, Alexandre M, Degee P, Monteverde F, Dubois P. Polylactide/montmorillonite nanocomposites: Study of the hydrolytic degradation. Pol Deg Stab 2005; 87: 535-542.

Peitl O, Zanotto ED, Hench LL. Highly bioactive P_2O_5-Na_2O-CaO-SiO_2 glass-ceramics. J. Non.- Cryst. Solids 2001; 292: 115-126.

Pena J, Corrales T, Izquierdo-Barba I, Doadrio AL, Vallet-Regi M. Long term degradation of poly(ε-caprolactone) films in biologically related fluids. Polym Degrad Stab 2006; 91: 1424-1432.

Pitt CG and Gu ZW. Modification of the rates of chain cleavage of poly(ε-caprolactone) and related polyesters in the solid state. J Control Rel 1987; 4: 283-292.

Porter AE, Patel N, Skepper JN, Best SM, Bonfield W. Comparison of in vivo dissolution processes in hydroxyapatite and silicon-substituted hydroxyapatite bioceramics. Biomaterials 2003; 24: 4609-4620.

Prabhakar RL, Brocchini S, Knowles J. Effect of glass composition on the degradation properties and ion release characteristics of phosphate glass-polycaprolactone composites. Biomaterials 2005: 26: 2209-2218.

Proikakis CS, Mamouzelos NJ, Tarantili PA, Andreopoulos AG. Swelling and hydrolytic degradation of poly(D,L-lactic acid) in aqueous solutions. Pol Degrad Stab 2006: 91: 614-619.

Qian Z, Li S, He Y, Zhang H, Liu X. Hydrolitic degradation study of biodegradable polyesteramide copolymers based on a ε-caprolactone and 11-aminoundecanoic acid. Biomaterials 2004; 25: 1975-1981.

Ramakrishna S, Huang ZM, Kumar GV, Batchelor AW, Mayer J. Vol. 1 Series on biomaterials and bioengineering. London: Imperial College Press, 2004. p. 1-15.

Rhee SH. Effect of the molecular weight of poly(ε-caprolactone) on interpenetrating network structure, apatite-forming ability, and degradability of poly(ε-caprolactone)/silica nano-hybrid materials. Biomaterials 2003; 24: 1721-1727.

Rich J, Jaakkola T, Tirri T, Narhi T, Yli-Urpo A, Seppala J. In vitro evaluation of poly(ε-caprolactone-co-DL-lactide) / bioactive glass composites. Biomaterials 2002; 23: 2143-2150.

Risbud M, Nabi Saheb D, Jog J, Bhonde R. Preparation, characterization and in vitro biocompatibility evaluation of poly(butylene terephthalate) / wollastonite composites. Biomaterials 2001; 22: 1591-1597.

Sahai N and Anseau M. Cyclic silicate active site and stereochemical match for apatite nucleation on pseudowollastonite bioceramic-bone interfaces. Biomaterials 2005; 26: 5763-5770.

Salgado AJ, Gomes ME, Coutinho OP, Reis RL. Bone and articular cartilage tissue engineering: the biological components. In: Reis RL and San Roman J, editors.

Biodegradable systems in tissue engineering and regenerative medicine. Boca Raton: CRC Press; 2005. p. 457-478.

Schiller C and Epple M. Carbonated calcium phosphates are suitable pH-stabilizing fillers for biodegradable polyesters. Biomaterials 2003; 24: 2037-2043.

Schliecker G, Schmidt C, Fuchs S, Kissel T. Characterization of a homologous series of D,L-lactic acid oligomers; a mechanistic study on the degradation kinetics in vitro. Biomaterials 2003; 24: 3835- 3844.

Seal BL, Otero TC, Panitch A. Polymeric biomaterials for tissue and organ regeneration. Mat Sci Eng 2001; 34: 147-230.

Seretoudi G, Bikiaris D, Panayiotou C. Synthesis, characterization and biodegradability of poly(ethylene succinate)/poly(ε-caprolactone block copolymers. Polymer 2002; 43: 5404-5415.

Shinzato S, Kobayashi M, Mousa WF, Kamimura M, Neo M, Choju K, Kokubo T, Nakamura T. Bioactive bone cement: Effect of surface curing properties on bone-bonding strength. J Biomed Mater Res 2000; 53: 51-61.

Sikavitsas VI, Temenoff JS, Mikos AG. Biomaterials and bone mechanotransduction. Biomaterials 2001; 22: 2581-2593.

Siriphannon P, Kameshima Y, Yasumori A, Okada K, Hayashi S. Formation of hydroxyapatite on $CaSiO_3$ powders in simulated body fluid. J Eur Cer Soc 2002; 22: 511-520.

Sousa RA, Mano JF, Reis RL, Cunha AM. Interfacial Interactions and Structure Development in Injection Molded HDPE/Hydroxyapatite Composites. Proc. 59th Annual Technical Conference of Plastic Engineers SPE 2001; 47: 2001.

Sousa RA, Mano JF, Reis RL, Cunha AM, Bevis MJ. Mechanical performance of starch based bioactive composite biomaterials molded with preferred orientation. Pol Eng Sci 2002; 42: 1032-1045.

Toquet J, Rohanizadeh R, Guicheux J, Couillaud S, Passuti N, Daculsi G, Heymann D. Osteogenic potential in vitro of human done marrow cells cultured on macroporous biphasic calcium phosphate ceramic. J Biomed Mater Res 1999; 44: 321-328.

Tserki V, Matzinos P, Pavlidou E, Vachliotis D, Panayiotou C. Biodegradable aliphatic polyesters. Part I. Synthesis and characterization of chain extended poly(butylene succinate-co-butylene adipate). Pol Degrad Stab 2006; 91: 367-376.

Tserki V, Matzinos P, Pavlidou E, Panayiotou C. Biodegradable aliphatic polyesters. Part II. Synthesis and characterization of chain extended poly(butylene succinate-co-butylene adipate). Pol Degrad Stab 2006; 91: 377-384.

Ural E, Kesenci K, Fambri L, Migliaresi C, Piskin E. Poly (D, L-lactide/ε-caprolactone) / hydroxyapatite composites. Biomaterials 2000; 21:2147-2154.

Vert M, Schwach G, Coudane J. Present and future of PLA polymer. J Mat Sci – Pure Appl Chem 1995; A32: 787-796.

Wan X, Chang C, Mao D, Jiang L, Li M. Preparation and in vitro bioactivities of calcium silicate nanophase materials. Mater Sci Eng C 2005; 25: 455-461.

Wang N, Ladizesky NH, Tanner KE, Ward IM, Bonfield W. Hydrostatically extruded HAPEX^{TM}. J Mat Sci 2000; 35: 1023-1030.

Wang M. Developing bioactive composite materials for tissue replacement. Biomaterials 2003; 24: 2133-2151.

Wei G and Ma PX. Polymer/Ceramic composite scaffolds for bone tissue engineering. In: Ma PX and Elisseeff J, editors. Scaffolding in tissue engineering. Boca Raton: CRC Taylor & Francis, 2006. p. 241-251.

Weiner S and Wagner HD. The material bone: Structure – mechanical function relations. Annu Rev Mater Sci 1998; 28: 271-298.

Weir NA, Buchanan FJ, Orr JF, Farrar DF, Dickson GR. Degradation of poly-L-lactide. Part 2: increased temperature accelerated degradation. Proc Instn Mech Engrs: J Engin in Med 2004; 218: 321-330.

Xanthos M, Young MY, Karayannidis GP, Bikiaris DN. Reactive modification of polyethylene terephthalate with polyepoxides, Pol Eng Sci 2001; 41: 643-655.

Xanthos M. Polymers and polymer composites. In: Xanthos M, editor. Functional fillers for plastics. Weinheim, Germany: Wiley VCH, 2005. p. 3-16.

Xin R, Leng Y, Chen J, Zhang Q. A comparative study of calcium phosphate formation on bioceramics in vitro and in vivo. Biomaterials 2005; 26: 6477-6486.

Xu XJ, Sy JC, Shastri VP. Towards developing surface eroding poly(α-hydroxy acids). Biomaterials 2006; 27: 3021-3030.

Yamamuro T, Shikata J, Kakutani Y, Yoshii S, Kitsugi T, Ono K. Novel methods for clinical applications of bioactive ceramics. In: Ducheyene P and Lemons JE, editors. Part II of Bioceramics: Material Characteristics Versus In Vivo Behavior. New York: The New York Academy of Sciences, 1988. p. 107-114.

Yao J, Radin S, Leboy PS, Ducheyne P. The effect of bioactive glass content on synthesis and bioactivity of composite poly (lactic-co-glycolic acid)/bioactive glass substrate for tissue engineering. Biomaterials 2005; 26: 1935-1943.